POLITECNICO DI MILANO
DIPARTIMENTO DI MATEMATICA
F. BRIOSCHI
PH.D. SCHOOL IN MATHEMATICAL MODELS AND METHODS IN ENGINEERING

ADJOINT-BASED PARAMETER ESTIMATION IN HUMAN VASCULAR ONE DIMENSIONAL MODELS

Doctoral Dissertation of:
Alessandro Melani

Advisors:
Prof. Luca Formaggia
Prof. Fabio Nobile

Tutor:
Prof. Davide Ambrosi

The Chair of the Doctoral Program:
Prof. Roberto Lucchetti

2013 – XXV Cycle

I discovered the works of Euler and my perception of the nature of mathematics underwent a dramatic transformation. I was de-Bourbakized, stopped believing in sets, and was expelled from the Cantorian paradise. I still believe in abstraction, but now I know that one ends with abstraction, not starts with it. I learned that one has to adapt abstractions to reality and not the other way around. Mathematics stopped being a science of theories but reappeared to me as a science of numbers and shapes.

A.Stepanov

Acknowledgements

THIS thesis has been developed within ERC Advanced Grant Mathcard (number 227058). I would like to thank Prof. Alfio Quarteroni for giving me the opportunity of being part of this project. I would also like to express my gratitude to all the people involved in the project that I had the pleasure to meet.

I would like to thank my advisors Prof. Luca Formaggia and Prof. Fabio Nobile for the attention and the time that they dedicated to me, even if it was not so simple to fit in three calendars. I am also thankful for giving me the possibility to move from virtually applied mathematics to really applied mathematics, for the amount of patience they had with me in this passage and all the knowledge necessary in this transition that they shared with me. I am grateful to them for giving me the opportunity to live in Milan and Lausanne and to experience what to be independent means.

I also thank my tutor Prof. Davide Ambrosi for helping me in inserting in MOX and in my first steps in research (and for his analyses of all my t-shirts graphics).

I would like to thank all the people involved in the project MACAREN@MOX, *MAthematichs for CARotid ENdarterectomy @ MOX*, and in particular Elena Faggiano for the preprocess of MRI data and Laura Azzimonti for the work on Echo Color Doppler imaging.

I thank all the people I met in MOX, especially the young people in the Laboratory and my PhD colleagues for being my first and most devoted friends in Milan. A special thank goes to Laura for all the chaos we have been able to create in couple both in Milan and in Lausanne and to Simone for the help and all the suggestions he gave me between a coffee and a beer and for all the passive smoking he absorbed.

Finally I would like to thank the non mathematic people involved in this experience: my family and my parents that supported me even if I am far away from them and Chiara for all the wonderful days we spent together, for the patience she had with me, especially in the last months I spent working by night, and for fattening me after two years of weight loss.

Abstract

VASCULAR network models are used to describe the propagation of pulse waves in the cardiovascular system. However they depend on several parameters that are difficult (if not impossible) to measure *in vivo* with sufficient confidence. Yet, their knowledge could provide useful information to physicians on the state of the vessels. It is therefore crucial to develop suitable techniques that allow to estimate these parameters adequately, starting from available measurements.

In this work, we focus on the estimation of the compliance of arterial walls in vascular networks. We represent the network as the combination of one-dimensional non linear models (one for each vessel) coupled through suitable interface conditions. The compliance of the vessel appears in the model as a parameter and, in general, it varies from one vessel to another and may even vary within a single vessel, for instance, because of the presence of a stenosis. We estimate this parameter by solving an *inverse problem* that fits the outputs of the state problem to measurements (typically section area or flow rate). The problem is formulated as the constrained minimization of a suitable cost function that we solve through the iterative resolution of three coupled problems (Karush-Kuhn-Tucker conditions), namely

1. *state problem*, that describes blood flow in the vessels and that depends on parameters;
2. *adjoint problem*, that gives us the sensitivity of state model to the variation of parameters and that depends on both state problem solution and parameters;
3. *optimality condition*, that permits us to update parameters and to understand when we reach the minimum and that depends on both state and adjoint problem solutions.

As a specific application, we consider the estimation of the compliance of the arteries of a carotid bifurcation, exploiting real medical data (area section inside the domain and flow rate at the inflow, respectively obtained by MRI and Eco Color Doppler exams).

Keywords: Parameter Estimation, Blood Flow Models, Networks Models, Carotid bifurcation.

Contents

List of Figures

Introduction

CARDIOVASCULAR diseases are the first cause of mortality in the world, thus motivating huge attention and economical investments in the research. Thanks to the increasing computational power and the progress in imaging and geometry reconstruction techniques, mathematical models and numerical simulations have become an effective tool to study and understand the physiology of the cardiovascular system as well as to predict the development of very common and dangerous cardiovascular pathologies. These models depend on a large number of parameters that may considerably differ from person to person and even in the same person in presence of anomalies.

The aim of this thesis is to develop and implement a mathematical method to estimate parameters in one dimensional network models of the circulatory system. In particular we are interested in estimating the compliance of the vessels. In the following, we first briefly recall the main elements of cardiovascular anatomy and the most common associated pathologies, to define the context of the thesis. Then, we provide an overview of the most recent achievements in the field of computational hemodynamics. More precisely, we recall the main models used to account for the different compartments of the cardiovascular system. Finally, we close the introduction presenting a brief overview of the thesis objectives and outline.

Cardiovascular physiology

The cardiovascular system provides the transport of blood (and its contained gases, cells, particles, and heat) among the different organs of the body. Due to the high resistance against flow in the microcirculation, the transport of blood requires a relatively high perfusion pressure. Maintenance of high levels of perfusion pressure without overloading the pumping heart is only possible when the arterial network is elastic (the windkessel effect).

The human cardiovascular system mainly consists of two parallel networks, the systemic and the pulmonary circulations. In the systemic circulation the oxygenated blood flows from the left atrium into the left ventricle through the mitral valve, which pre-

vents backflow. The contraction of the ventricle forces the blood into the aortic arch and the aorta. The coronary arteries stem from the aortic root and nourish the heart muscle itself. Three major arteries originate from the aortic arch (brachiocephalic, left common carotid and left subclavian arteries), supplying blood to the head and the upper limbs. The other major arteries originating from the aorta are (i) the renal arteries, which supply kidneys, (ii) the celiac and the superior and inferior mesenteric arteries, which supply intestines, spleen, and liver, and (iii) the iliac arteries, which branch out to the lower trunk and become the femoral and popliteal arteries of the thighs and legs, respectively. At the far end of the arterial circulation the blood flows through the capillary bed where it delivers nutrients and oxygen to organs and muscles and removes carbon dioxide. Then, the capillaries converge to form venules, which in turn form veins. The inferior vena cava returns blood to the heart from the legs and trunk; it is supplied by the iliac veins from the legs, the hepatic veins from the liver, and the renal veins from the kidneys. The subclavian veins, draining the arms, and the jugular veins, draining the head, join to form the superior vena cava. The two venae cavae, together with the coronary veins, return deoxygenated blood to the right atrium of the heart. There, the pulmonary circulation starts: the blood flows from the right atrium into the right ventricle through the tricuspid valve. The right ventricle contracts to force blood into the lungs through the pulmonary arteries. In the lungs oxygen is picked up and carbon dioxide eliminated, and the oxygenated blood returns to the left atrium of the heart via the pulmonary veins, thus completing the circuit. Indeed, in pulmonary circulation the arteries carry deoxygenated blood, and the veins bear oxygenated blood. Few schematic pictures describing the main elements of the circulatory system are shown in Figure 1.

The arterial system The structure and the mechanical properties of the arterial wall are rather complex. Large arteries range approximately from 2.5 cm to 0.1 cm of diameter and are made of three layers: the tunica intima (the inner coat), the tunica media (the middle coat), and the tunica adventitia (the outer coat). The tunica intima contains the endothelial cells, which sense and react to the normal and shear stress coming from the fluid. The tunica media is the thickest layer and is composed mainly of elastin and collagen fibers. The tunica adventitia is basically an outer covering and does not contribute significantly to the compliance of the vessel. Therefore, the mechanical properties of the wall are mainly determined by the tunica media, which has a nearly elastic behavior in physiological conditions. Regarding the small arteries, their wall is almost rigid and contains smooth muscle cells, which allow to change the intraluminal pressure and radius, in order to satisfy the needs of the surrounding tissues and to regulate the global arterial pressure. In the arterial tree, the pressure is kept at a relatively high value because the distal end of the arterial system bifurcates into many vessels with small diameters (arterioles) and hereby forms a large peripheral resistance. Pressure pulsations are reduced by the elasticity of the vessels (the windkessel effect). This elastic function of the arteries also helps perfusion during diastole and produces the wave-propagation phenomenon. Smooth muscle cells in the arterial wall can change their contractile state, thereby changing the diameter and hemodynamical resistance. In this way blood flow is distributed to the different vascular beds in accordance with the local instantaneous metabolic needs.

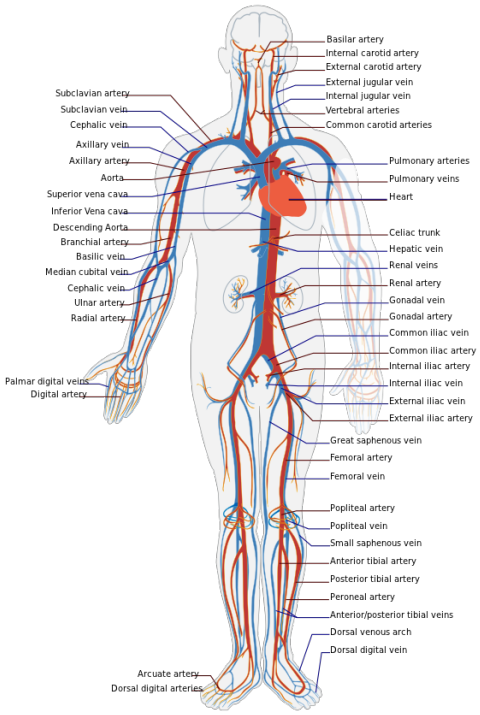

Figure 1: *Scheme of human circulatory system. Source: wikipedia.org*

The capillary system The capillary system is a network of small vessels with walls consisting of a single layer of endothelial cells lying on a basement membrane, The diameter of the capillaries is small enough that the whole blood may not be considered as a homogeneous fluid anymore. Blood cells move in a single-file train and deform strongly. The plasma, together with the glycocalyx layer covering the endothelial cells, acts as a lubrication layer. In the microcirculation, viscous forces dominate over inertia forces. Consequently, in its most simple form, the microcirculation, including the arterioles, can be approximated as a collection of parallel tubes or a porous medium with a linear relation between perfusion pressure and flow. In general, the peripheral resistance is not a constant and is principally controlled by the smooth muscle tone of the arterioles.

The venous system The blood is then collected in the venous system (venules and veins) in which the vessels rapidly merge into larger vessels directing the blood back to the heart. As the diameters in the venous system are of the same order of magnitude as in the arterial system, inertia forces may become influential again. However, both characteristic velocities and pressure amplitudes are lower than in the arterial system. As a consequence, in the venous system, unsteady inertia forces are of less importance than in the arterial system. Also the pressure within the veins is significantly lower than the arterial pressure. In certain situations the pressure can be low enough that the normal functioning vein will have an elliptic cross-sectional area or even collapse. Because of low pressures, gravitational forces become important, especially in the upright position. To cope with gravitational effects, veins have valves to prevent retrograde flow and ensure

unidirectional flow toward the heart.

The blood Blood is composed mainly of erythrocytes, or red blood cells, whose number ranges from 4.5 millions to 6 millions per cubic millimeter. They are responsible for the exchange of oxygen and carbon dioxide between the lungs and the body tissues. The leukocytes, or white blood cells, range approximately from 5000 to 10000 per cubic millimeter and defend the body against infecting organisms and foreign agents, both in the tissues and in the bloodstream itself. The blood also contains thrombocytes, or platelets, and several other factors active in blood clotting. Serum, a straw-colored liquid essentially composed of plasma (made 98% of water) without fibrinogen, makes up the liquid component of blood that separates from the clot. The behavior of blood is found to be non-Newtonian and its viscosity depends on the shear. The reason is that when the shear is low the red blood cells tend to interact, thus increasing the macroscopic viscosity of blood. For high shear there is no interaction and the viscosity of blood in large arteries is approximately constant (approximately between 0.03 g/cm/s and 0.04 g/cm/s).

For more details about the cardiovascular system and its components see [Boron and Boulpaep, 2008, Guyton and Hall, 2010, Netter and Colacino, 1989, Nichols et al., 2011] and references therein.

Cardiovascular pathology

Cardiovascular pathologies are a class of diseases that involve heart, arteries, or veins. In the following we briefly describe some of the main cardiovascular problems together with a possible treatment.

Heart failure. Heart failure refers to a cardiac dysfunction in which the heart may not pump blood at a sufficient rate in the arterial system. In systolic dysfunction, the myocardial contraction is diminished, and as a result, blood accumulates in the lungs or veins. Coronary artery disease, leading to a reduction of the flow of oxygen-rich blood to the heart muscle, is a common cause of systolic dysfunction. Also heart-valve disorders such as stenosis or leakage can cause systolic dysfunction as, over time, due to inadequate emptying of the ventricles, the heart enlarges and cannot pump adequately anymore. In diastolic dysfunction, the heart muscle has become stiffer and does not relax normally after contracting, which makes filling with blood less effective. High blood pressure is the most common cause of diastolic dysfunction. This is because the heart must eject blood against a too high pressure in the arterial system, causing the heart walls to thicken (hypertrophy) and stiffen.

Vascular disorders. Vascular disorders are primarily related to arteriosclerosis. Arteriosclerosis means hardening (sclerosis) of the arteries (arterio-) and usually affects all humans as part of the aging process. *Atherosclerosis*, in which fatty deposits (plaques) develop in the walls of medium-sized and large arteries, is the most common type of arteriosclerosis causing symptoms. Various factors, including high blood pressure, diabetes, and high levels of cholesterol in the blood, may contribute to its development. Hemodynamical factors such as disturbed

blood flow, low wall shear rate, and wall shear stress favor the development of atherosclerosis. This is why regions of disturbed blood flow, such as bifurcations and curved vessels, appear to be more prone to atherosclerosis. Plaques can grow and gradually cause the artery to narrow, compromising blood flow. Plaques can also rupture, exposing the lipid material within to the bloodstream. This can trigger the formation of a blood clot, which can suddenly block all blood flow or detach and travel downstream, creating an embolism. Heart attacks due to coronary artery disease and stroke (resulting from atherosclerosis that affects the arteries to the brain) are responsible for more deaths than all other causes combined. The main clinical procedures to treat stenotic arteries are the creation of arterial bypass, the insertion of a stent, a device which supports the vessel wall preserving the original lumen area, or the removal of the plaque and the insertion of a patch. Atherosclerotic processes are also seen as the most common cause of *aneurysms*. Atherosclerosis locally weakens the vascular wall. The transmural arterial pressure forces the weak area to remodel and bulge outward. An aortic aneurysm may rupture, resulting in an often fatal internal bleeding. High blood pressure, which is common among older people, increases the risk of aneurysm development. Aneurysms may also occur in the arteries of the brain (cerebral arteries). Rupture of a cerebral aneurysm may cause bleeding into the brain tissue, resulting in a hemorrhagic stroke. An aneurysm can be either fusiform or saccular. The former case is generally treated by grafting or by using stents. In contrast, a saccular aneurysm is either clipped or filled with thin metallic coils.

Numerical simulation of cardiovascular system: state of the art

Blood flow dynamics is governed by the classical laws of mass, momentum, and energy conservation. The constitutive equations of the vessel wall provide an additional constraint that strongly influences the dynamics of the blood; indeed, the deformation of the vessel has to be taken into account to correctly predict the pulse wave propagation along the systemic network of arteries. In addition, the macroscopic modeling of the blood flow as a Newtonian fluid and of the arterial wall as an elastic structure is justified only for large arteries, while the circulation in arterioles and capillaries should be simulated using more complex models accounting for the effects mentioned in the previous sections. Furthermore the mechanical propulsion is provided by the muscle of the heart, governed by its own constitutive equations including active components.

The selection of the appropriate model and geometrical dimension representation depends on the aims and on the required accuracy of the research study. Being the time constraint important in a medical environment, a compromise between model complexity and computational cost is mandatory. For this reason usually only few specific components of the problem are represented by complex three-dimensional models, while the remaining parts are in general accounted for through reduced models. Indeed, the dimensional-heterogeneity of the constituent components becomes unavoidable to correctly model the global and local circulation. Now we recall the main classes of models that are used in numerical simulations of cardiovascular system (see also [Formaggia et al., 2009]):

Three-dimensional (3-D) fluid-structure interaction (FSI) models provide a detailed

pointwise description of the flow dynamics in complex geometrical situations, such as those occurring at bifurcations, aneurysms, and stenoses among others. Moreover, thanks to the advancements in 3-D imaging techniques, they can now be employed to simulate patient-specific geometries starting from medical imaging data (see, e.g, [Canic et al., 2005], [Gerbeau et al., 2005], [Torii et al., 2008], [Taylor and Figueroa, 2009], [Vignon-Clementel et al., 2010] and [Faggiano et al., 2012]). Several techniques can be used to model the interaction between the blood and the vessel wall. Here we mention the arbitrary Lagrangian–Eulerian (ALE) formulation (see, e.g., [Nobile, 2001], [Deparis et al., 2006], [Küttler and Gee, 2010], [Crosetto, 2011], [Pozzoli, 2012] and references therein) and the Eulerian space-time formulation (see [Tezduyar et al., 2006, Tezduyar and Sathe, 2007]) to handle the domain movement and partitioned or monolithic algorithms to manage the fluid-structure interaction from a numerical point of view.

One-dimensional (1-D) FSI models are generally used to simulate the pulse wave propagation along large networks of arteries (see [Wemple and Mockros, 1972], [Avolio, 1980], [Stergiopulos et al., 1992], [Karamanoglu et al., 1994], [Olufsen et al., 2000], [Sherwin et al., 2003], [Vignon and Taylor, 2004], [Wang and Parker, 2004], [Formaggia et al., 2003], [Formaggia et al., 2006], [Alastruey et al., 2007], [Huo and Kassab, 2007], [Mynard and Nithiarasu, 2008], [Reymond et al., 2009], and references therein). Originally introduced in [Euler, 1844], they provide a cheap and accurate description of the main physiological quantities of interest (flow rate, pressure, and average wall deformation) along the global systemic network of arteries, thus accounting for the global interplay among the physical phenomena taking place in the different compartments.

Zero-dimensional (0-D) (also called lumped parameters models) provide averaged spatial information about the fundamental variables (pressure, flow rate, and volume) of the compartment of interest (organ, vessel, or part of vessel) at any instant in time, differentiating themselves from higher dimensional models that are also able to capture the spatial variation of these parameters. They are particularly appreciated in the description of complex multi-compartmental systems as they are easy to develop and prototype, fast to solve, and may be refined by adding equations for second-order effects and nonlinearities. Usually, lumped parameter models consist of sets of differential algebraic equations describing the conservation of mass and momentum which are complemented by a pressure-volume relation (see, e.g., [Stergiopulos et al., 1999], [Segers et al., 2003], [Milišić and Quarteroni, 2004], [Ottesen et al., 2004], and references therein). System models assembled from 0-D components generally feature the major components of the cardiovascular network (see, e.g., [Ursino, 1998], [Liang and Liu, 2005], and [Lanzarone et al., 2007]). For a recent review on lumped parameters models for cardiovascular problems see [Shi et al., 2011] and references therein.

The use of these dimensionally-heterogeneous models together with their correct mathematical coupling is called geometrical multiscale and has been firstly studied in [Formaggia et al., 1999]. Its efficient solution is a challenging task which has been addressed by several research groups with the final goal of accounting for the whole circulation and autoregulation of the systemic network of arteries (see [Migliavacca

et al., 2006], [Vignon-Clementel et al., 2006], [Blanco et al., 2007], [Grinberg and Karniadakis, 2008], [Kim et al., 2009], [Reichold et al., 2009], [Malossi, 2012], [Esmaily Moghadam et al., 2013] and references therein).

Thesis objectives and outline

The aim of this thesis is the development of a technique to estimate the elastic properties of a network of vessels. More precisely, we approximate the vessels network with 1D-FSI models and we make use of optimal control techniques to compute the compliance parameters that best fits the observations. To obtain the parameters, we solve the first order conditions (state equation, adjoint equation and optimality condition) iteratively and we update the parameters at each iteration, until a suitable tolerance is reached. The method is tested and finally applied to the estimation of the elastic properties of a carotid bifurcation that had been operated because affected by atherosclerotic plaque.

The main original contributions of this work include

- the development of continuous first order conditions for the network model, with particular attention to the adjoint coupling conditions and the adjoint compatibility conditions at each junction of the network;
- the implementation of the solvers of first order conditions and of some optimization techniques in the C++ finite element library `LifeV`;
- the verification and the tests of the developed optimal control technique with different optimization methods;
- the treatment of the real medical data and the application to real patient case.

This work is structured in four chapters in which we proceed from the preliminary knowledges necessary for the development of our method to the application to the real patient case. More precisely, the thesis is structured as follows.

In Chapter 1, we describe the preliminary background necessary to the development of our method. Firstly, we introduce and briefly describe the field of data assimilation, with specific attention to cardiovascular application. Then, we treat the variational approach of data assimilation and we deepen in optimal control theory, the Lagrangian approach and we focus on the particular case of hyperbolic problems. Finally, we present the finite dimension optimization techniques that we will use and their application to optimal control problems.

In Chapter 2, we describe the 1D-FSI model, starting from the derivation of the model, moving to the discretization that we choose and the boundary conditions that we impose and closing with the case of networks of vessels.

In Chapter 3, we describe the application of optimal control Lagrangian approach to the 1D-FSI model. Firstly, we analyze the first order conditions for single vessel 1D-FSI model: adjoint problem, its discretization, the treatment of boundary and compatibility conditions and the optimality condition. Then, we analyze the case of the network of vessels with particular attention to the adjoint coupling conditions. Finally, we focus on the implementation aspects.

In Chapter 4, we describe the application of our technique. Firstly, we present some tests to validate the model and our implementation. Then we show the application to a real case, employing medical data that come from the carotid bifurcation.

We close this thesis with a summary of the main conclusions drawn throughout the text and the full list of bibliographic references.

CHAPTER 1

Data assimilation and optimal control for partial differential equations

In this chapter we present the background knowledge that is necessary in this thesis. The chapter is organized as follows. In Section 1.1 we give a quick review on data assimilation techniques. In Section 1.2 we present basic concepts of optimal control theory for PDEs with particular attention to hyperbolic problems. In section 1.4 we describe some numerical methods used in optimization and their application to the solution of optimal control theory.

1.1 Data assimilation methods

Mathematical modeling is nowadays a major tool for the study of many physical evolutionary processes.

In many real-life situations, the following problems have to be faced:

(i) determine values of (part of) the input parameters, such as initial conditions, boundary conditions or model parameters, that best match given observation (values of output quantities).

(ii) determine which input parameters the output quantities are most sensitive to. In some situations, one will be interested in the sensitivities of outputs with respect to a large number of input parameters.

Data assimilation is the ensemble of techniques combining in an optimal way (in a sense to be defined) the mathematical information provided by the equations and the physical information given by the observation (generally sparse and noisy) into a

numerical model based on the approximation of physical and constitutive laws. In other words, the goal of data assimilation is to link together the heterogeneous (in nature, quality, and density) sources of information in order to retrieve a coherent state of the environment at a given date.

In the last decades, the study of geophysical fluids gave a huge impulse to the development of data assimilation [Blum et al., 2008, Evensen, 2009, Navon, 2009, Robinson and Lermusiaux, 2000, Wang et al., 2000], because of the maturity reached by mathematical models of the atmosphere, the growth of the available computing resources and the improvement in the collection of the observations. Originally, the problem of data assimilation was to determine the initial condition of a dynamical system from noisy observations taken during the time evolution. Using the same mathematical tools, data assimilation can also include the estimation of model parameters, boundary conditions or the state itself. The development of data assimilation methodology has mainly experienced three stages: objective analysis, statistical interpolation, stochastic methods and variational analysis. Simple analysis methods were mostly used in the 50's, when computers were unavailable; these techniques were the earliest bases of data assimilation. In the 60's and 70's, statistical considerations were introduced into the atmospheric data assimilation. Based on these considerations, some forms of optimal interpolation were used to assimilate observations into forecast models. In the same decades the Kalman filter (KF) was introduced and efficiently improved into many extensions. In the 80's and 90's, atmospheric data assimilation switched to variational methods ([Courtier et al., 1993]).

We can identify two main families in data assimilation methods:

Stochastic methods: The basic idea is to consider the state variables and initial conditions as the realization of a stochastic process and carry out Kalman filtering methods.

Variational methods: Data assimilation is set as being a problem of constrained optimization, then the tools of optimal control are used to solve it.

1.1.1 The stochastic approach

Stochastic methods are mainly based on the application of Kalman filter. The Kalman filter (KF) was developed by Kalman ([Kalman, 1960, Kalman and Bucy, 1961]) as a new approach to linear filtering and prediction problems. It is a recursive filter for the estimation of the state of a dynamic system from incomplete and noisy measurements ([du Plessis, 1967, Humpherys et al., 2012]). Because of its limitations in terms of models (designed for linear systems) and memory requirements for the storage of the structures involved (mainly the covariance matrix of the state variable at each time step), several modifications and improvements have been developed, such as the Extended KF (EKF), the Ensemble KF (EnKF) and the Unscented KF (UKF). We report briefly the formulation of the basic KF and we give some details of its extensions.

Consider a linear model representing the observation process:

$$\mathbf{y}_k = H_k \mathbf{u}_k + \varepsilon_k \tag{1.1}$$

where k is a multiple of the number of time steps between consecutive observations, $\mathbf{u}_k$ is the vector of state variables, $\mathbf{y}_k$ is the vector of the measures, H_k is the linear operator

which maps the state space into the observed space and ε_k is an additive Gaussian noise representing the error; this is assumed to be white with zero mean and covariance matrix R_k. For each time step we consider a discretized stochastic dynamic system

$$\mathbf{u}_k = M_{k-1}\mathbf{u}_{k-1} + B_k\mathbf{v}_k + \eta_{k-1} \tag{1.2}$$

where M_k describes the model dynamics, $\mathbf{v}_k$ is a set of parameters, B_k describes the dependence of the model on parameters, η_k is the random error associated with model parameters and we assume that η_k is an additive Gaussian noise with mean zero and with covariance matrix Q_k.

Kalman filter consists in averaging a prediction of the state with measures making a weighted mean, whose weights depend on the covariances of the dynamic system and of the observation process. The result is a new state that lies in between the predicted and measured state and has a better estimated uncertainty than either alone. This process is recursively repeated every time step and in each iteration it's possible to identify two distinct phases:

- **Prediction step** (or time update or forecast step) consists in making the dynamic system evolve without taking into account the observations and computing the *forecast* state $\mathbf{u}_k^f$.
- **Correction step** (or measurement update or analysis step) consists in updating the state computed in the previous step, by assimilating the observations into the model and computing the *assimilated* state $\mathbf{u}_k^a$.

Algorithm 1.1.1 (Kalman Filter time step)**.** Each time step of the Kalman filter can be represented with these stages:

(i) advance in time: $\begin{cases} \mathbf{u}_k^f = M_{k-1}\mathbf{u}_{k-1}^a + B_k\mathbf{v}_k \\ P_k^f = M_k P_{k-1}^a M_k^T + Q_k \end{cases}$

(ii) compute the Kalman gain: $K_k = P_k^f H_k^T (H_k P_k^f K_{k-1}^T + R_k)^{-1}$;

(iii) state update: $\mathbf{u}_k^a = \mathbf{u}_k^f + K_k(\mathbf{y}_k - H_k\mathbf{u}_k^f)$;

(iv) error covariance matrix update: $P_k^a = (I - K_k H_k)P_k^f$;

where P_k^f and P_k^a are the computed covariance matrix of $\mathbf{u}_k^f$ and $\mathbf{u}_k^a$.

The previous formulation can be extended to estimate also the vector of parameters $\mathbf{v}_k$ by applying the KF procedure to the system composed by the equation (1.2) coupled with the equation

$$\mathbf{v}_k = \mathbf{v}_{k-1} + \eta_{k-1}^{\mathbf{v}}. \tag{1.3}$$

In (1.3) we assume that $\eta_k^{\mathbf{v}}$ is the random error associated with the model parameters and we assume that $\eta_k^{\mathbf{v}}$ is an additive Gaussian noise with mean zero and with covariance matrix $Q_k^{\mathbf{v}}$. This procedure is equivalent to consider as state vector $\widehat{\mathbf{u}}_k = (\mathbf{u}_k, \mathbf{v}_k)^T$ instead of $\mathbf{u}_k$ and considering the modified algorithm

Algorithm 1.1.2 (Kalman Filter time step for parameter estimation)**.** Each time step of Kalman filter can be represented with these stages:

(i) advance in time: $\begin{cases} \widehat{\mathbf{u}}_k^f = \widehat{M}_{k-1}\widehat{\mathbf{u}}_{k-1}^a, \\ \widehat{P}_k^f = \widehat{M}_k\widehat{P}_{k-1}^a\widehat{M}_k^T + \widehat{Q}_k \end{cases}$

(ii) compute the Kalman gain: $K_k = \widehat{P}_k^f\widehat{H}_k^T(\widehat{H}_k\widehat{P}_k^f K_{k-1}^T + \widehat{R}_k)^{-1}$;

(iii) state update: $\widehat{\mathbf{u}}_k^a = \widehat{\mathbf{u}}_k^f + K_k(\widehat{\mathbf{y}}_k - \widehat{H}_k\widehat{\mathbf{u}}_k^f)$;

(iv) error covariance matrix update: $\widehat{P}_k^a = (I - K_k\widehat{H}_k)\widehat{P}_k^f$;

where

$$\widehat{M}_k = \begin{pmatrix} M_k & B_k \\ 0 & I \end{pmatrix}, \ \widehat{Q}_k = \begin{pmatrix} Q_k & 0 \\ 0 & Q_k^{\mathrm{y}} \end{pmatrix},$$

$$\widehat{\mathbf{y}}_k = \begin{pmatrix} \mathbf{y}_k \\ 0 \end{pmatrix} \ \widehat{H}_k = \begin{pmatrix} H_k & 0 \\ 0 & 0 \end{pmatrix}, \ \widehat{R}_k = \begin{pmatrix} R_k \\ 0 \end{pmatrix}$$

The classical formulation of KF works very well for low-dimensional, linear dynamical systems, but, often in real applications, none of this assumptions is valid. The main extensions of KF try to overcome this limitations [Simon, 2006].

Extended Kalman Filter The extended Kalman filter (EKF) has been developed to treat a nonlinear dynamical system where equations (1.1) and (1.2) are replaced by

$$\mathbf{y}_k = h(\mathbf{u}_k, \varepsilon_k) \quad \mathbf{u}_k = f(\mathbf{u}_{k-1}, \mathbf{v}_k, \eta_k), \tag{1.4}$$

where h and f are nonlinear functions. EKF consists in applying KF to a linearized version of (1.4) around the previous state. EKF has still some drawbacks:

- if the initial estimate of the state is wrong, or if the process is modeled incorrectly, the filter may be unstable or even diverge;
- the estimated covariance matrix tends to underestimate the true covariance matrix;
- it has high memory requirements, the matrices computed in Algorithms 1.1.1 and 1.1.2 are full and have dimension equal to the dimension of the state variable. To overcome this issue, low rank approximation techniques have been developed [Farrell and Ioannou, 2001, Tuan Pham et al., 1998].

Unscented Kalman Filter The unscented Kalman filter (UKF) [Julier et al., 2000, Julier and Uhlmann, 2004, Ambadan and Tang, 2009] represents a derivative-free alternative to the EKF and provides better performance at an equivalent computational complexity. In fact, in the UKF the state distribution is still Gaussian but it is specified using a minimal set of "carefully chosen" sample points or snapshots which completely capture the state mean and covariance. Furthermore, these points, when propagated through the nonlinear system, capture the mean and covariance at the subsequent step to the second order. Such sample points are chosen via unscented transform [van der Merwe and Wan, 2001, van der Merwe, 2004] of the state at the current time step. Also this method has high memory requirements if the state has high dimension. Another issue is the number of sample point: in fact $2N$ sample points are necessary, where N is the dimension of the state variable. Therefore, reduced rank approximations and dimensional reduction strategies have been developed [Chandrasekar et al., 2008].

Ensemble Kalman Filter The ensemble Kalman Filter (EnKF) [Evensen, 2003,Evensen, 2009, Reichle et al., 2002, Gillijns et al., 2006] is a Monte Carlo approximation of the KF that approximates the probability distributions by random samples. The starting point is choosing a set of sample points, that is, an ensemble of state estimates, that captures the initial probability distribution of the state. These sample points are then propagated through the true linear or nonlinear system and the probability density function of the actual state is approximated by the ensemble of the estimates. In the case of the UKF, the sample points are chosen deterministically. In fact, the number of sample points required is proportional to the dimension of the system. On the other hand, the number of ensembles required in the EnKF is heuristic. While one would expect that a large ensemble would be needed to obtain useful estimates, the literature on EnKF [Evensen, 2009] suggests that an ensemble of size 50 to 100 is often adequate for systems with thousands of state variables.

1.1.2 The variational approach

An optimal control approach considers the minimization of the misfit between the predicted state and the observations under the constraint of the partial differential equations (PDEs) governing the evolution of the system. Such optimization (or control) problem may be solved with a large variety of numerical methods for PDE constrained optimization problems. In the context of computational fluid dynamics there is a huge literature for the solution of inverse problems, among many others we mention [Blum et al., 2008, Gronskis et al., 2013, Gunzburger, 1987, Gunzburger, 2000, Hinze et al., 2009,Navon, 2009,Penenko, 2009] and some others will be mentioned in the following subsections.

The main ingredients of this kind of approaches are

- a deterministic state model that predict the physical behaviour of the system;
- a sparse and noisy set of observed values;
- a cost functional J that measures the distance between state variable and observations;
- a control variable that can be used to minimize the functional and on which the state model depends.

The control problem is solved by deriving and solving the system of first order necessary conditions:

- state model;
- adjoint model;
- optimality condition.

Optimal control methods can be grouped in two main categories;

***optimize-then-discretize* approach** (OD) consists in deriving the system of infinite dimensional first order necessary conditions and then discretize and solve this system;

***discretize-then-optimize* approach** (DO) consists in discretizing the state model and then derive and solve the system of finite dimensional first order necessary conditions.

For a deeper analysis of the differences of these two approaches, we refer the reader to [Hinze et al., 2009].

1.1.3 Data assimilation in cardiovascular system modelling

While data assimilation for geophysical models had a huge development in the last decades of the past century, data assimilation for cardiovascular models has featured great advancements only in the beginning of this century. This development was due to the tremendous increase of data gathering and the massive change in computational capabilities in the last few years. Therefore, well-established DA techniques are applied to cardiovascular problems and, furthermore, they feature an overlap between estimation theory, control theory and stochastic approaches. Moreover, they benefit from the continuous improvement of numerical methods for order reduction [Moireau and Chapelle, 2010, Bertoglio et al., 2012, Manzoni et al., 2012] and advanced discretization techniques. Among the others, we mention and briefly describe the most relevant works.

Stochastic approach

In [Devault et al., 2008] the circle of Willis was modelled with a network of one dimensional FSI models coupled with zero dimensional models to simulate outflow conditions. These latter models have been calibrated by using EnKF and employing real medical data for velocity and pressure of the blood and length and area of vessels.

In the same year, the group of Moireau and Chapelle applied the UKF to parameter identification in the context of cardiac biomechanics [Moireau et al., 2008, Moireau et al., 2009]. They also introduced an order reduction strategy [Moireau and Chapelle, 2010, Xi et al., 2011] and finally they applied these techniques also to the estimation of wall stiffness in a fluid structure interaction model for arterial flow simulations [Bertoglio et al., 2012], using also medical data [Moireau et al., 2012]. Their filtering strategy, usable for any choice of sampling points distribution, provides a tractable filtering algorithm that can be used with large-dimensional systems when the uncertainty space is of reduced size. Such algorithm invokes the original dynamical and observation operators, i.e. it does not require the computation of the tangent operator. Specifically, the covariance matrices are factorized in a form such that the costly computations are performed on a reduced-order matrix of the order of the uncertainty space. In [Marchesseau et al., 2013], MRI data are employed in reduced order UKF to personalize an electromechanical model of the heart. In [Lombardi, 2013], a sequential approach based on the UKF is applied to solve inverse problems in 1D hemodynamics, on a large systemic network.

Variational approach

In the last years, a great number of parameter estimation methods has been developed to minimize a cost functional that measures the misfit between state equation output

and observations in various fields in cardiovascular modelling (for example, stiffness in pure structural models [Stå lhand and Klarbring, 2005, Stå lhand, 2009, Balocco et al., 2010, Harb et al., 2011] or one dimensional FSI models [Dumas, 2008, Dumas et al., 2012, Bogaers et al., 2012], vascular territories resistance in one dimensional FSI models [Blanco et al., 2012], lumped cerebrovascular models [Pope et al., 2008], terminal parameters in three dimensional FSI models [Spilker and Taylor, 2010]), outflow boundary conditions in three dimensional imaged-based patient-specific models of the multi-branched pulmonary arteries and superior vena cava [Troianowski et al., 2011]. However, to the author's knowledge, only few works enforce adjoint-based techniques for the minimization of the cost functional:

- in [Lagrée, 2000], the author estimates the elastic parameter in a single vessel one dimensional model by using OD approach and employing as observations the output of the same one dimensional model,
- in [Martin et al., 2005], the authors estimate the elastic parameter in a single vessel one dimensional FSI model by using a DO approach and employing as observations the output of a three dimensional FSI problem,
- in [Sermesant et al., 2006], ventricular myocardium contractility is estimated with a DO strategy by making use of an electromechanical heart model on a patient specific geometry and simulated heart displacements;
- in [D'Elia et al., 2012, Perego et al., 2011], the Young modulus of the vessel wall in a three dimensional FSI model is estimated using a OD technique and assimilating vessel displacements from registered medical images,
- in [D'Elia, 2011], the velocity data is included in hemodynamics simulations by using a DO approach to recover an accurate and noise filtered approximation of the blood flow,
- in [Ismail et al., 2013b, Ismail et al., 2013a], the parameters of windkessel models at the outflow of a 3D FSI model are calibrated by using adjoint-based approach,
- in [Yang and Veneziani, 2013], the heart conductivity is estimated in the so called bidomain model by using a OD strategy.

The works that are closest to ours are [Lagrée, 2000] and [Martin et al., 2005], in which the elastic parameters of a single vessel one dimensional models are estimated. The main difference with our work are that we consider also a network and we use different and more sophisticated optimization methods. Then, differently from [Martin et al., 2005], we adopt OD approach in order to be able to change the numerical discretization of the differential models to our choice.

To the author's knowledge, in literature, no work has been done to estimate the elastic properties of arterial walls using a network of one dimensional vessel models and a OD variational approach.

1.2 Optimal control: Lagrangian formulation

The classical approach to optimal control for PDEs is based on the theory developed by J.L. Lions ([Lions, 1972, Lions, 1987]), which provides existence and uniqueness

results for optimal control problems described by elliptic, parabolic, hyperbolic and mixed PDEs. However, starting from the classical theory, a straightforward analysis for a broader class of optimal control problems (e.g. with non-linearities of boundary control) is not always easy. An alternative approach which allows to handle a wider class of optimal control problems is based on the *Lagrangian* formalism (see [Maurer and Zowe, 1979, Maurer, 1981]). This approach is suitable also for problems described by ordinary differential equations or integral equations, as well as for shape optimization problems [Jameson, 2003, Mohammadi and Pironneau, 2001, Sokolowski and Zolesio, 1992]. For these reasons we make use and discuss the optimal control theory based on the *Lagrangian* formalism, For a deeper study of optimal control theory, we refer the reader also to [Agoshkov, 2003, Alekseev et al., 1987, Aziz, 1977, Fernández-Cara and Zuazua, 2003, Hinze et al., 2009, Tröltzsch, 2010].

Remark 1.2.1. For the sake of simplicity, we present the Lagrangian formalism for scalar PDEs depending on scalar variables, but the analysis can be straightforwardly extended to vectorial PDEs with vectorial variables.

1.2.1 General case

The optimal control problem reads, in an abstract setting, as:

$$\text{find } v \in \mathcal{V},\ v = \underset{w \in \mathcal{V}}{\operatorname{argmin}}\, J(u, w), \text{ where } u \in \mathcal{U} \text{ is solution of } e(u, v) = 0 \text{ in } \mathcal{W}. \quad (1.5)$$

Here $J(u, v)$ is the cost functional, $e(u, v) = 0$ indicates a PDE (with appropriate boundary and initial conditions), which is called *state equation* (or *primal equation*). Consequently, the variable $u \in \mathcal{U}$ is called *state variable*, while $v \in \mathcal{V}$ is referred as the *control variable*. The spaces $\mathcal{U}$, $\mathcal{V}$ and $\mathcal{W}$ are, in general, Banach spaces. The *Lagrangian functional* is defined on the basis of (1.5) as

$$\mathcal{L}(\mathbf{x}) = \mathcal{L}(u, z, v) := J(u, v) + \langle z, e(u, v)\rangle_{\mathcal{W}^*,\mathcal{W}}, \quad (1.6)$$

where $\mathcal{W}^*$ is the dual space of $\mathcal{W}$ and $\langle\cdot,\cdot\rangle_{\mathcal{W}^*,\mathcal{W}}$ indicates the corresponding duality pairing. The Lagrange multiplier $z \in \mathcal{W}^*$ is called *adjoint variable* (or dual variable). With $\mathbf{x} \in \mathcal{X}$, we indicate the variables $\mathbf{x} := (u, z, v)$, where $\mathcal{X} := \mathcal{U} \times \mathcal{W}^* \times \mathcal{V}$. It follows that the Lagrangian function is defined as $\mathcal{L} : \mathcal{X} \to \mathbb{R}$. We now recall the following definitions.

Definition 1.2.1. By indicating with $\mathbf{y} := (u, v) \in \mathbf{U} \times \mathcal{V}$ and $e(\mathbf{y}) := e(u, v)$, we define the *feasible space* as $\mathcal{Y} := \{\mathbf{y} \in \mathbf{U} \times \mathcal{V} \ :\ e(\mathbf{y}) = 0\}$.

Definition 1.2.2. A feasible point $\mathbf{y}^{**} := (u^{**}, v^{**}) \in \mathcal{Y}$ is a *local optimal solution* if there exists $\delta > 0$ such that $J(\mathbf{y}^{**}) \leqslant J(\mathbf{y})\ \forall \mathbf{y} \in \mathcal{B}_\delta(\mathbf{y}^{**})$, being $\mathcal{B}_\delta(\mathbf{y}^{**}) := \{\mathbf{y} \in \mathcal{Y} \ : \ \|\mathbf{y}^{**} - \mathbf{y}\|_{\mathcal{Y}} \leqslant \delta\}$ with $\|\cdot\|_{\mathcal{Y}}$ a suitable norm of the space $\mathcal{Y}$.

Definition 1.2.3. A local optimal solution $\mathbf{y}^{**} \in \mathcal{Y}$ is a *global optimal solution* if $J(\mathbf{y}^{**}) \leqslant J(\mathbf{y})\ \forall \mathbf{y} \in \mathcal{Y}$.

Definition 1.2.4. Let $J(\mathbf{y})$ and $e(\mathbf{y})$ be continuously Fréchet differentiable[1] in $\mathcal{B}_\delta(\mathbf{y}^*)$, being $\mathbf{y}^* := (u^*, v^*) \in \mathcal{Y}$ a critical solution, i.e. satisfying the first order necessary conditions (1.7)-(1.9), and $\mathcal{C}(\mathbf{y}^*) := \mathcal{Y} \times \{\rho(v - v^*) \ :\ v \in \mathcal{V},\ \rho \geqslant 0\}$ a convex cone. We say that $\mathbf{y}^* \in \mathcal{Y}$ is a *regular point* if $\mathcal{W} \equiv \{e_y(\mathbf{y}^*)[\delta\mathbf{y}] \ :\ \delta\mathbf{y} \in \mathcal{C}(\mathbf{y}^*)\}$.

For first order necessary conditions for the local optimal solution of problem (1.5), we refer to the following theorem (for the proof see [Maurer, 1981] or [Tröltzsch, 2010]):

Theorem 1.2.1. *If $\mathbf{y}^{**} = (u^{**}, v^{**}) \in \mathcal{Y}$ is a regular point and a local optimal solution of problem (1.5), there exists a Lagrange multiplier $z^{**} \in \mathcal{Z}$ such that*

$$\mathcal{L}_z(\mathbf{y}^{**}, z^{**}) = e(\mathbf{y}^{**}) = 0 \text{ in } \mathcal{W}, \tag{1.7}$$

$$\mathcal{L}_u(\mathbf{y}^{**}, z^{**}) = J_u(\mathbf{y}^{**}) + e_u^*(\mathbf{y}^{**})[z^{**}] = 0 \text{ in } \mathcal{U}^*, \tag{1.8}$$

$$\mathcal{L}_v(\mathbf{y}^{**}, z^{**})[\psi] = \langle J_v(\mathbf{y}^{**}) + e_v^*(\mathbf{y}^{**})[z^{**}], \psi\rangle_{\mathcal{V}^*,\mathcal{V}} = 0 \; \forall \psi \in \mathcal{V}, \tag{1.9}$$

where the differentiation of the Lagrangian functional is in the Fréchet sense. The operators $e_u^*(\mathbf{y}^{**})$ and $e_v^*(\mathbf{y}^{**})$ are the dual Fréchet derivatives of $e(\mathbf{y})$ in $\mathbf{y}^{**}$ with respect to $u \in \mathcal{U}$ and $v \in \mathcal{V}$, respectively; similarly $J_u(\mathbf{y}^{**})$ and $J_v(\mathbf{y}^{**})$ are the Fréchet derivatives of $J(\mathbf{y})$ in $\mathbf{y}^{**}$ with respect to $u \in \mathcal{U}$ and $v \in \mathcal{V}$, respectively.

The first order necessary conditions (1.7)-(1.9) are usually called *Karush-Kuhn-Tucker conditions* (KKT conditions), while solutions $\mathbf{x}^{**} \in \mathcal{X}$ satisfying the KKT conditions are indicated as *critical solutions*. We note that equation (1.7) is the state equation. The equation (1.8) is referred to as the *adjoint equation* (or *dual equation*) while equation (1.9) is the *optimality condition*.

Theorem 1.2.1 is usually and conveniently used to find a local optimal solution, but we underline that a critical solution of first order is not necessarily a local optimal solution: therefore, we recall a second order sufficient optimality condition, whose proof is reported in [Maurer, 1981, Maurer and Zowe, 1979].

Theorem 1.2.2. *Let us suppose that $J(\mathbf{y})$ and $e(\mathbf{y})$ are twice Fréchet differentiable and let $\mathbf{x}^{**} = (\mathbf{y}^{**}, z^{**}) \in \mathcal{X}$ satisfy the first order necessary conditions (1.7)-(1.9). If there exists $\theta > 0$ such that(1.7)-(1.9)*

$$\mathcal{L}_{\mathbf{yy}}(\mathbf{x}^{**})[\mathbf{y}, \mathbf{y}] \geqslant \theta \|\mathbf{y}\|_{\mathcal{Y}}^2 \tag{1.10}$$

holds $\forall \mathbf{y} \in \mathcal{Y}$ for which

$$e_{\mathbf{y}}(\mathbf{y}^{**})[\mathbf{y}] = 0 \;\; in \;\; \mathcal{W}, \tag{1.11}$$

then $\mathbf{y}^{**}$ is a strict local optimal solution. In equation (1.10), we indicate with $\mathcal{L}_{\mathbf{yy}}(\mathbf{x}^{**})$ the second Fréchet derivative of the Lagrangian functional with respect to $\mathbf{y}$, which corresponds to the Hessian of $\mathcal{L}(\mathbf{x}^{**})$ with respect to $\mathbf{y}$. Analogously in equation (1.11), $e_{\mathbf{y}}(\mathbf{y}^{**})$ corresponds to the Jacobian of the state equation with respect to $\mathbf{y}$.

This theorem allows to find local optimal solutions of the problem (1.5), but for non-trivial problem is not easy if not impossible to compute $\mathcal{L}_{\mathbf{yy}}(\mathbf{x}^{**})$. Furthermore it is not always easy to understand if a local optimal solution is also a global one. This depends, in general, on the particular optimal control problem under consideration.

Remark 1.2.2. Throughout this work we indicate with the apex $**$ an optimal solution.

[1] Let be X and Y two spaces endowed with norm and $F(x) : x \in E \to Y$ an application defined on the open space $E \subset X$; we say that $F(x)$ is Fréchet differentiable in $\overline{x} \in E$ if there exists a linear and continuous operator $F_x(\overline{x}) \in \mathcal{L}(X, Y)$ s.t.:

$$\forall \varepsilon > 0, \; \exists \delta > 0 \; : \; \|F(\overline{x} + h) - F(\overline{x}) - F_x(\overline{x})[h]\|_Y \leqslant \varepsilon \|h\|_X \quad \forall h \in X \text{ s.t. } \|h\|_X < \delta.$$

The expression $F_x(\overline{x})[h]$, to which corresponds an element in Y for each $h \in X$, is said *Fréchet differential*, while the operator $F_x(\overline{x})$ is identified as *Fréchet derivative* of the application $F(x)$ in $\overline{x} \in E$. For a further deepening, we refer the reader to [Kolmogorov and Fomin, 1999]

1.3 Optimal control techniques for hyperbolic partial differential equations

In this section, we describe the computation of first necessary order conditions that have been illustrated in the previous section to a first-order hyperbolic PDE and we analyze the peculiar difficulties that arise in this kind of problems.

1.3.1 First order necessary conditions for hyperbolic partial differential equations

Using the same notation as in subsection 1.2.1, we start by introducing the time interval $[0,T]$ and the spatial domain Ω such that $\Omega \subset \mathbb{R}^n,\ n \geqslant 1$, with boundary $\partial\Omega$. In this case the spaces $\mathcal{V}$ and $\mathcal{U}$ are, in general, Banach spaces over the space–time domain $\Omega \times (0,T)$. We introduce the cost functionals of the form

$$J(u,v) = J_m(u) + \frac{1}{2}\gamma \int_0^T m_v(v - v_d, v - v_d)dt = \int_0^T j(u,v)dt, \tag{1.12}$$

where the term $J_m(u)$ has the forms

$$J_m(u) = \frac{1}{2}\int_0^T m_u(u - u_d, u - u_d)dt, \tag{1.13}$$

$$J_m(u) = \frac{1}{2}\sum_{i \in I_u} m_u(u^i - u_d^i, u^i - u_d^i) \tag{1.14}$$

or

$$J_m(u) = \frac{1}{2} m_u(u(T) - u_d, u(T) - u_d), \tag{1.15}$$

and $\gamma \geqslant 0$, $m_u(\cdot,\cdot)$ and $m_v(\cdot,\cdot)$ are positive and symmetric bilinear forms, u_d is the desired solution, while v_d the desired control, I_u is the set of couples (x_i, t_i) with $x_i \in \Omega$ and $t_i \in (0,T)$ on which the desired solution is given; the cost functional $J(u,v)$ is twice differentiable in $v \in \mathcal{V}$ and $u \in \mathcal{U}$. For the sake of simplicity, we neglect to indicate the space dependence of the variables explicitly. Starting from (1.5), we introduce the following state equation:

$$\begin{aligned} &\text{find } u \in \mathcal{U} \ :\ m\left(\frac{\partial u}{\partial t}, \varphi\right) + a(u,v)(\varphi) = F(\varphi), \quad \forall \varphi \in \mathcal{U}, \text{ with } v \in \mathcal{V},\ t \in (0,T) \\ &\text{with } u(0) = u_0, \end{aligned}$$

where $m(\cdot,\cdot)$ is a time–independent positive and symmetric bilinear form, $a(\cdot,\cdot)(\cdot)$ is a twice differentiable semilinear form (with linearity in the last argument), $F(\cdot)$ is a continuous and linear functional and u_0 is the initial condition. The space $\mathcal{U}$ is an appropriate functional space taking into account any Dirichlet homogeneous boundary conditions.

From (1.6), we define the Lagrangian functional for this particular case, which reads:

$$\begin{aligned} \mathcal{L}(\mathbf{x}) = \mathcal{L}(u,z,v) := \quad & J(u,v) + \textstyle\int_0^T F(z)dt - \int_0^T a(u,v)(z)dt \\ & - \textstyle\int_0^T m\left(\frac{\partial u}{\partial t}, z\right)dt - m(u(0) - u_0, z(0)) \end{aligned}$$

In order to obtain the first order necessary conditions (1.7)-(1.9) for the local optimal solution, we differentiate $\mathcal{L}(\mathbf{x})$ with respect to u, v and z. In particular, by differentiating $\mathcal{L}(\mathbf{x})$ with respect to u and integrating by parts, we obtain:

$$\begin{aligned}\mathcal{L}_u(\mathbf{x})[\vartheta] = \quad & J_u(u,v)[\vartheta] - \int_0^T a_u(u,v)(z,\vartheta)dt + \int_0^T m\left(\vartheta, \frac{\partial z}{\partial t}\right) dt \\ & -m(\vartheta(T), z(T)).\end{aligned} \tag{1.16}$$

where $a_u(u,v)(z,\vartheta)$ represents the differential of the form $a(v,u)(z)$ with respect to u evaluated in $\vartheta \in \mathcal{U}$. By using (1.16), we obtain the adjoint equation in weak form

$$\begin{aligned}&\text{find } z \in \mathbf{U} \ : \ -m\left(\vartheta, \frac{\partial z}{\partial t}\right) + a_u(u,v)(z,\vartheta) = J_u(u,v)[\vartheta] \quad \forall \vartheta \in \mathcal{U}, \ t \in (0,T). \\ &\text{with } z(T) = 0\end{aligned} \tag{1.17}$$

In the same way, by differentiating $\mathcal{L}(\mathbf{x})$ with respect to v, we obtain:

$$\mathcal{L}_v(\mathbf{x})[\vartheta] = J_v(u,v)[\psi] - \int_0^T a_v(u,v)(z,\psi)dt,$$

from which we deduce the optimality condition (1.9):

$$j_v(u^{**},v^{**})[\psi] - a_v(u^{**},v^{**})(z^{**},\psi) = 0 \quad \forall \psi \in \mathcal{V}, \ t \in (0,T)$$

where $a_v(u,v)(z,\vartheta)$ represents the differential of the form $a(v,u)(z)$ with respect to v evaluated in $\psi \in \mathcal{U}$ and $\mathbf{x}^{**} = (u^{**}, v^{**}, z^{**})$ indicates the critical solution.

Remark 1.3.1. The hyperbolic adjoint PDE (1.17) evolves "backward" in time with the "initial" conditions given at the final time $t = T$. From a numerical point of view, this could lead to large computational costs. In fact, we need to solve the state equation until the final time $t = T$ before solving the adjoint equation at each time step $t \in (0,T)$; this is due to the dependence of the adjoint problem on $u(t)$, $t \in (0,T)$.

From the beginning of this century, this classical framework has been seriously modified to take into account the presence of shocks and discontinuities in the solution u. Fortunately, shocks do not appear in typical hemodynamical applications: so we will not elaborate further this issue. For more details on optimal control for hyperbolic equations in presence of shocks, see [Ulbrich, 2001] and reference therein.

1.3.2 Well-poseness of optimal control problems for hyperbolic equations

In general, if $\gamma = 0$ in (1.13)-(1.15), the optimal control problem can be ill-posed in the sense that it can admit multiple local minima. The classical remedy for this difficulty is to set γ positive, but if no a priori information on the characterization of the optimal control variable are available, the choice of the bilinear form $m_v(\cdot,\cdot)$ is not easy. Another possible strategy to avoid local minima is the so called *multigrid method* [Bunks et al., 1995, Epanomeritakis et al., 2008, Banghert, 2008], which consists in decomposing the problem by scale and solving iteratively the problem in a hierarchical sequence of meshes from coarse to more refined ones, using the solution at the preceding level

as start point. At long scales there are fewer local minima and those that remain are further apart from each other. Thus, at long scales iterative methods can get closer to the neighborhood of the global minimum. To illustrate this behavior of hyperbolic problems, we consider the one dimensional wave equation

$$\begin{cases} \dfrac{\partial^2 u}{\partial t^2} - \tilde{c}^2 \dfrac{\partial^2 u}{\partial x^2} = 0 & x \in [0,1], \quad t \in [0,4], \\ u(0,t) = u(1,t), & t \in [0,4], \\ u(x,0) = \sum_{k=1}^{4} \cos(2k\pi x), & x \in [0,1]. \end{cases} \tag{1.18}$$

where the parameter $\tilde{c} > 0$. We solve (1.18) with different values of $\tilde{c}$ with a Lax-Wendroff finite difference scheme and with different discretization grid and we compute the functional

$$J(u,\tilde{c}) = \int_0^4 (u(L,t,\tilde{c}) - u_{ex}(L,t))^2 dt, \tag{1.19}$$

where $u_{ex}(x,t)$ is computed fixing $\tilde{c} = 1$. In Figure 1.1, we plot the functional (1.19) for different numbers of discretization intervals and the value of the parameter $\tilde{c}$.

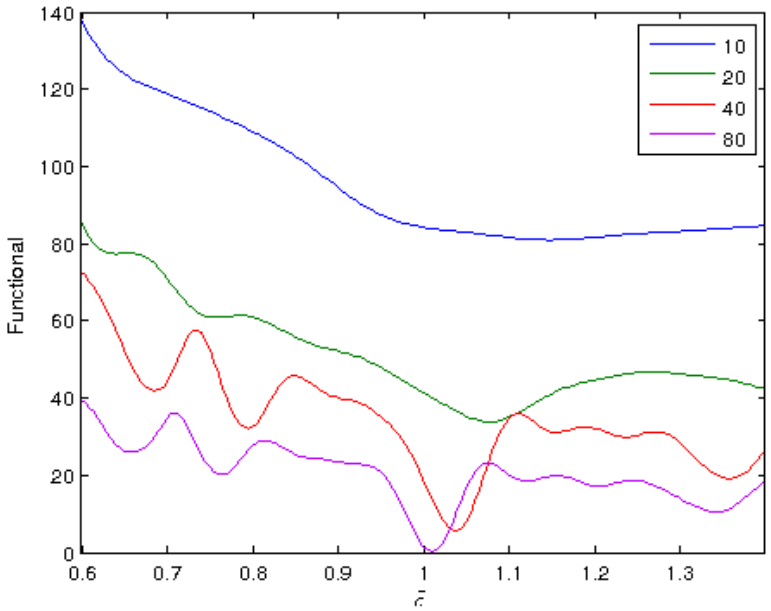

Figure 1.1: *Cost functional (1.19) for different numbers of discretization intervals ($N = 10,\ 20,\ 40,\ 80$) and the value of the parameter $\tilde{c}$*

We note that with few intervals the functional has only one minimum, but the functional is far from zero and the minimum is not close enough to the real global minimum ($\tilde{c} = 1$). Increasing the number of intervals, the number of local minima increase, the computed global minimum is closer to the real global minimum and the functional is closer to zero.

1.3.3 Controllability and observability of discretized hyperbolic equations

In this subsection, we describe the problems that arise when controlling a hyperbolic equation that has been discretized in space and time. In this review, we follow what is done in [Zuazua, 2005, Zuazua, 2007, Cannarsa and Coron, 2010]. For simplicity, we focus on the boundary controllability of the constant coefficient one dimensional equation

$$\begin{cases} u_{tt} - u_{xx} = 0 & 0 < x < 1,\ 0 < t < T \\ u(0,t) = u(1,t) = 0 & 0 < t < T \\ u(x,0) = u_0(x),\ u_t(x,0) = u_1(x) & 0 < x < 1 \end{cases} \tag{1.20}$$

but the same considerations remain valid for more complicate hyperbolic equations.

We say that this equation is *boundary controllable* if, for any $(z_0, z_1) \in L^2(0,1) \times H^{-1}(0,1)$, there exists $v \in L^2(0,T)$ such that the solution of the controlled wave equation

$$\begin{cases} z_{tt} - z_{xx} = 0 & 0 < x < 1,\ 0 < t < T \\ z(0,t) = 0;\ z(1,t) = v(t) & 0 < t < T \\ z(x,0) = z_0(x),\ z_t(x,0) = z_1(x) & 0 < t < T \end{cases} \tag{1.21}$$

satisfies

$$z(x,T) = z_t(x,T) = 0 \quad 0 < x < 1. \tag{1.22}$$

This problem corresponds to finding the control $v(t) = u_x(1,t) \in L^2(0,T)$, minimizing the functional

$$J(u_0,u_1) = \frac{1}{2}\int_0^T |u_x(1,t)|^2 dt + \int_0^1 z_0 u_1 dx - \int_0^1 z_1 u_0 dx \tag{1.23}$$

where u solves (1.20).

Remark 1.3.2. We note that (1.21) and (1.22) are the adjoint equation and the optimality condition, respectively.

We define the energy of the solution of (1.20) at time $t \in (0,T)$

$$E(t) = \frac{1}{2}\int_0^1 \left[|u_x(x,t)|^2 + |u_t(x,t)|^2\right] dx,$$

which is conserved i.e.

$$E(t) = E(0) \quad \forall t \in (0,T).$$

The problem of *boundary observability* of (1.20) consists in giving sufficient conditions on T such that there exists $C(T) > 0$ for which the boundary observability inequality

$$E(0) \leqslant C(T)\int_0^T |u_x(1,t)|^2 dt \tag{1.24}$$

holds for all solutions of (1.20). The constant $C(T)$ is called *observability constant*.

It can be proved that controllability and observability are equivalent problems and that the following observability result holds (see [Zuazua, 2005, Cannarsa and Coron, 2010])

Proposition 1.3.1. *For any $T \geqslant 2$, equation (1.20) is observable. In other words, for any $T \geqslant 2$ there exists $C(T) > 0$ such that (1.24) holds for any solution of (1.20). Conversely, if $T < 2$, (1.20) is not observable, or, equivalently*

$$\sup_{u \text{ solves } (1.20)} \left[\frac{E(0)}{\int_0^T |u_x(1,t)|^2 dt} \right] = \infty$$

Therefore (1.20) is boundary controllable iff $T \geqslant 2$. We note that the minimum observability time ($T = 2$) is twice the length of the domain: in fact, it is the time necessary for the information to propagate from an end point of the domain, reach the other end point and return back to the starting point.

We now analyze the continuous dependence of the constant $C(T)$ with respect to finite space discretization as the discretization parameter h tends to zero.

We consider a discretization of the interval $[0,1]$ into $N+1$ subintervals of length $h = 1/(N+1)$ with nodes $\{x_j = jh,\ j = 0, \dots, N+1\}$. We then consider the finite difference approximation of the wave equation (1.20):

$$\begin{cases} u_j'' - \dfrac{1}{h^2}\left[u_{j+1} + u_{j-1} - 2u_j\right] = 0 & 0 < t < T,\ j = 1, \dots, N, \\ u_j(t) = 0 & j = 0, N+1,\ 0 < t < T \\ u_j(0) = u_j^0,\ u_j'(0) = u_j^1, & j = 1, \dots, N, \end{cases} \tag{1.25}$$

where $u_j(t) = u(x_j, t),\ \forall j = 1, \dots, N$. The energy of the solution of (1.25)

$$E_h(t) = \frac{h}{2} \sum_{j=0}^{N} \left[\left| u_j' \right|^2 + \left| \frac{u_{j+1} - u_j}{h} \right|^2 \right] \tag{1.26}$$

is constant in time and it is also a natural discretization of the continuous energy (1.3.3). The problem of observability of the system (1.25) consists in find $T > 0$ and $C_h(T) > 0$ such that

$$E_h(0) \leqslant C_h(T) \int_0^T \left| \frac{u_N(t)}{h} \right|^2 dt \tag{1.27}$$

holds for all solutions of (1.25). We note that $u_x(1,t) \approx [u_{N+1}(t) - u_N(t)]/h$ and, taking into account that $u_{N+1} = 0$, $u_x(1,t) \approx -u_N(t)/h$. Therefore $|u_N(t)/h|^2$ is an approximation of $|u_x(1,t)|^2$ and the functional (1.23) can be discretized as

$$J_h((\mathbf{u}^0, \mathbf{u}^1)) = \frac{1}{2} \int_0^T \left| \frac{u_N(t)}{h} \right|^2 dt + h \sum_{j=1}^{N} z_j^0 u_j^1 - h \sum_{j=1}^{N} z_j^1 u_j^0, \tag{1.28}$$

where $(\mathbf{u}^0, \mathbf{u}^1)$ are the initial conditions of (1.25) and $(\mathbf{z}^0, \mathbf{z}^1)$ are the initial condition of the discretized version of the equation (1.21).

It can be proved (see [Zuazua, 2005, Cannarsa and Coron, 2010]) that the observability constant $C_h(T)$ in (1.27) tends to infinity as h tends to zero. This is due to the fact

that, while in the continuous problem all the frequencies that compose the spectrum of the solution travel at the same velocity, at discrete level, higher frequencies travel slower and velocity gap between two consecutive frequencies is proportional to $1/h$. In other words, the minimum observability time of the discretized problem tends to infinity, as h tends to zero, because the velocity of higher frequencies tends to zero. In figure 1.2, the velocity gap between frequencies is illustrated as the gap between the eigenvalues of the continuous wave problem (1.20) and the correspondent discretized problem. We note that this gap increase as the frequencies get higher. This considerations hold both for finite differences and standard finite elements discretizations.

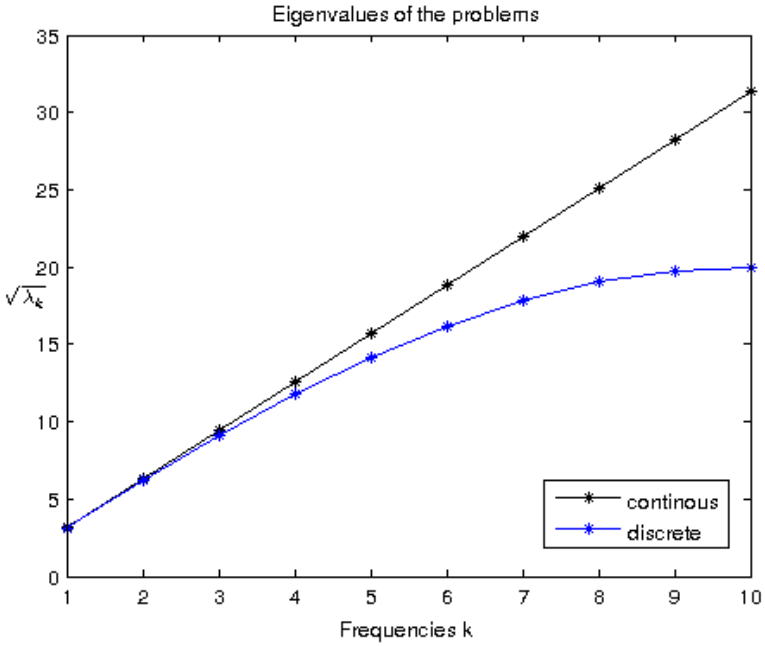

Figure 1.2: *Square roots of the eigenvalues associated to the wave problem in the continuous and discrete cases*

Several remedies have been proposed to keep $C_h(T)$ uniformly limited with h. We list some of them:

Fourier filtering mechanism [Zuazua, 2005] consists in eliminating the high frequency Fourier components and restricting the semidiscrete wave equation under consideration to the subspace of solutions generated by the Fourier components corresponding to the eigenvalues $\lambda \leqslant \gamma h^{-2}$ with $0 < \gamma < 4$.

Two-grid algorithm [Glowinski and Li, 1990, Glowinski, 1992] consists in using two grids: the computational one in which the discrete wave equations are solved, with step size h and a coarser one of size $2h$. In the fine grid, the eigenvalues satisfy the sharp upper bound $\lambda \leqslant 4/h^2$. And the coarse grid will "select" half of the eigenvalues, the ones corresponding to $\lambda \leqslant 2/h^2$. This indicates that in the fine grid the solutions obtained in the coarse one would behave very much as a filtered solutions.

Tychonov regularization [Glowinski et al., 1990] consists in adding an extra term in

the functional (1.23) and corresponds to relaxing the boundary observability inequality by adding an extra observation, distributed everywhere in the domain and at the right scale so that it asymptotically vanishes as h tends to zero but it is strong enough to capture the energy of the pathological high frequency components. In particular, by considering the functional

$$J_h^*((\mathbf{u}^0,\mathbf{u}^1)) = \frac{1}{2}\int_0^T \left|\frac{u_N(t)}{h}\right|^2 dt + h^3 \sum_{j=0}^{N} \int_0^T \left|\frac{u'_{j+1}u'_j}{h}\right|^2 dt + h\sum_{j=1}^{N} z_j^0 u_j^1 - h\sum_{j=1}^{N} z_j^1 u_j^0$$

in place of (1.28), we obtain that the observability inequality (1.27) becomes

$$E_h(0) \leqslant C_h(T)\left[\int_0^T \left|\frac{u_N(t)}{h}\right|^2 dt + h^3 \sum_{j=0}^{N} \int_0^T \left|\frac{u'_{j+1}u'_j}{h}\right|^2 dt\right], \tag{1.29}$$

that holds for all $T > 2$ for a suitable $C_h(T) > 0$ which is independent of h and of the solution of the semidiscrete equation (1.25), as observed in [Zuazua, 2005] and reference therein.

The considerations in this subsection hold also for more general hyperbolic problems and in particular for inverse problems and parameter estimation (see [Zuazua, 2005]). However, if initial data with a finite number of Fourier components are considered, also the solution has a finite number of frequencies and therefore a (possibly large) observability constant exists (see [Micu, 2002]).

1.4 Optimization methods

The resolution of optimal control problems requires the resolution of finite dimensional optimization problems. In this section we recall some of the most common optimization methods (the Steepest Descent, Barzilai-Borwein, Newton and Quasi Newton methods) and their application to optimal control problem described by PDEs. For a deeper analysis on optimization techniques, we refer mainly to [Dennis and Schnabel, 1987, Luenberger, 2003, Nocedal, 1992, Nocedal and Wright, 1999, Sun and Yuan, 2006].

1.4.1 A review of optimization methods

Let us consider the following finite-dimensional optimization problem

$$\text{find } \mathbf{x} \in \mathbb{R}^n,\ n \geqslant 1,\ \text{s.t. } \mathbf{x} = \underset{\mathbf{y}\in\mathbb{R}^n}{\operatorname{argmin}}\ f(\mathbf{y})$$

Let us suppose that $f(\mathbf{x}) : \mathbb{R}^n \to \mathbb{R}$ is twice differentiable in $\mathbf{x}$ and let us indicate with $\mathbf{g}(\mathbf{x}) \in \mathbb{R}^n$ and $H(\mathbf{x}) \in \mathbb{R}^{n\times n}$ the gradient and the Hessian of $f(\mathbf{x})$ with respect to $\mathbf{x}$ and with $\mathbf{x}^{**}$ and $f(\mathbf{x}^{**})$ the global minimizer and the value of the cost functional in it.

The classic schemes are iterative schemes which build a sequence $\mathbf{x}_k$; $k = 0, \dots$ with $\mathbf{x}_k \to \mathbf{x}^*$, being $\mathbf{x}^*$ a (local) minimizer. They all require to choose an initial guess $\mathbf{x}_0$ and fall into one of these two categories.

Line search We (approximately) minimize the function of a single variable α as

$$\psi(\alpha) = f(\mathbf{x}_k + \alpha \mathbf{d}_k);$$

being $\mathbf{d}_k$ the k-th *search direction* and

$$\mathbf{x}_{k+1} = \mathbf{x}_k + \alpha_k \mathbf{d}_k, \text{ where } \alpha_k = \underset{\alpha \in (0,+\infty)}{\operatorname{argmin}} \psi(\alpha).$$

Trust region The function f is approximated by a simpler function $\widetilde{f}_k$ in $B_{\delta_k}(\mathbf{x}_k)$, the closed ball of radius δ_k around $\mathbf{x}_k$, called the *trust region* and

$$\mathbf{x}_{k+1} = \underset{\mathbf{x} \in B_{\delta_k}(\mathbf{x}_k)}{\operatorname{argmin}} \widetilde{f}_k(\mathbf{x}).$$

Both methods operate through a simplification of the original problem. However, the underlying approach is rather different.

In a line search method the problem is simplified by reducing its dimensions to just one and we use the full information of the actual function f. In a trust region method, instead, the function f is replaced by an approximation $\widetilde{f}_k$ where the search of the minimizer is easier. Yet, the dimension of the problem we are facing has not changed. In this review, we limit ourselves to line search techniques.

Line search methods

As we said in the previous subsection, in line search methods, the sequence $\{\mathbf{x}_k\}_k$ is obtained by minimizing the one dimensional function $\psi(\alpha) = f(\mathbf{x}_k + \alpha \mathbf{d}_k)$ given a search direction $\mathbf{d}_k$. We describe with more details how line search methods work.

Definition 1.4.1. Given a point $\mathbf{x}_k \in \mathbb{R}^n$, a direction $\mathbf{d}_k \in \mathbb{R}^n$ is a descent direction if $\exists \delta > 0$ such that

$$f(\mathbf{x}_k + \alpha \mathbf{d}_k) < f(\mathbf{x}_k) \quad \forall \alpha \in (0; \delta) :$$

If f is continuously differentiable, we have that $\mathbf{d}_k$ is a descent direction in the point $\mathbf{x}_k$ if and only if $(\mathbf{g}(\mathbf{x}_k); \mathbf{d}_k) < 0$. In particular

$$\mathbf{d}_k = -B_k \mathbf{g}(\mathbf{x}_k) \tag{1.30}$$

is a descent direction for all symmetric positive definite matrices B_k.

We can sum up a generic line search method in the following algorithm

Algorithm 1.4.1 (Line search)**.** Given an initial guess $\mathbf{x}_0$, two positive constant $toll_{\mathbf{x}}$ and $toll_{\mathbf{g}}$ and a positive integer k_{max}.

For $k = 0, \ldots, k_{max}$ do

(i) Compute a suitable *search direction* $\mathbf{d}_k$;

(ii) Compute a suitable *step length* α_k;

(iii) Update: $\mathbf{x}_{k+1} = \mathbf{x}_k + \alpha_k \mathbf{d}_k$;

(iv) Convergence test: $\|\mathbf{x}_{k+1} - \mathbf{x}_k\| < toll_{\mathbf{x}}$ and $\|\mathbf{g}_{k+1}\| < toll_{\mathbf{g}}$. If true, stop; otherwise go back to (i) and increase k.

Remark 1.4.1. . The convergence criterion based on the difference between successive iterates is normally implemented only as a safeguard against stagnation of the algorithm. Terminating with $\|\mathbf{g}_{k+1}\| \geqslant toll_{\mathbf{g}}$ is considered as a *failure condition*.

Remark 1.4.2. For the sake of notation, in the following we will often use the suffix k to indicate quantities computed at $\mathbf{x} = \mathbf{x}_k$.

The choice of $\mathbf{d}_k$ (or equivalently B_k) determines the features of the line search method and we will discuss it in the following.

Concerning the choice of α_k, in principle, we should select

$$\alpha_k = \underset{\alpha \in (0,+\infty)}{\operatorname{argmin}} \ \psi(\alpha)$$

but, in practical, this way can not be followed. Therefore α_k is chosen with some heuristic rules so that $f_{k+1} < f_k$.

Armijo rule (or sufficient decrease condition) : for a given $c_1 \in (0, 1)$, we choose

$$f(\mathbf{x}_k + \alpha_k \mathbf{d}_k) \leqslant f_k + c_1 \alpha_k g_k^T d_k. \tag{1.31}$$

Nonmonotone step selection [Grippo et al., 1989, Grippo and Sciandrone, 2002]: for a given $c_1 \in (0, 1)$ and a positive integer M:

$$f(\mathbf{x}_k + \alpha_k \mathbf{d}_k) \leqslant \max_{0<j<\min(k,M)} f_{k-j} + c_1 \alpha_k g_k^T d_k. \tag{1.32}$$

Wolfe conditions : for given $c_1 \in (0, 1)$ and $c_2 \in (c_1, 1)$, we choose

$$\begin{aligned} &f(\mathbf{x}_k + \alpha_k \mathbf{d}_k) \leqslant f_k + c_1 \alpha_k g_k^T d_k, && \text{(Armijo rule)} \\ &|g_{k+1}^T d_k| \leqslant c_2 |g_k^T d_k|. && \text{(Curvature condition)} \end{aligned} \tag{1.33}$$

Due to its low computational request, the Armijo rule (1.31) is probably the most used, but it can be proved that it is not always enough to ensure the global convergence of line search method sequence, and, for this reason, a backtracking strategy is usually associated to it. The nonmonotone step selection rule (1.32) is similar to Armijo rule (1.31), but allows a local increase of the function f. The Wolfe conditions ensure that the sequence globally converges, but it is clearly more complex than the other two strategies.

Choice of $\mathbf{d}_k$

As said, the choice of the search direction $\mathbf{d}_k$ determines the features of the line search method and characterizes the different methods. In literature a huge number a line search methods have been proposed, but in this subsection we focus only on those that we have used in our application (see Chapter 4).

Steepest descent method The steepest descent method (SD or gradient method) is the simplest and most classical methods for unconstrained optimization (it was firstly proposed by Cauchy in [Cauchy, 1847]). It consists in choosing minus gradient as the search direction i.e.

$$\mathbf{d}_k = -\mathbf{g}_k \quad B_k = I_n$$

where I_n is the $n \times n$ identity matrix. This method is very robust and requires a very low amount of memory (at every iteration no previous step information is needed), but it has only linear convergence rate and, therefore, a large number of iterations is needed to converge.

Barzilai-Borwein method The Barzilai-Borwein method (BB or spectral gradient method) was firstly proposed by Barzilai and Borwein in their pioneeristic work [Barzilai and Borwein, 1988] and, then, analyzed in detail in [Raydan, 1993, Raydan, 1997, Raydan and Svaiter, 2002, Fletcher, 2005, Dai and Fletcher, 2005]. The search direction is proportional to minus gradient and, in particular,

$$\mathbf{d}_k = -\gamma_k \mathbf{g}_k \quad B_k = \gamma_k I_n.$$

Two choices of γ_k are possible

$$\gamma_k^1 = \frac{\mathbf{s}_{k-1}^T \mathbf{s}_{k-1}}{\mathbf{s}_{k-1}^T \mathbf{y}_{k-1}} \quad \gamma_k^2 = \frac{\mathbf{y}_{k-1}^T \mathbf{s}_{k-1}}{\mathbf{y}_{k-1}^T \mathbf{y}_{k-1}}$$

where $\mathbf{s}_{k-1} = \mathbf{x}_k - \mathbf{x}_{k-1}$ and $\mathbf{y}_{k-1} = \mathbf{g}_k - \mathbf{g}_{k-1}$. The first choice is the most studied and used. We underline that at every iteration BB method makes use of information referring also to the previous step. BB method is part of the family of *fast gradient* methods ([van den Doel and Ascher, 2012]), whose descent direction is proportional to minus gradient but have better convergence properties than standard SD method.

BB method is usually coupled with nonmonotone line search technique (1.32) ([Grippo and Sciandrone, 2002]) because it has been proved in [Raydan, 1997] that with this choice BB methods has results comparable to conjugate gradient methods, especially for non-quadratic and large scale problems. There is numerical evidence that BB method has superlinear convergence rate. These properties and its simplicity make this method very appealing for complex applications.

Newton and quasi-Newton methods Newton and quasi-Newton methods are probably the most used unconstrained optimization methods. Therefore they are largely discussed in most of the classical numerical optimization monographies like [Dennis and Schnabel, 1987, Kelley, 1995, Luenberger, 2003, Nocedal, 1992, Nocedal and Wright, 1999].

Newton method makes use of second order information, i.e. the Hessian matrix H_k, to choose the search direction

$$\mathbf{d}_k = -H_k^{-1} \mathbf{g}_k \quad B_k = H_k^{-1}.$$

It is widely known that in a suitable neighbourhood of the solution $\mathbf{x}^{**}$ Newton method converges quadratically. The drawback of this method is that at each iteration, the computation of the Hessian matrix and the solution of a linear system is needed. This could lead to high computational cost, especially for large optimization, and second order information are not always available or easy to compute.

To overcome these difficulties, in quasi-Newton methods, the matrix B_k is chosen to be an approximation of H_k^{-1}. There are a large number of quasi-Newton methods that differ each other in the type of approximation used. One of the most effective and

used quasi-Newton methods is the *BFGS method* (named after its creators Broyden, Fletcher, Goldfarb and Shanno), in which, starting from an initial approximation, at each iteration a rank-one update is performed to obtain B_{k+1} from B_k

$$B_{k+1} = B_k - \frac{B_k \mathbf{s}_k \mathbf{s}_k^T B_k}{\mathbf{s}_k^T B_k \mathbf{s}_k} + \frac{\mathbf{y}_k \mathbf{y}_k^T}{\mathbf{y}_k^T \mathbf{s}_k} \tag{1.34}$$

It can be proved (see [Nocedal, 1992]) that BFGS method converges superlinearly and it has a large computational saving respect to Newton method.

1.4.2 Optimization methods for optimal control problem described by PDEs

In this Section we briefly discuss how to solve optimal control problems described by PDEs by means of the optimization methods reported in Section 1.4,

By referring to Section 1.2, the solution of the optimal control problems (1.6) is obtained by solving the first order conditions (1.7)-(1.9). The resulting system is in general fully coupled in the sense that each equation (or system of equations) depends on (u, z, v), with the exception of the state equation which does not depend on the adjoint variable z.

In Section 1.4 we have introduced several iterative methods, which can be conveniently used also for the solution of optimal control problems described by PDEs. With this aim, we need to use a numerical method for the approximation of the state, adjoint and optimality equations which define the first order necessary conditions.

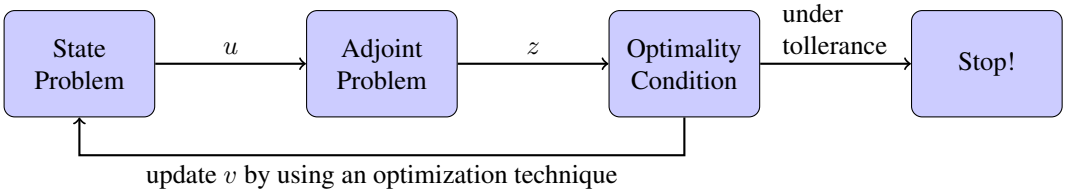

Figure 1.3: *Schematic representation of Algorithm 1.4.2*

It is possible to solve the approximated optimal control problem by means of an optimization iterative method, such as SD, BB, Newton or BFGS methods.

Algorithm 1.4.2 (Optimal control problem resolution)**.** For a given approximated optimal control problem, the iterative algorithm reads:

(i) choose an initial guess v ;

(ii) solve the state equation (1.7) given v in order to obtain u and compute the cost functional $J(u, v)$;

(iii) solve the adjoint equation (1.8) given v and u in order to obtain z;

(iv) compute the optimality condition given u, v and z;

(v) if the optimality condition is below a certain tolerance, stop the algorithm; otherwise update v according with one of the optimization methods introduced in Section 1.4 and return to Step (ii).

CHAPTER 2

One dimensional fluid structure interaction models for cardiovascular system

In this chapter we introduce and describe the one dimensional fluid structure interaction model (or 1D-FSI model) that is conveniently used to describe blood vessels and that we adopt as the state model in our work.

The chapter is organized as follows. In section 2.1 we describe the 1D-FSI model, from its derivation to the analysis of the numerical approximation employed and the boundary and compatibility conditions necessary to close the system. In section 2.2 we describe how the model presented in section 2.1 can be extended to consider networks of vessels.

2.1 One dimensional FSI models

One dimensional models provide simplified representation of the blood flow in deformable vessels. Although inadequate to give a detailed description of the full real phenomena of flow field (e.g. recirculation or wall shear stress cannot be computed in simplified models), they describe well wave propagation phenomena due to the compliance of the wall.

2.1.1 Deriving the equations

There are several ways to derive a 1D model of an incompressible fluid flowing in a compliant pipe. Here we follow the approach presented in Chapter 10 of [Formaggia et al., 2009], that consists in deriving the equations from conservation principles.

We model an artery as a simple compliant tube (as illustrated in figure 2.1) that is

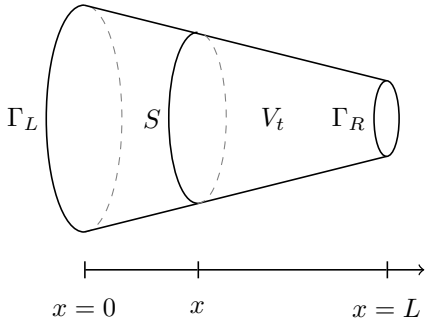

Figure 2.1: *Scheme of a simple compliant tube and notations*

assumed to be axial symmetric with the axis of vessel rectilinear and aligned to the x axis. For the derivation of 1D equations, we start from Reynolds' transport theorem for an arbitrary control volume V_t with boundary ∂V_t and outer normal $\mathbf{n}$. It asserts that

$$\frac{d}{dt}\int_{V_t} f dV = \int_{V_t} \frac{\partial f}{\partial t} dV + \int_{\partial V_t} f \mathbf{u}_b \cdot \mathbf{n} d\sigma, \tag{2.1}$$

where $f = f(t, \mathbf{x})$ is a generic continuous function and $\mathbf{u}_b$ is the velocity of the boundary ∂V_t, composed by the arterial wall $\partial V_{t,w}$ and the two end sections S_1 and S_2 that are assumed normal to the axis. On S_1 and S_2 the normal component of $\mathbf{u}_b$ is 0, while on $\partial V_{t,w}$ the velocity $\mathbf{u}_b$ coincides with the velocity $\mathbf{u}_w$ of the arterial wall, so that

$$\int_{\partial V_t} f \mathbf{u}_b \cdot \mathbf{n} d\sigma = \int_{\partial V_{t,w}} f \mathbf{u}_w \cdot \mathbf{n} d\sigma. \tag{2.2}$$

To obtain the one-dimensional equations, we have to consider values averaged on the section of the pipe: the area-averaged value $\bar{f}$ of f is given by

$$\bar{f} = \frac{1}{A}\int_S f d\sigma \tag{2.3}$$

where $A = A(x,t) = \int_S d\sigma$ is the area of the cross section S. Then, we can write

$$\int_{V_t} f dV = \int_{x_1}^{x_2} \left[\int_S f d\sigma\right] dx = \int_{x_1}^{x_2} A\bar{f} dx, \tag{2.4}$$

where x_1 and x_2 are the coordinates of cross sections S_1 and S_2. As x_1 and x_2 are independent of time, we have that the left hand side of (2.1) is

$$\frac{d}{dt}\int_{V_t} f dV = \int_{x_1}^{x_2} \frac{\partial}{\partial t}(A\bar{f}) dx. \tag{2.5}$$

We note that $\mathbf{u}_w$ is different from the fluid velocity $\mathbf{u}$ because the lumen is permeable. The relative velocity between arterial wall and fluid is given by

$$\mathbf{w} = \mathbf{u}_w - \mathbf{u}.$$

With this equality the second term of the right hand side of equation (2.1) can be written as

$$\int_{\partial V_{t,w}} f \mathbf{u}_w \cdot \mathbf{n} d\sigma = \int_{\partial V_{t,w}} f \mathbf{w} \cdot \mathbf{n} d\sigma + \int_{\partial V_{t,w}} f \mathbf{u} \cdot \mathbf{n} d\sigma.$$

We also observe that

$$\int_{\partial V_{t,w}} f\mathbf{u}\cdot\mathbf{n}d\sigma = \int_{\partial V_t} f\mathbf{u}\cdot\mathbf{n}d\sigma - \int_{S_1} f\mathbf{u}\cdot\mathbf{n}d\sigma - \int_{S_2} f\mathbf{u}\cdot\mathbf{n}d\sigma = \\ = \int_{\partial V_t} f\mathbf{u}\cdot\mathbf{n}d\sigma + \int_{S_1} fu_1 d\sigma - \int_{S_2} fu_1 d\sigma,$$

where u_1 is the x-component of the velocity $\mathbf{u}$. Invoking Gauss' theorem, we have

$$\int_{\partial V_{t,w}} f\mathbf{u}\cdot\mathbf{n}d\sigma = \int_{V_t} \nabla\cdot(f\mathbf{u})dV + \int_{S_1} fu_1 d\sigma - \int_{S_2} fu_1 d\sigma,$$

and, averaging on the section, at the end we obtain

$$\int_{\partial V_{t,w}} f\mathbf{u}_w\cdot\mathbf{n}d\sigma = \int_{\partial V_{t,w}} f\mathbf{w}\cdot\mathbf{n}d\sigma - \int_{x_1}^{x_2} \frac{\partial}{\partial x}\left[A\overline{(fu_1)}\right]dx + \\ \int_{V_t} \nabla\cdot(f\mathbf{u})dV. \tag{2.6}$$

Finally, including the expressions (2.5) and (2.6) into (2.1), we have

$$\int_{x_1}^{x_2} \frac{\partial}{\partial t}(A\bar{f})dx = \int_{x_1}^{x_2}\left(\int_S \frac{\partial f}{\partial t}d\sigma\right)dx + \int_{x_1}^{x_2}\left(\int_{\partial S} f\mathbf{w}\cdot n d\gamma\right)dx - \\ \int_{x_1}^{x_2} \frac{\partial}{\partial x}\left[A\overline{(fu_1)}\right]dx + \int_{x_1}^{x_2}\left(\int_S \nabla\cdot(f\mathbf{u})d\sigma\right)dx.$$

This equation is true for any values of the coordinates and, consequently, we obtain the final form of the one-dimensional transport theorem for a generic variable f

$$\frac{\partial}{\partial t}\left(A\bar{f}\right) + \frac{\partial}{\partial x}\left[A\overline{(fu_1)}\right] = \int_S \left[\frac{\partial f}{\partial t} + \nabla\cdot(f\mathbf{u})\right]d\sigma + \int_{\partial S} f\mathbf{w}\cdot n d\gamma \tag{2.7}$$

This relation is general. Now we will proceed to derive the governing equations by invoking the principles of conservation of mass and balance of momentum.

Conservation of mass The equation representing the conservation of mass can be obtained by taking $f = 1$ in (2.7) and, with assuming the assumption of incompressibility (i.e. $\nabla\cdot\mathbf{u} = 0$), we have

$$\frac{\partial A}{\partial t} + \frac{\partial}{\partial x}\left(A\overline{u}_1\right) = \int_{\partial S} \mathbf{w}\cdot\mathbf{n}d\gamma, \tag{2.8}$$

where the right-hand side term is the volumetric outflow per unit length and unit time.

Balance of momentum We take $f = u_1$ and assume that the fluid is incompressible. The area-averaged Reynolds' transport law (2.7) becomes

$$\frac{\partial}{\partial t}(A\overline{u}_1) + \frac{\partial}{\partial x}\left(A\overline{u}_1^2\right) = \int_S \left[\frac{\partial u_1}{\partial t} + \mathbf{u}\cdot\nabla u_1\right]d\sigma + \int_{\partial S} u_1\mathbf{w}\cdot\mathbf{n}d\gamma,$$

that can be written as

$$\frac{\partial}{\partial t}(A\overline{u}_1) + \frac{\partial}{\partial x}\left(A\overline{u}_1^2\right) = \int_S \frac{Du_1}{Dt} d\sigma + \int_{\partial S} u_1 \mathbf{w}\cdot\mathbf{n} d\gamma, \tag{2.9}$$

where $\dfrac{Du_1}{Dt} = \dfrac{\partial u_1}{\partial t} + \mathbf{u}\cdot\nabla u_1$ denotes the *material derivative*. We now recall the balance of the momentum on the control volume V_t

$$\int_{V_t} \frac{D}{Dt}(\rho\mathbf{u}) dV = \int_{V_t} \rho\mathbf{f}^b dV + \int_{\partial V_t} \mathbf{T}\mathbf{n} d\sigma,$$

where $\mathbf{f}^b$ represents the body force per unit volume and $\mathbf{T}$ is the Cauchy stress tensor. Assuming that the density ρ is constant and using divergence theorem, the previous equation can be written as

$$\int_{V_t} \frac{D\mathbf{u}}{Dt} dV = \int_{V_t} \mathbf{f}^b dV + \frac{1}{\rho}\int_{V_t} \nabla\cdot\mathbf{T} d\sigma. \tag{2.10}$$

The constitutive equation for the fluid states that

$$\mathbf{T} = -p\mathbf{I} + \mathbf{D}, \tag{2.11}$$

where p is the pressure, $\mathbf{I}$ is the identity tensor and $\mathbf{D}$ is the tensor of deviatoric stresses due to viscosity. Setting $\nabla\cdot\mathbf{D} = \mathbf{d}$ and assuming that the pressure is homogeneous on each cross section of the vessel, we have that

$$\nabla\cdot\mathbf{T} = -\nabla p + \mathbf{d},$$

and therefore, by (2.10), we obtain

$$\int_{x_1}^{x_2}\left(\int_S \frac{D\mathbf{u}}{Dt} d\sigma\right) = \int_{x_1}^{x_2}\left\{\int_S \left[\mathbf{f}^b + \frac{1}{\rho}\left(-\nabla p + \mathbf{d}\right)\right] d\sigma\right\}.$$

The coordinates x_1 and x_2 are arbitrarily chosen and so we can write the first component of this equation as

$$\int_S \frac{Du_1}{Dt} d\sigma = \int_S \left[f_1^b + \frac{1}{\rho}\left(-\frac{\partial p}{\partial x} + d_1\right)\right] d\sigma. \tag{2.12}$$

Now, we substitute (2.12) in (2.9)

$$\frac{\partial}{\partial t}\left(A\overline{u}\right) + \frac{\partial}{\partial x}\left(A\overline{u_1^2}\right) = \int_S \left[f_1^b + \frac{1}{\rho}\left(-\frac{\partial p}{\partial x} + d_1\right)\right] d\sigma + \int_{\partial S} u_1\mathbf{w}\cdot\mathbf{n} d\sigma$$

which can be expressed in area-averaged values as

$$\frac{\partial}{\partial t}\left(A\overline{u}\right) + \frac{\partial}{\partial x}\left(A\overline{u_1^2}\right) = \frac{A}{\rho}\left(\rho\bar{f}_1^b - \frac{\partial\bar{p}}{\partial x} + \bar{d}_1\right) + \int_{\partial S} u_1\mathbf{w}\cdot\mathbf{n} d\sigma.$$

The term $\overline{u_1^2}$ is handled by defining the Coriolis coefficient α which is a function of the velocity profile

$$\overline{u_1^2} = \frac{1}{A}\int_S u_1^2 d\sigma = \alpha\overline{u}_1^2.$$

For a flat profile, we have $\alpha = 1$ and for a parabolic profile we have $\alpha = 4/3$. The viscous force term $\bar{d}_1$ is taken as a linear function of area-averaged velocity $\overline{u}_1$

$$\frac{A}{\rho}\bar{d}_1 = -K_R\overline{u}_1, \tag{2.13}$$

where K_R is a strictly positive quantity which represents the viscous resistance of the flow per unit length.

Finally, the balance of momentum equation is

$$\frac{\partial}{\partial t}\left(A\overline{u}\right) + \frac{\partial}{\partial x}\left(\alpha A\overline{u}_1^2\right) = \frac{A}{\rho}\bar{f}_1^b - \frac{A}{\rho}\frac{\partial \bar{p}}{\partial x} - K_R\overline{u}_1 + \int_{\partial S} u_1 \mathbf{w}\cdot\mathbf{n}d\sigma. \tag{2.14}$$

Now we assume that the lumen is impermeable ($\mathbf{w}\cdot\mathbf{n} = 0$) and that the body forces are negligible ($\bar{f}_1^b = 0$) and we also simplify the notation, denoting u instead of $\bar{u}_1$ and p instead of $\bar{p}$. Defining the mass flux across a section as $Q = Au = \int_S u_1 d\sigma$, the resulting governing equations for continuity of mass and momentum become

$$\begin{cases} \dfrac{\partial A}{\partial t} + \dfrac{\partial Q}{\partial x} = 0 & x \in (0,L),\ t \in (0,T) \\ \dfrac{\partial Q}{\partial t} + \dfrac{\partial}{\partial x}\left(\alpha\dfrac{Q^2}{A}\right) + \dfrac{A}{\rho}\dfrac{\partial p}{\partial x} + K_R\dfrac{Q}{A} = 0 & x \in (0,L),\ t \in (0,T) \end{cases} \tag{2.15}$$

2.1.2 Arterial wall model

The unknowns in the system of equations (2.15) are p, A and Q. We have three unknowns and only two equations. Therefore we need one more relation between two of these quantities to close the system. We enforce a simple 1-D structural model for the vessel wall, which is assumed to be axial symmetric and only radial displacement are considered. This results in a pressure-area relation which may account for several phenomena, as described in [Formaggia et al., 2003]. In this work, we consider only an elastic response of the vessel wall and a pressure-area relation of the form

$$p = P_{ext} + \psi(A, x) \tag{2.16}$$

with P_{ext} the external pressure (here taken constant) and

$$\psi(A,x) = \beta(x)\left(\sqrt{\frac{A}{A^0(x)}} - 1\right) \tag{2.17}$$

where

$$\beta(x) = \sqrt{\frac{\pi}{A^0(x)}}\frac{h_0(x)E(x)}{1-\nu^2}, \tag{2.18}$$

A^0 is the vessel reference area, h_0 is the vessel thickness, E is the Young modulus and ν is the Poisson ratio, that is tipically taken equal $1/2$ for biological tissues. The relations (2.16), (2.17) and (2.18) are derived from a mechanical model for the vessel-wall displacement [Quarteroni et al., 2000], as shown in [Formaggia et al., 2003].

Remark 2.1.1 (Choice of ψ)**.** Note that (2.17) is only one of the possible choices of ψ and more complex and general laws that take into account viscoelastic contributions can be found e.g. in [Malossi et al., 2012]

With the wall mechanism described by (2.16) and (2.17), the system (2.15) can be written in conservative form

$$\frac{\partial \mathbf{U}}{\partial t} + \frac{\partial \mathbf{F}(\mathbf{U})}{\partial x} + \mathbf{S}(\mathbf{U}) = \mathbf{0} \tag{2.19}$$

with

$$\begin{aligned} \mathbf{U} = \begin{pmatrix} A \\ Q \end{pmatrix}, \ \mathbf{F}(\mathbf{U}) = \begin{pmatrix} Q \\ \alpha \dfrac{Q^2}{A} + \dfrac{\beta A^0}{3\rho} \left(\dfrac{A}{A^0} \right)^{3/2} \end{pmatrix} \quad \text{and} \\ \mathbf{S}(\mathbf{U}) = \begin{pmatrix} 0 \\ K_R \dfrac{Q}{A} - \dfrac{\beta}{3\rho} \left(\dfrac{A}{A^0} \right)^{3/2} \dfrac{\partial A^0}{\partial x} + \dfrac{A}{\rho} \left[\dfrac{2}{3} \left(\dfrac{A}{A^0} \right)^{1/2} - 1 \right] \dfrac{\partial \beta}{\partial x} \end{pmatrix} \end{aligned} \tag{2.20}$$

The system is closed by providing a proper set of of boundary conditions on the inflow and outflow boundaries Γ_L and Γ_R that we describe in subsection 2.1.5. We postpone the discussion on the boundary conditions to subsection (2.1.5).

2.1.3 Characteristic variables

The system (2.19) can be written in quasi-linear form as

$$\frac{\partial \mathbf{U}}{\partial t} + \mathbf{F}_{\mathbf{U}} \frac{\partial \mathbf{U}}{\partial x} + \mathbf{S}(\mathbf{U}) = \mathbf{0}, \tag{2.21}$$

where

$$\mathbf{F}_{\mathbf{U}} = \frac{\partial \mathbf{F}}{\partial \mathbf{U}} = \begin{pmatrix} 0 & 1 \\ -\alpha \dfrac{Q^2}{A^2} + \dfrac{\beta}{2\rho} \left(\dfrac{A}{A^0} \right)^{1/2} & 2\alpha \dfrac{Q}{A} \end{pmatrix}.$$

Under the assumption $A > 0$ (that is a necessary condition to have a physical relevant solution), the matrix $\mathbf{F}_{\mathbf{U}}$ has two real eigenvalues λ_1 and λ_2 and the corresponding left eigenmatrix L is

$$L = \begin{pmatrix} \mathbf{l}_1^T \\ \mathbf{l}_2^T \end{pmatrix},$$

where $\mathbf{l}_i$ indicates the i-th eigenvector such that $\mathbf{l}_i \mathbf{F}_{\mathbf{U}} = \lambda_i \mathbf{l}_i$. For the typical values of velocity, vessel area and elastic parameter β under physiological conditions, we have that $\lambda_1 > 0$ and $\lambda_2 < 0$. Therefore the system is strictly hyperbolic and subcritical (see [LeVeque, 2002] for these definitions).

The characteristic variables can be determined by integrating the differential system

$$\frac{\partial \mathbf{W}}{\partial \mathbf{U}} = L.$$

It may be shown (see [Quarteroni and Formaggia, 2004]) that the two characteristic variables are

$$W_1 = \frac{Q}{A} + 4\sqrt{\frac{\beta}{2\rho} \left(\frac{A}{A^0} \right)^{1/2}}, \tag{2.22}$$

$$W_2 = \frac{Q}{A} - 4\sqrt{\frac{\beta}{2\rho}\left(\frac{A}{A^0}\right)^{1/2}}. \tag{2.23}$$

For a detailed analysis of characteristic variables of the system (2.19), we refer the reader to [Quarteroni and Formaggia, 2004].

2.1.4 Numerical approximation

In literature, several approaches have been proposed for the numerical approximation of the one dimensional system of conservation laws (2.15) (see [Sherwin et al., 2003, Blanco et al., 2007, Reymond et al., 2009]). Following [Formaggia et al., 2003], in this work we use an explicit second order Taylor-Galerkin discretization of the system (2.19). We write the Taylor expansion truncated to the second order at time t^n such that $\Delta t = t^{n+1} - t^n$, yielding

$$\mathbf{U}^{n+1} = \mathbf{U}^n + \Delta t \left.\frac{\partial \mathbf{U}}{\partial t}\right|^n + \frac{\Delta t^2}{2}\left.\frac{\partial^2 \mathbf{U}}{\partial t^2}\right|^n. \tag{2.24}$$

We replace the time derivative by space derivative, exploiting (2.19). We define the matrix

$$\mathbf{S}_\mathbf{U} = \frac{\partial \mathbf{S}}{\partial \mathbf{U}} = \begin{pmatrix} 0 & 0 \\ -K_R\dfrac{Q}{A^2} + \dfrac{\beta}{2\rho A^0}\left(\dfrac{A}{A^0}\right)^{1/2}\dfrac{\partial A^0}{\partial x} + \dfrac{1}{\rho}\left(\dfrac{A}{A^0}\right)^{1/2}\dfrac{\partial \beta}{\partial x} & \dfrac{K_R}{A} \end{pmatrix}$$

and we obtain

$$\frac{\partial \mathbf{U}}{\partial t} = -\mathbf{S} - \frac{\partial \mathbf{F}}{\partial x} \tag{2.25}$$

$$\begin{aligned} \frac{\partial^2 \mathbf{U}}{\partial t^2} &= -\frac{\partial \mathbf{S}}{\partial t} - \frac{\partial^2 \mathbf{F}}{\partial t \partial x} = -\mathbf{S}_\mathbf{U}\frac{\partial \mathbf{U}}{\partial t} - \frac{\partial}{\partial x}\left(\mathbf{F}_\mathbf{U}\frac{\partial \mathbf{U}}{\partial t}\right) \\ &= \mathbf{S}_\mathbf{U}\left(\mathbf{S} + \frac{\partial \mathbf{F}}{\partial x}\right) + \frac{\partial}{\partial x}\left(\mathbf{F}_\mathbf{U}\mathbf{S}\right) + \frac{\partial}{\partial x}\left(\mathbf{F}_\mathbf{U}\frac{\partial \mathbf{F}}{\partial x}\right). \end{aligned} \tag{2.26}$$

Remark 2.1.2. We point out that the derivation of the scheme is slightly more complex than the standard Lax-Wendroff scheme, because of the presence of a non-constant source term and of the explicit dependence of the momentum flux $\mathbf{F}$ on x through β and A^0.

From (2.24), (2.25) and (2.26), we obtain the temporal scheme

$$\begin{aligned} \mathbf{U}^{n+1} = \; & \mathbf{U}^n - \Delta t\frac{\partial}{\partial x}\left(\mathbf{F}(\mathbf{U}^n) - \frac{\Delta t}{2}\mathbf{F}_\mathbf{U}(\mathbf{U}^n)\mathbf{S}(\mathbf{U}^n)\right) \\ & + \frac{\Delta t^2}{2}\left[\mathbf{S}_\mathbf{U}(\mathbf{U}^n)\frac{\partial \mathbf{F}(\mathbf{U}^n)}{\partial x} + \frac{\partial}{\partial x}\left(\mathbf{F}_\mathbf{U}(\mathbf{U}^n)\frac{\partial \mathbf{F}(\mathbf{U}^n)}{\partial x}\right)\right] \\ & - \Delta t\left(\mathbf{S}(\mathbf{U}^n) - \frac{\Delta t}{2}\mathbf{S}_\mathbf{U}(\mathbf{U}^n)\mathbf{S}(\mathbf{U}^n)\right). \end{aligned} \tag{2.27}$$

For space discretization, we employ linear finite elements. We subdivide the domain Ω into N_{el} finite elements Ω_e of size h_e. We indicate by $\mathcal{V}_h$ the space of continuous

vector functions defined on Ω, linear on each element and $\mathcal{V}_h^0$ the subspace of $\mathcal{V}_h$ whose functions are zero at the endpoints. The finite element solution of (2.27) requires, for $n \geqslant 0$, to find $\mathbf{U}_h^{n+1}$ in $\mathcal{V}_h$ such that, for all $\varphi_h \in \mathcal{V}_h^0$,

$$\begin{aligned}(\mathbf{U}_h^{n+1}, \varphi_h) = \; & (\mathbf{U}_h^n, \varphi_h) - \Delta t \left[\mathbf{F}(\mathbf{U}_h^n) - \frac{\Delta t}{2} \mathbf{F}_{\mathbf{U}}(\mathbf{U}_h^n) \left(\mathbf{S}(\mathbf{U}_h^n) + \frac{\partial \mathbf{F}(\mathbf{U}_h^n}{\partial x} \right), \frac{\partial \varphi_h}{\partial x} \right] \\ & - \Delta t \left[\mathbf{S}(\mathbf{U}_h^n) - \frac{\Delta t}{2} \mathbf{S}_{\mathbf{U}}(\mathbf{U}_h^n) \left(\mathbf{S}(\mathbf{U}_h^n + \frac{\partial \mathbf{F}(\mathbf{U}_h^n}{\partial x}) \right), \varphi_h \right]\end{aligned} \tag{2.28}$$

At a discrete level, this scheme is closed by introducing two boundary and two compatibility conditions, that we will discuss in subsections 2.1.5 and 2.1.6.

The main advantage of this scheme is the low computational cost of each time step, due to the explicit nature of the scheme. However, the explicit time discretization has a drawback: it implies a limitation on the time step related to the so-called Courant-Friedrichs-Lewy (CFL) condition. In particular, from [Quartapelle, 1993], a Von Neumann stability analysis leads to the condition

$$\lambda_M \frac{\Delta t}{h} \leqslant \frac{\sqrt{3}}{3}, \tag{2.29}$$

where $\lambda_M = \max\{\lambda_1, \lambda_2\}$.

2.1.5 Boundary conditions

From the analysis of the characteristics (see [Formaggia et al., 2009]), we can argue that only one boundary condition can be imposed at each end of the tube. For the sake of simplicity, we focus only on the left boundary ($x = 0$). We recall that W_1 is the characteristic variable entering the domain (2.22) and W_2 is the characteristic variable going out (2.23). Let here $\mathbf{U} = \mathbf{U}(t)$ be the vector of variables at the boundary point. A boundary condition has the general form

$$G(\mathbf{U}(t)) = g(t), \quad \text{for } t > 0, \tag{2.30}$$

where G is a C^1 function and g a given function of time. Not all the choices are possible: we require that

$$\mathbf{r}_1^T(\mathbf{U}) \frac{\partial G(\mathbf{U})}{\partial \mathbf{U}} \neq 0, \tag{2.31}$$

where $\mathbf{r}_1$ is the right eigenvector of $\mathbf{F}_{\mathbf{U}}(\mathbf{U}(t))$ associated to the characteristic variable W_1. This condition corresponds to the request that the boundary condition is not on the outgoing characteristic.

In practice, we are interested only in two specific types of boundary conditions that we are now going to describe

Proximal and distal conditions

It is simple to verify that the prescription of the flow rate Q, the section area A or the flow velocity u at one end of the tube is allowable (i.e. it satisfies (2.31)). For example, at $x = 0$, we can impose

$$Q(0, t) = g(t), \quad \text{for } t > 0,$$

where g is a given function of time. This type of condition is clearly reflective and a simple wave associated to the outgoing characteristic is partially reflected into the domain. This kind of boundary conditions is useful when we have to impose data coming from real measurements.

Absorbing boundary conditions

Absorbing boundary conditions (or non-reflecting boundary conditions) allow the simple wave associated to the exiting characteristic variable to go out without spurious reflections. Therefore, this type of boundary conditions can be useful at the distal boundary ($x = L$). If we indicate the second left eigenvector of $\mathbf{F_U}$ with $\mathbf{l}_2$, following [Thompson, 1987] and [Hedstrom, 1979], absorbing boundary conditions at $x = L$ are provided by

$$\mathbf{l}_2^T \left[\frac{\partial \mathbf{U}}{\partial t} - \mathbf{S}(\mathbf{U}) \right]_{x=L} = 0, \tag{2.32}$$

which is equivalent to require that

$$\frac{dW_2(t)}{dt} - \mathbf{l}_2^T \mathbf{S}(W_2(\mathbf{U}(t)) = 0, \tag{2.33}$$

where $W_2(t) = W_2(L, t)$, $\mathbf{U}(t) = \mathbf{U}(L, t)$ and we recall that the characteristic variables can be expressed in function of the physical variables. As this is a condition on the incoming characteristics, the condition (2.31) is satisfied. From a numerical point of view, the absorbing boundary condition (2.33) can be temporally discretized at time $t^{n+1} = t^n + \Delta t$ as

$$W_2^{n+1} = W_2^n + \Delta t \mathbf{l}_2^T \mathbf{S}^n = 0,$$

where $\mathbf{l}_2$ and $\mathbf{S}$ are computed from the solution at time t^n.

2.1.6 Compatibility conditions

As we have noted, the boundary conditions prescribe only one unknown at each end of the tube or one nonlinear function relating the two unknowns. However to solve problem (2.28), we need to know both A and Q at the endpoints. Therefore, we need two more conditions, that are called compatibility conditions and that are based on the extrapolation of outgoing characteristics. These conditions have been described in [Formaggia et al., 2003] and extended in [Malossi et al., 2012].

Let us consider the quasi-linear form of problem (2.19)

$$\frac{\partial \mathbf{U}}{\partial t} + \mathbf{F_U}(\mathbf{U}) \frac{\partial \mathbf{U}}{\partial x} + \mathbf{S}(\mathbf{U}) = \mathbf{0}. \tag{2.34}$$

Let Λ and L the eigenvalue and left eigenvector matrix of $\mathbf{F_U}$, such that $L\mathbf{F_U}L^{-1} = \Lambda$. They have the form

$$\Lambda = \begin{pmatrix} \lambda_1 & 0 \\ 0 & \lambda_2 \end{pmatrix}, \quad L = \varsigma \begin{pmatrix} -\lambda_2 & 1 \\ -\lambda_1 & 1 \end{pmatrix}, \tag{2.35}$$

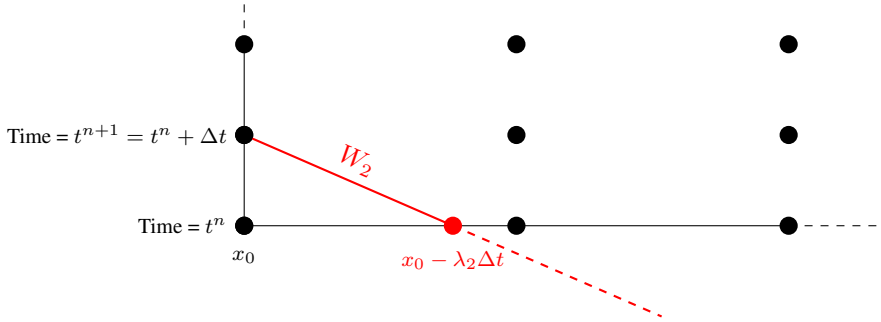

Figure 2.2: *Characteristic extrapolation for the 1D-FSI problem on the left side of the domain*

where $\varsigma = 1/A$ (as detailed in [Formaggia et al., 2003]) and

$$\begin{aligned}\lambda_{1,2} &= \alpha\frac{Q}{A} \pm \sqrt{\alpha(\alpha-1)\left(\frac{Q}{A}\right)^2 + \frac{A}{\rho}\frac{\partial\psi}{\partial A}} \\ &= \alpha\frac{Q}{A} \pm \sqrt{\alpha(\alpha-1)\left(\frac{Q}{A}\right)^2 + \frac{\beta}{2\rho}\left(\frac{A}{A^0}\right)^{1/2}}.\end{aligned} \tag{2.36}$$

We recall that the characteristic variable $\mathbf{W}$ are defined as

$$\frac{\partial \mathbf{W}}{\partial \mathbf{U}} = L$$

and, therefore, by left multiplying (2.34) by L, we obtain

$$L\frac{\partial \mathbf{U}}{\partial t} + L\mathbf{F}_{\mathbf{U}}(\mathbf{U})L^{-1}L\frac{\partial \mathbf{U}}{\partial x} + L\mathbf{S}(\mathbf{U}) = \mathbf{0}, \tag{2.37}$$

and, by $\dfrac{\partial \mathbf{W}}{\partial x} = \dfrac{\partial L}{\partial x}\mathbf{U} + L\dfrac{\partial \mathbf{U}}{\partial x}$, (2.37) can be written as

$$L\frac{\partial \mathbf{U}}{\partial t} + \Lambda\left[\frac{\partial \mathbf{W}}{\partial x} - \frac{\partial L}{\partial x}\mathbf{U}\right] + L\mathbf{S}(\mathbf{U}) = \mathbf{0}. \tag{2.38}$$

We note that, assuming that L is constant in time,

$$\frac{D\mathbf{W}}{Dt} = L\frac{\partial \mathbf{U}}{\partial t} + \Lambda\frac{\partial \mathbf{W}}{\partial x}$$

and, consequently, (2.38) is equivalent to

$$\frac{D\mathbf{W}}{Dt} = \Lambda\frac{\partial L}{\partial x}\mathbf{U} - L\mathbf{S}(\mathbf{U}). \tag{2.39}$$

On each end point, we are interested only in the outgoing characteristic that we assume for simplicity to be W_i. Therefore, we consider only one equation of the system (2.39)

$$\frac{D\mathbf{W}_i}{Dt} = \lambda_i\frac{\partial l_i^T}{\partial x}\mathbf{U} - l_i^T\mathbf{S}(\mathbf{U}). \tag{2.40}$$

By introducing the same time discretization used in the Taylor-Galerkin formulation, we can write the compatibility condition

$$l_i^T(\mathbf{U}^{n+1} - \mathbf{U}_\star^n) = \Delta t \left(\lambda_i \frac{\partial l_i^T}{\partial x} \mathbf{U}_\star^n - l_i^T \mathbf{S}(\mathbf{U}_\star^n) \right), \tag{2.41}$$

where $\mathbf{U}_\star^n = (A_\star^n, Q_\star^n)^T$ is the foot of the characteristic.

The final set of boundary conditions for the finite element problem is computed by solving a 2×2 linear system on each side of the tube whose first equation is the numerical compatibility condition and the second equation is the physical boundary condition (for simplicity here we consider only boundary conditions on flow rate or section area):

$$\begin{aligned} &\text{Left} \quad \begin{pmatrix} L_{21} & L_{22} \\ & \\ 1/0 & 0/1 \end{pmatrix} \begin{pmatrix} A^{n+1} \\ \\ Q^{n+1} \end{pmatrix} = \begin{pmatrix} f_L^n \\ \\ g_L^n \end{pmatrix}, \\ &\text{Right} \quad \begin{pmatrix} L_{11} & L_{12} \\ & \\ 1/0 & 0/1 \end{pmatrix} \begin{pmatrix} A^{n+1} \\ \\ Q^{n+1} \end{pmatrix} = \begin{pmatrix} f_R^n \\ \\ g_R^n \end{pmatrix}, \end{aligned} \tag{2.42}$$

where g_L^n and g_R^n are the values of the prescribed boundary condition on the left and on the right side, respectively, and

$$\begin{aligned} f_L^n = \; & L_{21} A_\star^n + L_{22} Q_\star^n \\ & + \Delta t \left(\lambda_2 \left(\frac{\partial L_{21}}{\partial x} A_\star^n + \frac{\partial L_{22}}{\partial x} Q_\star^n \right) - L_{21} S_1(\mathbf{U}_\star^n) - L_{22} S_2(\mathbf{U}_\star^n) \right) \\ f_R^n = \; & L_{11} A_\star^n + L_{12} Q_\star^n \\ & + \Delta t \left(\lambda_1 \left(\frac{\partial L_{11}}{\partial x} A_\star^n + \frac{\partial L_{12}}{\partial x} Q_\star^n \right) - L_{11} S_1(\mathbf{U}_\star^n) - L_{12} S_2(\mathbf{U}_\star^n) \right) \end{aligned}$$

2.2 Network of vessels

The model described in the previous section can be easily extended to handle a network of vessels by a domain splitting technique, following what is done in [Formaggia et al., 2009]. We split the network into a set of pipes and each one is modelled by a 1D-FSI model. At every bifurcation or branch of the tree, the models are coupled with suitable interface (or coupling) conditions.

For simplicity, we now detail only the case of a single bifurcation (see figure 2.3) that is the simplest network. It can be described by a triplet of one dimensional models, three boundary conditions (one inflow and two outflow conditions) and a set of coupling conditions. Let us denote with x^* the bifurcation point and with $\mathbf{U}_i,\ i = 1, 2, 3$ the unknowns of corresponding models. In x^* we have six unknowns in total. Therefore, we need six coupling conditions. Three equations are obtained by the continuity of

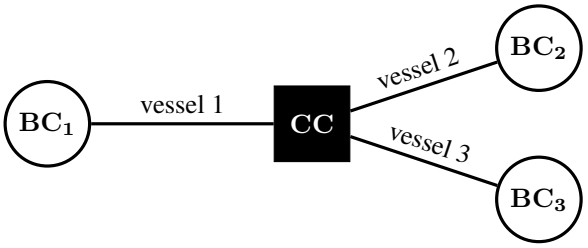

Figure 2.3: *Schematic representation of a bifurcation*

mass flux and total pressure

$$P_T = \frac{\rho}{2}\frac{Q^2}{A} + \beta\left(\sqrt{\frac{A}{A^0}} - 1\right)$$

across x^*:

$$Q_1(x^*) = Q_2(x^*) + Q_3(x^*), \tag{2.43}$$

$$\frac{\rho}{2}\frac{Q_1^2(x^*)}{A_1(x^*)} + \beta_1\left(\sqrt{\frac{A_1(x^*)}{A^0}} - 1\right) = \frac{\rho}{2}\frac{Q_2^2(x^*)}{A_2(x^*)} + \beta_2\left(\sqrt{\frac{A_2(x^*)}{A^0}} - 1\right), \tag{2.44}$$

$$\frac{\rho}{2}\frac{Q_1^2(x^*)}{A_1(x^*)} + \beta_1\left(\sqrt{\frac{A_1(x^*)}{A^0}} - 1\right) = \frac{\rho}{2}\frac{Q_3^2(x^*)}{A_3(x^*)} + \beta_3\left(\sqrt{\frac{A_3(x^*)}{A^0}} - 1\right). \tag{2.45}$$

Then, at a numerical level, three compatibility conditions (one per vessel) are defined to close the numerical system, in analogy with the compatibility conditions (2.41) for the single vessel case.

The three equations (2.43)-(2.45) and the three compatibility conditions define a nonlinear system that we solve to have the six unknowns that are used as boundary conditions for the 1D-FSI models. We can now summarize how we proceed to solve the network system at each time step:

(i) we solve the non-linear system of coupling conditions to compute $\mathbf{U}_i$ at each bifurcation and branch of the network;

(ii) we solve each model using endpoints values $\mathbf{U}_i$ coming from either the coupling conditions at network junctions or boundary conditions at proximal and distal points.

CHAPTER 3

Optimal control for one dimensional FSI models

In this chapter we apply the Lagrangian formalism described in Section 1.2 to the model presented in the previous chapter to estimate a parameter of the model. In particular, we want to estimate the compliance parameter β (depending on the spatial variable x), given some measurements inside the domain of the model.

The chapter is organized as follows. In Section 3.1, we present the adjoint model (subsection 3.1.2) and the optimality condition (subsection 3.1.6) for the single vessel problem, with particular attention to the numerical discretization of the adjoint problem (subsection 3.1.3) and the derivation of the boundary and compatibility conditions (subsection 3.1.4 and 3.1.5, respectively). Then, in Section 3.2, we describe how to extend the framework to network problems, with particular attention to the treatment of adjoint coupling conditions (subsection 3.2.2), and we show an application to a bifurcation (subsection 3.2.5). Finally, in Section 3.3 we discuss the overall optimal control problem framework.

3.1 Optimal control for a single one dimensional FSI model

3.1.1 Lagrangian functional

As described in Section 1.2, we have to define a Lagrangian functional to guide the parameter estimation procedure. We consider problem (2.19), as state equation, endowed with two generic scalar boundary conditions

$$G_0(\mathbf{U}(0,t)) = g_0(t) \quad G_L(\mathbf{U}(L,t)) = g_L(t),$$

where G_0 and G_L can be any appropriate functions of the state variables $\mathbf{U}(x,t) = (A(x,t), Q(x,t))$ evaluated on the boundaries that satisfy (2.31), and g_0 and g_t are

prescribed functions of time.

With these assumptions we can write the Lagrangian functional:

$$\begin{aligned}\mathcal{L}(\mathbf{U},\beta,\overline{\mathbf{m}}) :=& J(\mathbf{U},\beta)+\langle \mathbf{e}(\mathbf{U},\beta),\overline{\mathbf{m}}\rangle \\ =& J(\mathbf{U},\beta)+\int_0^T\int_0^L\left(\left(\frac{\partial \mathbf{U}}{\partial t}+\frac{\partial \mathbf{F}(\mathbf{U};\beta)}{\partial x}+\mathbf{S}(\mathbf{U};\beta)\right),\mathbf{m}\right)dxdt \\ &+\int_0^T[((G_0(\mathbf{U}(0,t))-g_0(t)),m_{C0})+((G_L(\mathbf{U}(L,t))-g_L(t)),m_{CL})]dt \\ &+\int_0^L((\mathbf{U}(x,0)-\mathbf{U}_0(x)),\mathbf{m}_0)dx\end{aligned} \tag{3.1}$$

where $\overline{\mathbf{m}}=(\mathbf{m},m_{C0},c_{CL},\mathbf{m}_0)^T$ is the set of adjoint variables and $e(\mathbf{U},\beta)$ is the state model. We observe that $\mathbf{m}(x,t)$ and $\mathbf{m}_0(x)$ are vector functions, while $m_{C0}(t)$ and $m_{CL}(t)$ are scalar functions.

We define $J(\mathbf{U},\beta)$ as cost functional that take into account the difference between the solution of (2.19) and some measurements, and can be written in a general way

$$J(\mathbf{U},\beta)=J^{in}(\mathbf{U},\beta)+J^{rb}(\mathbf{U},\beta)+J^{lb}(\mathbf{U},\beta)$$

where $J^{in}(\mathbf{U},\beta)$ depends only on quantities that are internal to the domain $(0,L)$ and $J^{rb}(\mathbf{U},\beta)$ and $J^{lb}(\mathbf{U},\beta)$ depend on quantities on the right and left side of the boundary, respectively.

In particular in real applications, we will consider the functional

$$J(\mathbf{U})=\frac{1}{2}\sum_{k=0}^{N_t}\sum_{j=0}^{N_x}\left(A(x_j,t_k)-A_M(x_j,t_k)\right)^2. \tag{3.2}$$

where $A(x,t)$ is the first component of the state equation solution $\mathbf{U}(x,t)$, namely the section area of the vessel, $A_M(x,t)$ are section area measurements and $\{x_j\}_{j=1}^{N_x}$ and $\{t_k\}_{k=0}^{N_t}$ are the space and time nodes on which measurements are taken.

Remark 3.1.1. From this point on, we will put on evidence all the quantities that depends directly on the compliance parameter β.

3.1.2 Adjoint state equation

We recall that the adjoint problem is the derivative of the Lagrangian functional with respect to the state variable: $\mathcal{L}_{\mathbf{U}}(\mathbf{U},\beta,\overline{\mathbf{m}})=0$. To compute $\mathcal{L}_{\mathbf{U}}(\mathbf{U},\beta,\overline{\mathbf{m}})=0$ we

integrate by parts the first integral in (3.1):

$$\begin{aligned}\mathcal{L}(\mathbf{U},\beta,\overline{\mathbf{m}}) =& J(\mathbf{U},\beta)+\int_0^T\int_0^L\left(-\mathbf{U}^T\frac{\partial\mathbf{m}}{\partial t}-\mathbf{F}^T(\mathbf{U};\beta)\frac{\partial\mathbf{m}}{\partial x}+\mathbf{S}^T(\mathbf{U};\beta)\mathbf{m}\right)dxdt\\ &+\int_0^T[((G_0(\mathbf{U}(0,t))-g_0(t)),m_{C0})-(\mathbf{F}^T(\mathbf{U};\beta)\mathbf{m})(0,t)]dt\\ &+\int_0^T[((G_L(\mathbf{U}(L,t))-g_L(t)),m_{CL})+(\mathbf{F}^T(\mathbf{U};\beta)\mathbf{m})(L,t)]dt\\ &+\int_0^L[((\mathbf{U}(x,0)-\mathbf{U}_0(x)),\mathbf{m}_0)-(\mathbf{U}^T\mathbf{m})(x,0)]dx\\ &+\int_0^L(\mathbf{U}^T\mathbf{m})(x,T)dx.\end{aligned}$$

From this form of the Lagrangian functional we can easily write the adjoint equation.

$$\begin{cases}\dfrac{\partial\mathbf{m}}{\partial t}+\mathbf{F}^T_{\mathbf{U}}(U;\beta)\dfrac{\partial\mathbf{m}}{\partial x}-\mathbf{S}^T_{\mathbf{U}}(U;\beta)\mathbf{m}=J^{in}_{\mathbf{U}}(\mathbf{U},\beta) & x\in(0,L),\ t\in(0,T),\\ \dfrac{\partial G_0(U(0,t))}{\partial\mathbf{U}}^T m_{C0}-(\mathbf{F}^T_{\mathbf{U}}(\mathbf{U};\beta)\mathbf{m})(0,t)+J^{lb}_{\mathbf{U}}(\mathbf{U},\beta)=\mathbf{0} & t\in(0,T),\\ \dfrac{\partial G_L(U(L,t))}{\partial\mathbf{U}}^T m_{CL}+(\mathbf{F}^T_{\mathbf{U}}(\mathbf{U};\beta)\mathbf{m})(L,t)+J^{rb}_{\mathbf{U}}(\mathbf{U},\beta)=\mathbf{0} & t\in(0,T),\\ \mathbf{m}_0=\mathbf{m}(x,0) & x\in(0,L)\\ \mathbf{m}(x,T)=\mathbf{0} & x\in(0,L)\end{cases}\tag{3.3}$$

where $J^{(\bullet)}_{\mathbf{U}}(\mathbf{U},\beta)=\dfrac{\partial J^{(\bullet)}(U,\beta)}{\partial U}$ is the Fréchet derivative of the functional $J(\mathbf{U},\beta)$ with respect to $\mathbf{U}$. We note that the adjoint equation is a linear hyperbolic equation evolving backward in time, i.e. it evolves from the final time T to the initial time 0. We also observe that the flux matrix $\mathbf{F}^T_{\mathbf{U}}(\mathbf{U};\beta)$ is the transpose of the Jacobian matrix of the state problem (2.19) and, therefore, the two matrices have the same eigenvalues and the left eigenvectors of the one are the right eigenvectors of the other.

3.1.3 Numerical approximation

We solve the adjoint equation using a discretization analogous to that used to solve the state equation i.e. a second order Taylor-Galerkin scheme. As in subsection 2.1.4 we write the Taylor expansion truncated to the second order at time t^n, but with $\Delta t = t^n - t^{n+1} < 0$

$$\mathbf{m}^n=\mathbf{m}^{n+1}+\Delta t\left.\frac{\partial\mathbf{m}}{\partial t}\right|^{n+1}+\frac{\Delta t^2}{2}\left.\frac{\partial^2\mathbf{m}}{\partial t^2}\right|^{n+1},$$

where $\mathbf{m}^n=\mathbf{m}(x,t^n)$. For the sake of simplicity, from this point on, in this subsection we omit the dependence of $\mathbf{F}_{\mathbf{U}}$. $\mathbf{S}_{\mathbf{U}}$ and $J_{\mathbf{U}}$ on $\mathbf{U}$ and β.

We replace the time derivative by space derivative, exploiting the first equation of (3.3), and we obtain

$$\frac{\partial \mathbf{m}}{\partial t} = -\mathbf{F}_{\mathbf{U}}^T \frac{\partial \mathbf{m}}{\partial x} + \mathbf{S}_{\mathbf{U}}^T \mathbf{m} + J_{\mathbf{U}}^{int}, \tag{3.4}$$

and

$$\frac{\partial^2 \mathbf{m}}{\partial t^2} = \frac{\partial}{\partial t}\left(-\mathbf{F}_{\mathbf{U}}^T \frac{\partial \mathbf{m}}{\partial x} + \mathbf{S}_{\mathbf{U}}^T \mathbf{m} + J_{\mathbf{U}}^{int}\right) \tag{3.5}$$

We note that, using Einstein notation,[1] the terms in the right hand side of (3.5) can be written as

$$\frac{\partial}{\partial t}\left(\frac{\partial F_j}{\partial u_i}\frac{\partial m_j}{\partial x}\right) = \left(\frac{\partial}{\partial t}\frac{\partial F_j}{\partial u_i}\right)\frac{\partial m_j}{\partial x} + \frac{\partial F_j}{\partial u_i}\left(\frac{\partial}{\partial t}\frac{\partial m_j}{\partial x}\right) = \underbrace{\frac{\partial^2 F_j}{\partial u_i \partial u_k}\frac{\partial u_k}{\partial t}\frac{\partial m_j}{\partial x}}_{-T_1} + \underbrace{\frac{\partial F_j}{\partial u_i}\left(\frac{\partial}{\partial t}\frac{\partial m_j}{\partial x}\right)}_{-T_2}$$

$$\frac{\partial}{\partial t}\left(\frac{\partial S_j}{\partial u_i} m_j\right) = \left(\frac{\partial}{\partial t}\frac{\partial S_j}{\partial u_i}\right) m_j + \frac{\partial S_j}{\partial u_i}\frac{\partial m_j}{\partial t} = \underbrace{\frac{\partial^2 S_j}{\partial u_i \partial u_k}\frac{\partial u_k}{\partial t} m_j}_{T_3} + \underbrace{\frac{\partial S_j}{\partial u_i}\frac{\partial m_j}{\partial t}}_{T_4}$$

$$\frac{\partial}{\partial t}\frac{\partial J^{in}}{\partial u_i} = \underbrace{\frac{\partial^2 J^{in}}{\partial u_i \partial u_k}\frac{\partial u_k}{\partial t}}_{T_5}$$

We point out that m is independent of u and consequently we find out that

$$\begin{aligned} T_1 + T_3 + T_5 &= \frac{\partial u_k}{\partial t}\left[-\frac{\partial^2 F_j}{\partial u_i \partial u_k}\frac{\partial m_j}{\partial x} + \frac{\partial^2 S_j}{\partial u_i \partial u_k} m_j + \frac{\partial^2 J^{in}}{\partial u_i \partial u_k}\right] = \\ &= \frac{\partial u_k}{\partial t}\frac{\partial}{\partial u_k}\left[-\frac{\partial F_j}{\partial u_i}\frac{\partial m_j}{\partial x} + \frac{\partial S_j}{\partial u_i} + \frac{\partial J^{in}}{\partial u_i}\right] = \frac{\partial u_k}{\partial t}\frac{\partial}{\partial u_k}\left(\frac{\partial m_i}{\partial t}\right) = 0 \end{aligned} \tag{3.6}$$

Therefore, thanks to (3.6), (3.5) simplifies as

$$\frac{\partial^2 \mathbf{m}}{\partial t^2} = -\mathbf{F}_{\mathbf{U}}^T \frac{\partial}{\partial x}\left(-\mathbf{F}_{\mathbf{U}}^T \frac{\partial \mathbf{m}}{\partial x} + \mathbf{S}_{\mathbf{U}}^T \mathbf{m} + J_{\mathbf{U}}^{in}\right) + \mathbf{S}_{\mathbf{U}}^T\left(-\mathbf{F}_{\mathbf{U}}^T \frac{\partial \mathbf{m}}{\partial x} + \mathbf{S}_{\mathbf{U}}^T \mathbf{m} + J_{\mathbf{U}}^{in}\right) \tag{3.7}$$

Finally, from (3.4) and (3.7), after time discretization we obtain the scheme

$$\begin{aligned} \mathbf{m}^n = \mathbf{m}^{n+1} - \Delta t \left(\mathbf{F}_{\mathbf{U}}^T \frac{\partial \mathbf{m}}{\partial x} - \mathbf{S}_{\mathbf{U}}^T \mathbf{m} - J_{\mathbf{U}}^{in}\right)\Big|^{n+1} + \\ + \frac{\Delta t^2}{2}\left[-\mathbf{F}_{\mathbf{U}}^T \frac{\partial}{\partial x}\left(-\mathbf{F}_{\mathbf{U}}^T \frac{\partial \mathbf{m}}{\partial x} + \mathbf{S}_{\mathbf{U}}^T \mathbf{m} + J_{\mathbf{U}}^{in}\right) + \mathbf{S}_{\mathbf{U}}^T\left(-\mathbf{F}_{\mathbf{U}}^T \frac{\partial \mathbf{m}}{\partial x} + \mathbf{S}_{\mathbf{U}}^T \mathbf{m} + J_{\mathbf{U}}^{in}\right)\right]\Big|^{n+1} \end{aligned} \tag{3.8}$$

[1] Repeated indexes on the same side of an expression are implicitly summed, for instance

$$a_i b_i \equiv \sum_i a_i b_i$$

and

$$a_{i,k} b_i \equiv \sum_i a_{i,k} b_i.$$

Remark 3.1.2. We remind that, due to the fact that the adjoint equation evolves backward in time, in (3.8) we compute the n-th temporal value exploiting the $(n+1)$-th temporal value. We stress moreover that the time step $\Delta t = t^n - t^{n+1}$ we use in the adjoint equation is negative.

For the space discretization of the adjoint equation, we make use of the same strategy that we employed to discretize the state equation in subsection 2.1.4, i.e. linear finite elements. We subdivide the domain $\Omega = [0, L]$ into N_{el} finite elements Ω_e of size h_e. We indicate by $\mathcal{V}_h$ the space of continuous vector functions defined on Ω, linear on each element and $\mathcal{V}_h^0$ the subspace of $\mathcal{V}_h$ whose functions are zero on the end points of Ω. The finite element solution of (2.27) requires to find $\mathbf{m}_h^{n+1}$ in $\mathcal{V}_h$ such that, for all $\varphi_h \in \mathcal{V}_h^0$ and for $n \geqslant 0$,

$$\begin{aligned}(\mathbf{m}^n, \varphi_h) = \left(\mathbf{m}^{n+1}, \varphi_h\right) - \Delta t \left(\left(\mathbf{F}_{\mathbf{U}}^T \frac{\partial \mathbf{m}}{\partial x} - \mathbf{S}_{\mathbf{U}}^T \mathbf{m} - J_{\mathbf{U}}^{in}\right), \varphi_h\right) \\ + \frac{\Delta t^2}{2} \left(-\mathbf{F}_{\mathbf{U}}^T \frac{\partial}{\partial x} \left(-\mathbf{F}_{\mathbf{U}}^T \frac{\partial \mathbf{m}}{\partial x} + \mathbf{S}_{\mathbf{U}}^T \mathbf{m} + J_{\mathbf{U}}^{in}\right), \varphi_h\right) \\ + \frac{\Delta t^2}{2} \left(\mathbf{S}_{\mathbf{U}}^T \left(-\mathbf{F}_{\mathbf{U}}^T \frac{\partial \mathbf{m}}{\partial x} + \mathbf{S}_{\mathbf{U}}^T \mathbf{m} + J_{\mathbf{U}}^{in}\right), \varphi_h\right).\end{aligned} \tag{3.9}$$

We now integrate by parts the second term in the right hand side of (3.9)

$$\begin{aligned}&\left(-\mathbf{F}_{\mathbf{U}}^T \frac{\partial}{\partial x} \left(-\mathbf{F}_{\mathbf{U}}^T \frac{\partial \mathbf{m}}{\partial x} + \mathbf{S}_{\mathbf{U}}^T \mathbf{m} + J_{\mathbf{U}}^{in}\right), \varphi_h\right) \\ &\qquad = \left(-\mathbf{F}_{\mathbf{U}}^T \frac{\partial \mathbf{m}}{\partial x} + \mathbf{S}_{\mathbf{U}}^T \mathbf{m} + J_{\mathbf{U}}^{in}, \frac{\partial \mathbf{F}_{\mathbf{U}} \varphi_h}{\partial x}\right) \\ &= -\left(\mathbf{F}_{\mathbf{U}}^T \frac{\partial \mathbf{m}}{\partial x}, \frac{\partial \mathbf{F}_{\mathbf{U}} \varphi_h}{\partial x}\right) + \left(\mathbf{S}_{\mathbf{U}}^T \mathbf{m}, \frac{\partial \mathbf{F}_{\mathbf{U}} \varphi_h}{\partial x}\right) + \left(J_{\mathbf{U}}^{in}, \frac{\partial \mathbf{F}_{\mathbf{U}} \varphi_h}{\partial x}\right) \\ &\qquad = -\left(\frac{\partial \mathbf{F}_{\mathbf{U}}^T}{\partial x} \mathbf{F}_{\mathbf{U}}^T \frac{\partial \mathbf{m}}{\partial x}, \varphi_h\right) - \left(\mathbf{F}_{\mathbf{U}}^T \mathbf{F}_{\mathbf{U}}^T \frac{\partial \mathbf{m}}{\partial x}, \frac{\partial \varphi_h}{\partial x}\right) \\ &\qquad\quad + \left(\frac{\partial \mathbf{F}_{\mathbf{U}}^T}{\partial x} \mathbf{S}_{\mathbf{U}}^T \mathbf{m}, \varphi_h\right) + \left(\mathbf{F}_{\mathbf{U}}^T \mathbf{S}_{\mathbf{U}}^T \frac{\partial \mathbf{m}}{\partial x}, \frac{\partial \varphi_h}{\partial x}\right) \\ &\qquad\quad + \left(\frac{\partial \mathbf{F}_{\mathbf{U}}^T}{\partial x} J_{\mathbf{U}}^{in}, \varphi_h\right) + \left(\mathbf{F}_{\mathbf{U}}^T J_{\mathbf{U}}^{in}, \frac{\partial \varphi_h}{\partial x}\right).\end{aligned}$$

Replacing into (3.9) and rearranging the terms, we get

$$
\begin{aligned}
(\mathbf{m}^n, \varphi_h) = \left(\mathbf{m}^{n+1}, \varphi_h\right) + \Delta t \Bigg[& \left(\left(\mathbf{S}_{\mathbf{U}}^T + \frac{\Delta t}{2} \frac{\partial \mathbf{F}_{\mathbf{U}}^T}{\partial x} \mathbf{S}_{\mathbf{U}}^T + \frac{\Delta t}{2} \mathbf{S}_{\mathbf{U}}^T \mathbf{S}_{\mathbf{U}}^T \right) \mathbf{m}, \varphi_h \right) \\
& + \left(\left(-\mathbf{F}_{\mathbf{U}}^T - \frac{\Delta t}{2} \frac{\partial \mathbf{F}_{\mathbf{U}}^T}{\partial x} \mathbf{F}_{\mathbf{U}}^T - \frac{\Delta t}{2} \mathbf{S}_{\mathbf{U}}^T \mathbf{F}_{\mathbf{U}}^T \right) \frac{\partial \mathbf{m}}{\partial x}, \varphi_h \right) \\
& - \left(\frac{\Delta t}{2} \left(\mathbf{F}_{\mathbf{U}}^T \mathbf{F}_{\mathbf{U}}^T - \mathbf{F}_{\mathbf{U}}^T \mathbf{S}_{\mathbf{U}}^T \right) \frac{\partial \mathbf{m}}{\partial x}, \frac{\partial \varphi_h}{\partial x} \right) \Bigg] \\
& + \Delta t \left[\left(\left(I + \frac{\Delta t}{2} \mathbf{S}_{\mathbf{U}}^T + \frac{\Delta t}{2} \frac{\partial \mathbf{F}_{\mathbf{U}}^T}{\partial x} \right) J_{\mathbf{U}}^{in}, \varphi_h \right) + \frac{\Delta t}{2} \left(\mathbf{F}_{\mathbf{U}}^T J_{\mathbf{U}}^{in}, \frac{\partial \varphi_h}{\partial x} \right) \right].
\end{aligned}
$$

We observe that for this scheme we have to fulfill the same CFL condition for the state equation i.e. (2.29), because the flux operator of the state and adjoint problem have the same eigenvalues. Therefore, to be sure to satisfy the condition we use the same space and time discretization for both the problems.

3.1.4 Boundary conditions

We observe that in (3.3) have two scalar boundary conditions at each end, involving the variables m_{C0} and $\mathbf{m}(0,t)$ on the left boundary and m_{CL} and $\mathbf{m}(L,t)$ on the right boundary, respectively. We are interested primarily in the variable $\mathbf{m}$. To eliminate the Lagrangian multipliers m_{C0} and m_{CL}, we premultiply the second and third equation of (3.3) by the vectors $\mathbf{v}_0$ and $\mathbf{v}_L$ that are in the orthogonal space to $\dfrac{\partial G_0(\mathbf{U}(0,T))}{\partial \mathbf{U}}$ and $\dfrac{\partial G_L(\mathbf{U}(L,T))}{\partial \mathbf{U}}$ respectively, thus obtaining

$$
\begin{aligned}
\mathbf{v}_0^T [(\mathbf{F}_{\mathbf{U}}^T(\mathbf{U};\beta)\mathbf{m})(0,t) - J_{\mathbf{U}}^{lb}(\mathbf{U}(0,t))] = \mathbf{0}, \\
\mathbf{v}_L^T [(\mathbf{F}_{\mathbf{U}}^T(\mathbf{U};\beta)\mathbf{m})(L,t) + J_{\mathbf{U}}^{rb}(\mathbf{U}(L,t))] = \mathbf{0}.
\end{aligned}
$$

We obtain then one scalar boundary condition per end point, involving only $\mathbf{m}(0,t)$ and $\mathbf{m}(L,t)$, respectively:

$$
\begin{aligned}
\mathbf{v}_0^T (\mathbf{F}_{\mathbf{U}}^T(\mathbf{U};\beta)\mathbf{m})(0,t) &= \mathbf{v}_0^T J_{\mathbf{U}}^{lb}(\mathbf{U}(0,t)), \\
\mathbf{v}_L^T (\mathbf{F}_{\mathbf{U}}^T(\mathbf{U};\beta)\mathbf{m})(L,t) &= -\mathbf{v}_L^T J_{\mathbf{U}}^{rb}(\mathbf{U}(L,t)).
\end{aligned}
\tag{3.10}
$$

In Table 3.1 we represent the quantities that appear in the adjoint boundary conditions, depending to the state boundary conditions that are described in subsection 2.1.5.

State Condition	$\partial G/\partial \mathbf{U}$	$\mathbf{v}$	$\mathbf{v}^T \mathbf{F}_{\mathbf{U}}^T$	$\mathbf{v}^T J_{\mathbf{U}}$
A	$(1,0)^T$	$(0,1)^T$	$((\mathbf{F}_{\mathbf{U}})_{12}, (\mathbf{F}_{\mathbf{U}})_{22})$	$(J_{\mathbf{U}})_2$
Q	$(0,1)^T$	$(1,0)^T$	$((\mathbf{F}_{\mathbf{U}})_{11}, (\mathbf{F}_{\mathbf{U}})_{21})$	$(J_{\mathbf{U}})_1$
p	$\left(\frac{\beta}{2(AA_0)^{1/2}}, 0\right)^T$	$(0,1)^T$	$((\mathbf{F}_{\mathbf{U}})_{12}, (\mathbf{F}_{\mathbf{U}})_{22})$	$(J_{\mathbf{U}})_2$
u	$(-u,1)^T$	$(1,u)^T$	$((\mathbf{F}_{\mathbf{U}})_{11} + u(\mathbf{F}_{\mathbf{U}})_{12}, (\mathbf{F}_{\mathbf{U}})_{22}) + u(\mathbf{F}_{\mathbf{U}})_{22})$	$(J_{\mathbf{U}})_1 + u(J_{\mathbf{U}})_2$

Table 3.1: *Terms in adjoint boundary conditions in relation to the state boundary conditions*

Remark 3.1.3 (Computation of m_{C0} and m_{CL})**.** We note that once we compute the value of $\mathbf{m}$ on the boundaries, it is easy to compute m_{C0} and m_{CL} with the formulae

$$\begin{aligned} m_{C0} =& \frac{1}{\left(\dfrac{\partial G_0(U(0,T))}{\partial \mathbf{U}}\right)_1} \left((F_{\mathbf{U}})_{2,1} m_2(0,t) - \left(J^{lb}_{\mathbf{U}}(\mathbf{U}(0,t))\right)_1\right), \\ m_{CL} =& -\frac{1}{\left(\dfrac{\partial G_L(U(L,T))}{\partial \mathbf{U}}\right)_1} \left((F_{\mathbf{U}})_{2,1} m_2(L,t) + \left(J^{rb}_{\mathbf{U}}(\mathbf{U}(L,t))\right)_1\right) \end{aligned} \tag{3.11}$$

that is obtained from the boundary conditions in (3.3) and by noting that $(F_{\mathbf{U}})_{1,1} = 0$

3.1.5 Compatibility conditions

As for the state equation, the adjoint boundary conditions (3.10) are composed by a single scalar condition for the two unknowns on each boundary side. To solve the problem (3.3) we have to add two more conditions (the compatibility conditions) and we use the same approach of subsection 2.1.6, i.e. the extrapolation of the outgoing characteristics, which consists in extending the equation on the boundary and we getting the value of an unknown from the value at the previous time step.

Let Λ and R be the matrices of eigenvalues and right eigenvectors of the $\mathbf{F}_{\mathbf{U}}$ respectively, such that $R^{-1}\mathbf{F}_{\mathbf{U}}R = \Lambda$. They have the form

$$\Lambda = \begin{pmatrix} \lambda_1 & \\ & \lambda_2 \end{pmatrix} \quad R = L^{-1} = \frac{1}{\varsigma(\lambda_1 - \lambda_2)} \begin{pmatrix} 1 & -1 \\ \lambda_1 & -\lambda_2 \end{pmatrix} =: \begin{pmatrix} \mathbf{r}_1 & \mathbf{r}_2 \end{pmatrix},$$

where L is the left eigenvectors matrix of $\mathbf{F}_{\mathbf{U}}$ in (2.35), $\varsigma = 1/A$, $\mathbf{r}_1$ and $\mathbf{r}_2$ are the right eigenvectors of $\mathbf{F}_{\mathbf{U}}$ and λ_1 and λ_2 are the eigenvectors of $\mathbf{F}_{\mathbf{U}}$ defined in (2.36).

We define the characteristic variable $\mathbf{V}$ such that

$$\frac{\partial \mathbf{V}}{\partial \mathbf{m}} = R^T.$$

Multiplying by R^T equation (3.3) we obtain

$$R^T \frac{\partial \mathbf{m}}{\partial t} + R^T \mathbf{F}^T_{\mathbf{U}} R^{-T} R^T \frac{\partial \mathbf{m}}{\partial x} = R^T \left(\mathbf{S}^T_{\mathbf{U}} \mathbf{m} + J^{in}_{\mathbf{U}}\right),$$

so that

$$\frac{\partial \mathbf{V}}{\partial t} + \Lambda R^T \frac{\partial \mathbf{m}}{\partial x} = R^T \left(\mathbf{S}^T_{\mathbf{U}} \mathbf{m} + J^{in}_{\mathbf{U}}\right).$$

Therefore

$$\frac{\partial \mathbf{V}}{\partial t} + \Lambda \left(\frac{\partial \mathbf{V}}{\partial x} - \frac{\partial R^T}{\partial x}\mathbf{m}\right) = R^T \left(\mathbf{S}^T_{\mathbf{U}} \mathbf{m} + J^{in}_{\mathbf{U}}\right). \tag{3.12}$$

We note that, assuming that R is constant in time,

$$\frac{D\mathbf{V}}{Dt} = R^T \frac{\partial \mathbf{m}}{\partial t} + \Lambda \frac{\partial \mathbf{V}}{\partial x}$$

and, consequently, (3.12) is equivalent to

$$\frac{D\mathbf{V}}{Dt} = \Lambda \frac{\partial R^T}{\partial x}\mathbf{m} + R^T\left(\mathbf{S}_{\mathbf{U}}^T\mathbf{m} + J_{\mathbf{U}}^{in}\right). \tag{3.13}$$

On each end point, we are interested only in the outgoing characteristic that we assume for simplicity to be V_i. Therefore, we consider only one equation of the system (3.13)

$$\frac{D\mathbf{V}_i}{Dt} = \lambda_i \frac{\partial \mathbf{r}_i^T}{\partial x}\mathbf{U} - \mathbf{r}_i^T\mathbf{S}(\mathbf{U}). \tag{3.14}$$

By introducing the same time grid used in Taylor-Galerkin formulation and given the value $\mathbf{V}^{n+1}$, we compute the value $\mathbf{V}_i^n$ using the characteristic outgoing from the foot $\mathbf{V}_{i,*}^{n+1}$

$$\frac{1}{\Delta t}\left(\mathbf{V}_i^n - \mathbf{V}_{i,*}^{n+1}\right) - \lambda_i^{n+1}\left(\frac{\partial \mathbf{r}_i^T}{\partial x}\right)^{n+1}\mathbf{m}_*^{n+1} - \left(\mathbf{r}_i^T\right)^{n+1}\left[\left(\mathbf{S}_{\mathbf{U}}^T\right)^{n+1}\mathbf{m}_*^{n+1} + \left(J_{\mathbf{U}}^{in}\right)^{n+1}\right] = 0.$$

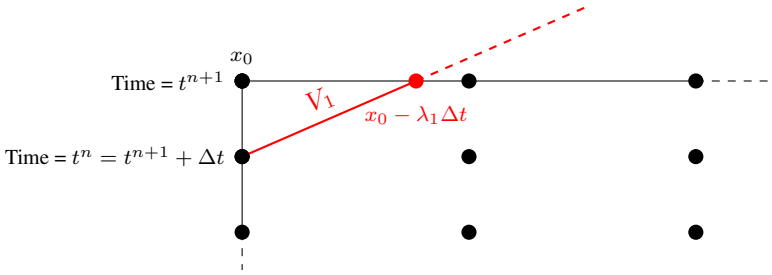

Figure 3.1: *Characteristic extrapolation for the adjoint problem on the left side of the domain*

Thus, the compatibility condition is

$$\left(\mathbf{r}_i^T\right)^{n+1}\mathbf{m}^n = \left(\mathbf{r}_i^T\right)^{n+1}\left\{\mathbf{m}_*^{n+1} + \Delta t\left[\left(\mathbf{S}_{\mathbf{U}}^T\right)^{n+1}\mathbf{m}_*^{n+1} + \left(J_{\mathbf{U}}^{in}\right)^{n+1}\right]\right\} + \Delta t\,\lambda_i^{n+1}\left(\frac{\partial \mathbf{r}_i^T}{\partial x}\right)^{n+1}\mathbf{m}_*^{n+1}.$$

Furthermore, the derivative of R with respect to x is

$$\frac{\partial R}{\partial x} = -\frac{1}{\varsigma(\lambda_1-\lambda_2)^2}\left(\frac{\partial \lambda_1}{\partial x} - \frac{\partial \lambda_2}{\partial x}\right)\begin{pmatrix}1 & -1\\ \lambda_1 & -\lambda_2\end{pmatrix} + \frac{1}{\varsigma(\lambda_1-\lambda_2)}\begin{pmatrix}0 & 0\\ \dfrac{\partial \lambda_1}{\partial x} & -\dfrac{\partial \lambda_2}{\partial x}\end{pmatrix},$$

where the derivatives of the eigenvalues with respect to x are computed by deriving the equation (2.36)

Finally, we impose the boundary and compatibility conditions solving a 2×2 linear system on each side of the domain

$$\begin{pmatrix}\mathbf{r}_1^T\\ \mathbf{v}_0^T\mathbf{F}_{\mathbf{U}}^T(\mathbf{U}(0,t^n))\end{pmatrix}\begin{pmatrix}m_1^n\\ m_2^n\end{pmatrix} = \begin{pmatrix}\mathbf{r}_1^T\left[\mathbf{m}_*^{n+1} + \Delta t\left(\mathbf{S}_{\mathbf{U}}^T\mathbf{m}_*^{n+1} + J_{\mathbf{U}}^{in}\right)\right] + \Delta t\,\Lambda\dfrac{\partial \mathbf{r}_1^T}{\partial x}\mathbf{m}_*^{n+1}\\ \mathbf{v}_0^T J_{\mathbf{U}}^{lb}(\mathbf{U}(0,t^n))\end{pmatrix},$$

$$\begin{pmatrix}\mathbf{r}_2^T\\ \mathbf{v}_L^T\mathbf{F}_{\mathbf{U}}^T(\mathbf{U}(L,t^n))\end{pmatrix}\begin{pmatrix}m_1^n\\ m_2^n\end{pmatrix} = \begin{pmatrix}\mathbf{r}_2^T\left[\mathbf{m}_*^{n+1} + \Delta t\left(\mathbf{S}_{\mathbf{U}}^T\mathbf{m}_*^{n+1} + J_{\mathbf{U}}^{in}\right)\right] + \Delta t\,\Lambda\dfrac{\partial \mathbf{r}_2^T}{\partial x}\mathbf{m}_*^{n+1}\\ \mathbf{v}_L^T J_{\mathbf{U}}^{rb}(\mathbf{U}(L,t^n))\end{pmatrix}.$$

3.1.6 Optimality condition

Once we have computed the solutions of the state and the adjoint problems, we still need to enforce the optimality condition given by the last KKT condition in (1.7)-(1.9). We recall that such condition is obtained as the derivative of the Lagrangian with respect to the parameter. We write the relation explicitly.

$$\begin{aligned}
\frac{\partial \mathcal{L}}{\partial \beta}(\mathbf{U},\beta,\overline{\mathbf{m}}) &= \frac{\partial J}{\partial \beta}(\mathbf{U},\beta) + \frac{\partial}{\partial \beta}\left\langle \mathbf{e}(\mathbf{U},\beta),\overline{\mathbf{m}}\right\rangle \\
&= \frac{\partial J}{\partial \beta}(\mathbf{U},\beta) + \frac{\partial}{\partial \beta}\left\{ \int_0^T \int_0^L \left(\frac{\partial \mathbf{U}}{\partial t} + \frac{\partial \mathbf{F}}{\partial x}(\mathbf{U};\beta) + \mathbf{S}(\mathbf{U};\beta),\mathbf{m}\right) dxdt \right. \\
&+ \int_0^T [((G_0(\mathbf{U}(0,t)) - g_0(t)), m_{C0}) + ((G_L(\mathbf{U}(L,t)) - g_L(t)), m_{CL})]dt \\
&\left. + \int_0^L ((\mathbf{U}(x,0) - \mathbf{U}_0(x)),\mathbf{m}_0)dx \right\} \\
&= \frac{\partial J}{\partial \beta}(\mathbf{U},\beta) + \int_0^T \int_0^L \left(\frac{\partial}{\partial \beta}\frac{\partial \mathbf{F}}{\partial x}(\mathbf{U};\beta) + \frac{\partial \mathbf{S}}{\partial \beta}(\mathbf{U};\beta),\mathbf{m}\right) dxdt \\
&+ \int_0^T \left[\left(\frac{\partial G_0(\mathbf{U}(0,t))}{\partial \beta}, m_{C0}\right) + \left(\frac{\partial G_L(\mathbf{U}(L,t))}{\partial \beta}, m_{CL}\right)\right] dt
\end{aligned} \tag{3.15}$$

where

$$\frac{\partial S}{\partial \beta}(U;\beta) = \begin{pmatrix} 0 \\ -\frac{1}{3\rho}\left(\frac{A}{A^0}\right)^{3/2}\frac{\partial A^0}{\partial x} \end{pmatrix},$$

and

$$\frac{\partial}{\partial \beta}\frac{\partial F}{\partial x}(U;\beta) = \begin{pmatrix} 0 \\ \frac{1}{2\rho}\sqrt{\frac{A}{A^0}}\frac{\partial A}{\partial x} - \frac{1}{6\rho}\left[\left(\frac{A}{A^0}\right)^{3/2}\right]\frac{\partial A^0}{\partial x} \end{pmatrix}.$$

We note that the term involving the initial conditions disappears because it does not depend on β. For the same reason, the terms that contain the multipliers m_{C0} or m_{CL} are present only if the functions G_L or G_0 depend explicitly on β, for instance when we impose conditions on the pressure or absorbing boundary conditions. Therefore we need to compute explicitly m_{C0} or m_{CL} from (3.11) only in these cases.

For example, in the simplest case in which

- we do not take into account the vessel tapering (i.e. $\partial A_0/\partial x = 0$),
- we do not have any explicit dependence on β in the cost functional J (e.g. the one in (3.2)) ,
- we do not have any explicit dependence on β in the boundary functions G_L and G_0 (e.g. conditions on flow rate or section area),

equation (3.15) simplifies as

$$\frac{\partial \mathcal{L}}{\partial \beta}(\mathbf{U}, \beta, \overline{\mathbf{m}}) = \int_0^T \int_0^L \frac{(\mathbf{m})_2}{2\rho} \sqrt{\frac{A}{A_0}} \frac{\partial A}{\partial x} dx dt. \tag{3.16}$$

3.2 Optimal control for a network of 1D-FSI models

The previous framework can be extended to handle the more general case of a network of vessels. We consider, as state model, the model described in section 2.2 composed by the set $\mathcal{N}_m$ of models connected by the set $\mathcal{N}_c$ of coupling nodes:

$$\begin{cases} \dfrac{\partial \mathbf{U}_i}{\partial t} + \dfrac{\partial \mathbf{F}}{\partial x}(\mathbf{U}_i; \beta_i) = \mathbf{S}(\mathbf{U}_i; \beta_i) & x \in (0, L_i),\ t \in (0, T), & \forall i \in \mathcal{N}_m \\ G_0^k(\mathbf{U}_k(0,t), \beta) = g_0^k(t) & t \in (0, T), & \forall k \in \mathcal{N}_m^{init} \\ G_L^k(\mathbf{U}_k(L_k,t), \beta) = g_L^k(t) & t \in (0, T), & \forall k \in \mathcal{N}_m^{term} \\ \sum_{i \in \mathcal{N}_m^{R_j}} Q_i(L_i, t) = \sum_{i \in \mathcal{N}_m^{L_j}} Q_i(0, t) & t \in (0, T), & \forall j \in \mathcal{N}_c \\ P_{\bar{i}}(L_{\bar{i}}, t) = P_k(L_k, t) & t \in (0, T), & \bar{i} \in \mathcal{N}_m^{R_j},\ \forall j \in \mathcal{N}_c, \\ & & \forall k \in \mathcal{N}_m^{R_j},\ k \neq \bar{i} \\ P_{\bar{i}}(L_{\bar{i}}, t) = P_k(0, t) & t \in (0, T), & \bar{i} \in \mathcal{N}_m^{R_j},\ \forall j \in \mathcal{N}_c, \\ & & \forall k \in \mathcal{N}_m^{L_j} \\ \mathbf{U}_i(x, 0) = \mathbf{U}_{0,i}(x) & x \in (0, L_i), & \forall i \in \mathcal{N}_m \end{cases} \tag{3.17}$$

where $U_{TOT} = \{\mathbf{U}_i\}^{i \in \mathcal{N}_m}$, $\beta_{TOT} = \{\beta_i\}^{i \in \mathcal{N}_m}$ and $\mathcal{N}_m^{term}$, $\mathcal{N}_m^{init}$, $\mathcal{N}_m^{R_j}$, $\mathcal{N}_m^{L_j}$ are the subsets of $\mathcal{N}_m$ that are formed by the distal vessels, the proximal vessels, the vessels on the right of the j-th coupling node and the vessels on the left of the j-th coupling node, respectively. For each coupling node, we call $\bar{i}$ the first element of $\mathcal{N}_m^{R_j}$.

The conditions

$$G_0^k(\mathbf{U}_k(0,t), \beta) = g_0^k(t), \quad G_L^k(\mathbf{U}_k(L_k,t), \beta) = g_L^k(t)$$

are generic scalar boundary conditions on proximal and distal vessels, where G_0^k and G_L^k can be any appropriate functions of the state variables evaluated on the boundaries that satisfy (2.31) and g_0^k and g_t^k are the given functions of time.

We recall that this model consists in the splitting of the network into a set of pipes, which are modelled by a set of 1D-FSI models (one for each vessel) and they are coupled with coupling conditions at every bifurcation or branch that enforce the conservation of the mass (fourth equation in (3.17)) and continuity of the total pressure (fourth and fifth equations of (3.17))

3.2.1 Lagrangian functional

The Lagrangian associated to the state problem (3.17) can be easily written as

$$
\begin{aligned}
&\mathcal{L}(\mathbf{U}_{TOT}, \beta_{TOT}, \overline{\mathbf{m}}_{TOT}) = \\
&\quad = J(\mathbf{U}_{TOT}, \beta_{TOT}) + \sum_{i \in \mathcal{N}_m} \int_0^T \int_0^{L_i} \left(\left(\frac{\partial \mathbf{U}_i}{\partial t} + \frac{\partial \mathbf{F}(\mathbf{U}_i; \beta_i)}{\partial x} + \mathbf{S}(\mathbf{U}_i; \beta_i) \right), \mathbf{m}_i \right) dxdt + \\
&\qquad + \sum_{k \in \mathcal{N}_m^{init}} \int_0^T \left(G_0^k(\mathbf{U}_k(0,t)) - g_0^k(t), m_{C0,k} \right) dt \\
&\qquad + \sum_{k \in \mathcal{N}_m^{term}} \int_0^T \left(G_L^k(\mathbf{U}_k(L_k,t)) - g_L^k(t), m_{CL,k} \right) dt + \\
&\qquad + \sum_{j \in \mathcal{N}_c} \int_0^T \left(\sum_{i \in \mathcal{N}_m^{R_j}} Q_i(L_i,t) - \sum_{i \in \mathcal{N}_m^{L_j}} Q_i(0,t), m_{CC,j} \right) dt \\
&\qquad + \sum_{j \in \mathcal{N}_c} \sum_{\substack{k \in \mathcal{N}_m^{R_j} \\ k \neq \bar{i}}} \int_0^T \left(P_{\bar{i}}(L_{\bar{i}},t) - P_k(L_k,t), m_{CCR_j,k} \right) \\
&\qquad + \sum_{j \in \mathcal{N}_c} \sum_{k \in \mathcal{N}_m^{L_j}} \int_0^T \left(P_{\bar{i}}(L_{\bar{i}},t) - P_k(0,t), m_{CCL_j,k} \right) \\
&\qquad + \sum_{i \in \mathcal{N}_m} \int_0^{L_i} \left(\mathbf{U}_i(x,0) - \mathbf{U}_{0,i}(x), \mathbf{m}_{0,i} \right) dx
\end{aligned}
\tag{3.18}
$$

where $\mathbf{m}_{TOT}$ is the set of all the adjoint variables. As in the single vessel case (3.1), $\mathbf{m}_i$ and , $\mathbf{m}_{0,i}, i \in \mathcal{N}_m$ are vector functions, while all the other adjoint variables are scalar variables.

We define $J(\mathbf{U}_{TOT}, \beta_{TOT})$ as cost functional that takes into account the difference between the solution of (2.19) and some measurements, and can be written in a general way

$$
\begin{aligned}
J(\mathbf{U}_{TOT}, \beta_{TOT}) = &\sum_{i \in \mathcal{N}_m} J^{in}(\mathbf{U}_i, \beta_i) + \sum_{k \in \mathcal{N}_m^{init}} J^{lb}(\mathbf{U}_k, \beta_k) + \sum_{k \in \mathcal{N}_m^{term}} J^{rb}(\mathbf{U}_k, \beta_k) \\
&+ \sum_{j \in \mathcal{N}_c} \left(\sum_{k \in \mathcal{N}_m^{R_j}} J^{rb}(\mathbf{U}_k, \beta_k) + \sum_{k \in \mathcal{N}_m^{L_j}} J^{lb}(\mathbf{U}_k, \beta_k) \right),
\end{aligned}
$$

where

- $J^{in}(\mathbf{U}_i, \beta_i)$ depends only on the quantities inside the i-th vessel;
- $J^{lb}(\mathbf{U}_k, \beta_k)$ depends on the quantities on the left extreme of the k-th vessel;
- $J^{rb}(\mathbf{U}_k, \beta_k)$ depends on the quantities on the right extreme of the k-th vessel.

3.2.2 Adjoint problem

To obtain the adjoint problem we have to compute the derivative of the Lagrangian functional with respect to the state variable, namely $\mathcal{L}_{\mathbf{U}_{TOT}}(\mathbf{U}_{TOT}, \beta_{TOT}, \overline{\mathbf{m}}_{TOT}) = \mathbf{0}$. After some computations, the adjoint problem can be written as

$$
\begin{cases}
\dfrac{\partial \mathbf{m}_i}{\partial t} + \mathbf{F}_{\mathbf{U}}^T(\mathbf{U}_i;\beta_i)\dfrac{\partial \mathbf{m}_i}{\partial x} - \mathbf{S}_{\mathbf{U}}^T(\mathbf{U}_i;\beta_i)\mathbf{m}_i = J_{\mathbf{U}}^{in}(\mathbf{U}_i) & x \in (0, L_i),\ t \in (0,T), \\ & \forall i \in \mathcal{N}_m, \\
\dfrac{\partial G_0^k(\mathbf{U}_k(0,T))}{\partial \mathbf{U}}^T m_{C0,k} - (\mathbf{F}_{\mathbf{U}}^T(\mathbf{U}_k;\beta_k)\mathbf{m}_k)(0,t) = J_{\mathbf{U}}^{lb}(\mathbf{U}_k) & t \in (0,T), \\ & \forall k \in \mathcal{N}_m^{init}, \\
\dfrac{\partial G_L^k(\mathbf{U}_k(L_k,T))}{\partial \mathbf{U}}^T m_{CL,k} + (\mathbf{F}_{\mathbf{U}}^T(\mathbf{U}_k;\beta_k)\mathbf{m}_k)(L,t) = J_{\mathbf{U}}^{rb}(\mathbf{U}_k) & t \in (0,T), \\ & \forall k \in \mathcal{N}_m^{term}, \\
\dfrac{\partial Q_{\bar{i}}(L_{\bar{i}},t)}{\partial \mathbf{U}} m_{CC,j} + & \\
\quad + \dfrac{\partial P_{\bar{i}}(L_{\bar{i}},t)}{\partial \mathbf{U}} \left(\sum_{\substack{k \in \mathcal{N}_m^{R_j} \\ k \neq \bar{i}}} m_{CCR_j,k} + \sum_{k \in \mathcal{N}_m^{L_j}} m_{CCL_j,k} \right) + & \\
\quad + (\mathbf{F}_{\mathbf{U}}^T(\mathbf{U}_{\bar{i}};\beta_{\bar{i}})\mathbf{m}_{\bar{i}})(L_{\bar{i}},t) = -J_{\mathbf{U}}^{rb}(\mathbf{U}_{\bar{i}}) & t \in (0,T), \\ & \bar{i} \in \mathcal{N}_m^{R_j}, \\ & \forall j \in \mathcal{N}_c \\
\dfrac{\partial Q_k(L_k,t)}{\partial \mathbf{U}} m_{CC,j} - \dfrac{\partial P_k(L_k,t)}{\partial \mathbf{U}} m_{CCR_j,k} + & \\
\quad + (\mathbf{F}_{\mathbf{U}}^T(\mathbf{U}_k;\beta_k)\mathbf{m}_k)(L_k,t) = -J_{\mathbf{U}}^{rb}(\mathbf{U}_k) & t \in (0,T), \\ & \forall j \in \mathcal{N}_c, \\ & \forall k \in \mathcal{N}_m^{R_j}, k \neq \bar{i} \\
\dfrac{\partial Q_k(0,t)}{\partial \mathbf{U}} m_{CC,j} + \dfrac{\partial P_k(0,t)}{\partial \mathbf{U}} m_{CCL_j,k} + & \\
\quad + (\mathbf{F}_{\mathbf{U}}^T(\mathbf{U}_k;\beta_k)\mathbf{m}_k)(0,t) = J_{\mathbf{U}}^{lb}(\mathbf{U}_k) & t \in (0,T), \\ & \forall j \in \mathcal{N}_c, \\ & \forall k \in \mathcal{N}_m^{L_j} \\
\mathbf{m}_{0,i} = \mathbf{m}_i(x,0) & x \in (0, L_i), \\ & \forall i \in \mathcal{N}_m \\
\mathbf{m}_i(x,T) = 0 & x \in (0, L_i), \\ & \forall i \in \mathcal{N}_m.
\end{cases}
\tag{3.19}
$$

The adjoint problem for a network of vessel (3.19) has a structure similar to the

adjoint problem for a single vessel (3.3). They are both composed by linear hyperbolic backward-in-time equations and have analogous boundary conditions (for the treatment of adjoint boundary conditions we refer to 3.1.4). The main difference lays in the presence of coupling conditions.

We solve numerically problem (3.19) by considering each vessel model in parallel, discretized by a second order Taylor-Galerkin scheme in time and linear finite element method in space (exactly as we described for the single vessel model in subsection 3.1.3). At end points of each vessel we impose boundary conditions, int the same way as we described in subsection 3.1.4) if the vessel is distal or proximal as well as coupling conditions. Then we close the system with numerical compatibility conditions as in subsection 3.1.5.

3.2.3 Adjoint coupling conditions

We now describe how we treat the coupling conditions in the adjoint problem. We consider a generic coupling node j inside the network. We define $\mathcal{N}_m^{R_j}$ the ordered set of models that enter the node and $\mathcal{N}_m^{L_j}$ the ordered set of models that leave the node, as shown in figure 3.2. Obviously, each set has at least one member. We call $\bar{i}$ the first member of $\mathcal{N}_m^{R_j}$. We define n_R^j the cardinality of $\mathcal{N}_m^{R_j}$, n_L^j the cardinality of $\mathcal{N}_m^{L_j}$ and $n^j = n_R^j + n_L^j$.

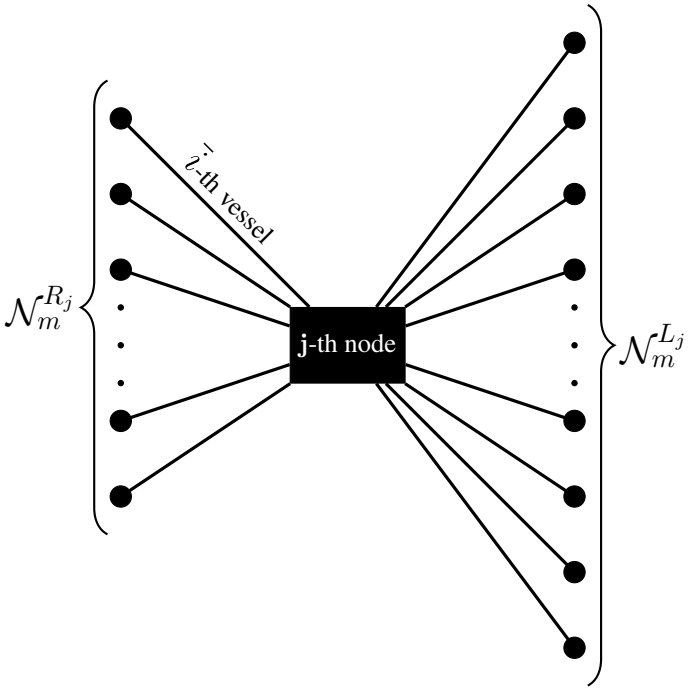

Figure 3.2: *Generic coupling node configuration*

We recall that the adjoint coupling conditions have the form

$$
\begin{aligned}
&\frac{\partial Q_{\bar{i}}(L_{\bar{i}},t)}{\partial \mathbf{U}_{\bar{i}}} m_{CC,j} + \\
&\quad + \frac{\partial P_{\bar{i}}(L_{\bar{i}},t)}{\partial \mathbf{U}_{\bar{i}}} \left(\sum_{\substack{k\in\mathcal{N}_m^{R_j} \\ k\neq\bar{i}}} m_{CCR_j,k} + \sum_{k\in\mathcal{N}_m^{L_j}} m_{CCL_j,k} \right) + \\
&\qquad + (\mathbf{F}^T_{\mathbf{U}_{\bar{i}}}(\mathbf{U}_{\bar{i}};\beta_{\bar{i}})\mathbf{m}_{\bar{i}})(L_{\bar{i}},t) = -J^{rb}_{\mathbf{U}_{\bar{i}}}(\mathbf{U}_{\bar{i}}) \qquad && t\in(0,T), \\
&\qquad\qquad && \bar{i}\in\mathcal{N}_m^{R_j}, \\
&\qquad\qquad && \forall j\in\mathcal{N}_c \\
&\frac{\partial Q_k(L_k,t)}{\partial \mathbf{U}_k} m_{CC,j} - \frac{\partial P_k(L_k,t)}{\partial \mathbf{U}_k} m_{CCR_j,k} + \\
&\qquad + (\mathbf{F}^T_{\mathbf{U}_k}(\mathbf{U}_k;\beta_k)\mathbf{m}_k)(L_k,t) = -J^{rb}_{\mathbf{U}_k}(\mathbf{U}_k) \qquad && t\in(0,T), \\
&\qquad\qquad && \forall j\in\mathcal{N}_c, \\
&\qquad\qquad && \forall k\in\mathcal{N}_m^{R_j}, k\neq\bar{i} \\
&\frac{\partial Q_k(0,t)}{\partial \mathbf{U}_k} m_{CC,j} + \frac{\partial P_k(0,t)}{\partial \mathbf{U}_k} m_{CCL_j,k} + \\
&\qquad + (\mathbf{F}^T_{\mathbf{U}_k}(\mathbf{U}_k;\beta_k)\mathbf{m}_k)(0,t) = J^{lb}_{\mathbf{U}_k}(\mathbf{U}_k) \qquad && t\in(0,T), \\
&\qquad\qquad && \forall j\in\mathcal{N}_c, \\
&\qquad\qquad && \forall k\in\mathcal{N}_m^{L_j}
\end{aligned}
$$

We observe that these conditions constitute a system of $2n^j$ equations in the $3n^j$ variables $(m_{CC,j}, \mathbf{m}_{CCR_j}, \mathbf{m}_{CCL_j}, \mathbf{m}_{R_j}, \mathbf{m}_{L_j})$ where

$$
\begin{aligned}
&\mathbf{m}_{CCR_j} = \{m_{CCR_j,k},\ k\in\mathcal{N}_m^{R_j}, k\neq\bar{i}\} && \mathbf{m}_{CCL_j} = \{m_{CCL_j,k},\ k\in\mathcal{N}_m^{L_j}\} \\
&\mathbf{m}_{R_j} = \{\mathbf{m}_i(L_i,t),\ i\in\mathcal{N}_m^{R_j}\} && \mathbf{m}_{L_j} = \{\mathbf{m}_i(0,t),\ i\in\mathcal{N}_m^{L_j}\}
\end{aligned}
$$

We write this system in matrix form

$$
A\mathbf{m}^j_{CC} + \mathcal{F}^j\mathbf{m}^j = \mathcal{J}^j, \tag{3.20}
$$

where

$$
\mathbf{m}^j = \begin{pmatrix} \mathbf{m}_{R_j} \\ \mathbf{m}_{L_j} \end{pmatrix} \in \mathbb{R}^{2n^j},\ \mathbf{m}^j_{CC} = \begin{pmatrix} m_{CC,j} \\ \mathbf{m}_{CCR_j} \\ \mathbf{m}_{CCL_j} \end{pmatrix} \in \mathbb{R}^{n^j},
$$

and

$$
A = \begin{pmatrix}
\frac{\partial Q_{\bar{i}}(L_{\bar{i}},t)}{\partial \mathbf{U}_{\bar{i}}} & \frac{\partial P_{\bar{i}}(L_{\bar{i}},t)}{\partial \mathbf{U}_{\bar{i}}} & \cdots & \frac{\partial P_{\bar{i}}(L_{\bar{i}},t)}{\partial \mathbf{U}_{\bar{i}}} & \frac{\partial P_{\bar{i}}(L_{\bar{i}},t)}{\partial \mathbf{U}_{\bar{i}}} & \cdots & \frac{\partial P_{\bar{i}}(L_{\bar{i}},t)}{\partial \mathbf{U}_{\bar{i}}} \\
\mathbf{Q}_{\mathbf{U},R_j} & \mathbf{P}^2_{\mathbf{U},R} & \cdots & \mathbf{P}^{n^j_R}_{\mathbf{U},R} & & & \\
\mathbf{Q}_{\mathbf{U},L_j} & & & & \mathbf{P}^1_{\mathbf{U},L} & \cdots & \mathbf{P}^{n^j_L}_{\mathbf{U},L}
\end{pmatrix} \in \mathbb{R}^{(2n^j)\times n^j},
$$

$$\mathcal{F}^j = \begin{pmatrix} \mathcal{F}_1^{R_j} & & & & & & \\ & \ddots & & & & & \\ & & \mathcal{F}_{n_R^j}^{R_j} & & & & \\ & & & \mathcal{F}_1^{L_j} & & & \\ & & & & \ddots & & \\ & & & & & \mathcal{F}_{n_L^j}^{L_j} \end{pmatrix} \in \mathbb{R}^{2n^j \times 2n^j},$$

$$\mathcal{J}^j \in \mathbb{R}^{2\times n^j}, \quad (\mathcal{J}^j)_k = \begin{cases} -J_{\mathbf{U}}^{rb}(\mathbf{U}_{\bar{i}}) & k = 1, \\ -J_{\mathbf{U}}^{rb}(\mathbf{U}_k) & 1 < k \leqslant n_R^j, \\ J_{\mathbf{U}}^{lb}(\mathbf{U}_k) & n_R^j < k \leqslant n^j \end{cases}$$

and

$$\mathbf{Q}_{\mathbf{U},R_j} \in \mathbb{R}^{2(n_{R_j}^j - 1)} \quad (\mathbf{Q}_{\mathbf{U},R_j})_k = \begin{cases} 0 & \text{if } k \text{ is odd,} \\ 1 & \text{if } k \text{ is even,} \end{cases}$$

$$\mathbf{Q}_{\mathbf{U},L_j} \in \mathbb{R}^{2n_{L_j}^j} \qquad (\mathbf{Q}_{\mathbf{U},L_j})_k = \begin{cases} 0 & \text{if } k \text{ is odd,} \\ 1 & \text{if } k \text{ is even,} \end{cases}$$

$$\mathbf{P}_{\mathbf{U},R}^k \in \mathbb{R}^{2(n_{R_j}^j - 1)\times 2}, \quad k \in \mathcal{N}_m^{R_j}, k \neq \bar{i},$$

$$\left(\mathbf{P}_{\mathbf{U},R}^k\right)_{l,*} = \begin{cases} (\ 0,\ 0\ ) & l \neq k \\ \left(-\left(\dfrac{\partial P_k(L_k,t)}{\partial \mathbf{U}_k}\right)_1,\ -\left(\dfrac{\partial P_k(L_k,t)}{\partial \mathbf{U}_k}\right)_2 \right) & l = k \end{cases}$$

$$\mathbf{P}_{\mathbf{U},L}^k \in \mathbb{R}^{2n_{L_j}^j \times 2}, \quad k \in \mathcal{N}_m^{L_j},$$

$$\left(\mathbf{P}_{\mathbf{U},L}^k\right)_{l,*} = \begin{cases} (\ 0,\ 0\ ) & l \neq k \\ \left(\left(\dfrac{\partial P_k(0,t)}{\partial \mathbf{U}_k}\right)_1,\ \left(\dfrac{\partial P_k(0,t)}{\partial \mathbf{U}_k}\right)_2 \right) & l = k \end{cases}$$

$$\mathcal{F}_k^{R_j} = \mathbf{F}_{\mathbf{U}_k}^T(\mathbf{U}_k(L_k,t);\beta_k) \in \mathbb{R}^{2\times 2}, \quad k \in \mathcal{N}_m^{R_j},$$

$$\mathcal{F}_k^{L_j} = \mathbf{F}_{\mathbf{U}_k}^T(\mathbf{U}_k(0,t);\beta_k) \in \mathbb{R}^{2\times 2}, \quad k \in \mathcal{N}_m^{L_j},$$

As for the boundary conditions, we are interested primarily in the variables $\mathbf{m}_j$ and, therefore, to eliminate the Lagrangian multipliers $\mathbf{m}_{CC}^j$, we premultiply the system (3.20) by a matrix

$$B = \begin{pmatrix} \mathbf{b}_{1,1} & \mathbf{b}_{1,2} & \mathbf{b}_{1,3} & \cdots & \mathbf{b}_{1,n^j} \\ \mathbf{b}_{2,1} & \mathbf{b}_{2,2} & & & \\ \mathbf{b}_{3,1} & & \mathbf{b}_{3,3} & & \\ \vdots & & & \ddots & \\ \mathbf{b}_{n^j,1} & & & & \mathbf{b}_{n^j,n^j} \end{pmatrix} \in \mathbb{R}^{n^j \times (2n^j)}$$

where

$$\mathbf{b}_{1,1} = \begin{pmatrix} \dfrac{1}{\left(\dfrac{\partial P_{\bar{i}}}{\partial \mathbf{U}_{\bar{i}}}\right)_1} & 0 \end{pmatrix}$$

$$\mathbf{b}_{1,k} = \begin{cases} \begin{pmatrix} \dfrac{1}{\left(\dfrac{\partial P_k}{\partial \mathbf{U}_k}\right)_1} & 0 \end{pmatrix} & 1 < k \leqslant n^j_{R_j} \\ \begin{pmatrix} -\dfrac{1}{\left(\dfrac{\partial P_k}{\partial \mathbf{U}_k}\right)_1} & 0 \end{pmatrix} & n^j_{R_j} < k \leqslant n^j_{L_j} \end{cases}$$

$$\mathbf{b}_{k,1} = \begin{pmatrix} -\dfrac{\left(\dfrac{\partial P_{\bar{i}}}{\partial \mathbf{U}_{\bar{i}}}\right)_2}{\left(\dfrac{\partial P_{\bar{i}}}{\partial \mathbf{U}_{\bar{i}}}\right)_1} & 1 \end{pmatrix}$$

$$\mathbf{b}_{k,k} = \begin{cases} \begin{pmatrix} -\dfrac{\left(\dfrac{\partial P_k}{\partial \mathbf{U}_k}\right)_2}{\left(\dfrac{\partial P_k}{\partial \mathbf{U}_k}\right)_1} & 1 \end{pmatrix} & 1 < k \leqslant n^j_{R_j} \\ \begin{pmatrix} \dfrac{\left(\dfrac{\partial P_k}{\partial \mathbf{U}_k}\right)_2}{\left(\dfrac{\partial P_k}{\partial \mathbf{U}_k}\right)_1} & -1 \end{pmatrix} & n^j_{R_j} < k \leqslant n^j_{L_j} \end{cases}$$

The rows of B are orthogonal to the columns of A. In this way, we eliminate the variable $\mathbf{m}^j_{CC}$ and we have to solve the linear system of size $2n^j \times 2n^j$

$$B\mathcal{F}^j\mathbf{m}^j = B\mathcal{J}^j. \tag{3.21}$$

Remark 3.2.1 (Computation of m_{C0} and m_{CL})**.** We note that once we have computed $\mathbf{m}^j$, we recover easily to compute m^j_{CC} by inverting the relations (3.20)

$$\mathbf{m}^j_{CC} = A^\dagger(\mathcal{J}^j - \mathcal{F}^j\mathbf{m}^j),$$

where $A^\dagger$ is the pseudo-inverse of A.

3.2.4 Optimality condition

Once we compute $\mathbf{U}_{TOT}$ from the state problem (3.17) and $\overline{\mathbf{m}}_{TOT}$ from the adjoint problem (3.19), we can compute the optimality condition, deriving the Lagrangian (3.18) with respect to β_{TOT}

$$
\begin{aligned}
\frac{\partial \mathcal{L}}{\partial \beta_{TOT}}(\mathbf{U}_{TOT}, \beta_{TOT}, \overline{\mathbf{m}}_{TOT}) &= \frac{\partial J}{\partial \beta_{TOT}}(\mathbf{U}_{TOT}, \beta_{TOT}) \\
&+ \sum_{i \in \mathcal{N}_m} \int_0^T \int_0^{L_i} \left(\left(\frac{\partial}{\partial \beta_i} \frac{\partial \mathbf{F}(\mathbf{U}_i; \beta_i)}{\partial x} + \frac{\partial \mathbf{S}}{\partial \beta_i}(\mathbf{U}_i; \beta_i) \right), \mathbf{m}_i \right) dx dt + \\
&+ \sum_{k \in \mathcal{N}_m^{init}} \int_0^T \left(\frac{\partial G_0^k}{\partial \beta_k}(\mathbf{U}_k(0,t), \beta_k), m_{C0,k} \right) dt \\
&+ \sum_{k \in \mathcal{N}_m^{term}} \int_0^T \left(\frac{\partial G_L^k}{\partial \beta_k}(\mathbf{U}_k(L_k,t), \beta_k), m_{CL,k} \right) dt + \\
&+ \sum_{j \in \mathcal{N}_c} \sum_{\substack{k \in \mathcal{N}_m^{R_j} \\ k \neq \bar{i}}} \int_0^T \left(\frac{\partial P_{\bar{i}}}{\partial \beta_{\bar{i}}}(L_{\bar{i}}, t) - \frac{\partial P_k}{\partial \beta_k}(L_k, t), m_{CCR_j,k} \right) \\
&+ \sum_{j \in \mathcal{N}_c} \sum_{k \in \mathcal{N}_m^{L_j}} \int_0^T \left(\frac{\partial P_{\bar{i}}}{\partial \beta_{\bar{i}}}(L_{\bar{i}}, t) - \frac{\partial P_k}{\partial \beta_k}(0, t), m_{CCL_j,k} \right)
\end{aligned}
\tag{3.22}
$$

where

$$
\frac{\partial P_i}{\partial \beta_i}(x,t) = \left(\sqrt{\frac{A_i(x,t)}{A_i^0}} - 1 \right).
$$

We note that the optimality condition does not depend on $\mathbf{m}_{0,i}$ and $m_{CC,j}$ because initial conditions as well as the coupling conditions stating the conservation of mass are independent of the compliance parameter. In the same way, if the boundary conditions are independent of β_{TOT} (i.e. conditions on area, flow rate or velocity), the adjoint variables on the boundaries do not appear in (3.22). either.

3.2.5 The example of a bifurcation

We now analyze the particular case of a bifurcation composed of three vessels (see figure 3.3), that is the simplest type of network. From this point on, we refer to the vessels using the numbering introduced in the figure. We consider the following state problem

$$
\begin{cases}
\dfrac{\partial \mathbf{U}_i}{\partial t} + \dfrac{\partial \mathbf{F}(\mathbf{U}_i; \beta_i)}{\partial x} + \mathbf{S}(\mathbf{U}_i; \beta_i) = 0, & x \in (0, L_i),\ t \in (0,T), & i = 1,2,3 \\
G_0^1(\mathbf{U}_1(0,t), \beta_1) = g_0^1(t) & t \in (0,T) & \\
G_{L_i}^i(\mathbf{U}_i(L_i,t), \beta_i) = g_{L_i}^i(t) & t \in (0,T), & i = 2,3 \\
Q_1(L,t) = Q_2(0,t) + Q_3(0,t) & t \in (0,T), & \\
P_1(L,t) = P_2(0,t) & t \in (0,T), & \\
P_1(L,t) = P_3(0,t) & t \in (0,T), & \\
\mathbf{U}_i(x,0) = \mathbf{U}_{0,i}(x) & x \in (0, L_i), & i = 1,2,3
\end{cases}
\tag{3.23}
$$

where the unknowns are $\mathbf{U}_{TOT} = (\mathbf{U}_1, \mathbf{U}_2, \mathbf{U}_3)^T$ and the set of parameters is $\beta_{TOT} = (\beta_1, \beta_2, \beta_3)^T$. In this simple model:

- the set of models is $\mathcal{N}_m = \{1, 2, 3\}$;
- the set of proximal models is $\mathcal{N}_m^{init} = \{1\}$;
- the set of distal models is $\mathcal{N}_m^{term} = \{2, 3\}$;
- the set of coupling nodes is $\mathcal{N}_c = \{1\}$;
- the set of models entering the only coupling node is $\mathcal{N}_m^{R_j} = \{1\}$;
- the set of models leaving the only coupling node is $\mathcal{N}_m^{L_j} = \{2, 3\}$.

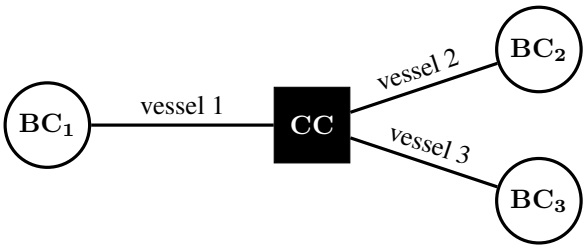

Figure 3.3: *Schematic representation of a bifurcation*

We impose boundary conditions at the inlet of the bifurcation i.e. at the inlet of the first vessel (second equation in the system (3.23)) and at the outlet of the bifurcation i.e. at the outlet of the second and third vessels (third equation in the system (3.23)). Then, to link the three models, we apply coupling conditions on the continuity of the total pressure and the conservation of the flow, that involve the value of $\mathbf{U}_1$ at the outlet and of $\mathbf{U}_2$ and $\mathbf{U}_3$ at the inlet (third, fourth and sixth equation in the system (3.23)).

We consider a cost functional $J(\mathbf{U}_{TOT}, \beta_{TOT})$ that takes into account the difference between the solution of (3.23) and the measurements, and can be split in the following way.

$$J(\mathbf{U}_{TOT}, \beta_{TOT}) = \sum_{i=1}^{3} J^{in}(\mathbf{U}_i, \beta_i) + \sum_{i=1}^{3} J^{lb}(\mathbf{U}_i, \beta_i) + \sum_{i=1}^{3} J^{rb}(\mathbf{U}_i, \beta_i)$$

where $J^{in}(\mathbf{U}_i, \beta_i)$ depends only on quantities that are internal to the i-th vessel, $J^{lb}(\mathbf{U}_i, \beta_i)$ depends on quantities on the left side of the i-th vessel and $J^{rb}(\mathbf{U}_i, \beta_i)$ depends on quantities on the right side of the i-th vessel. Therefore we can define the Lagrangian and then we can derive the adjoint problem for the bifurcation case. We detail all the terms thereafter.

$$
\begin{cases}
\dfrac{\partial \mathbf{m}_i}{\partial t} + \mathbf{F}_{\mathbf{U}}^T(\mathbf{U}_i;\beta_i)\dfrac{\partial \mathbf{m}_i}{\partial x} - \mathbf{S}_{\mathbf{U}}^T(U_i;\beta_i)\mathbf{m}_i = J_{\mathbf{U}}^{int}(\mathbf{U}_i) & x \in (0,L_i),\ t \in (0,T),\ i=1,2,3 \\
\dfrac{\partial G_0^1(\mathbf{U}_1(0,T)),\beta_1}{\partial \mathbf{U}}^T m_{C0,1} - (\mathbf{F}_{\mathbf{U}}^T(\mathbf{U}_1;\beta_1)\mathbf{m}_1)(0,t) = J_{\mathbf{U}}^{lb}(\mathbf{U}_1) & t \in (0,T), \\
\dfrac{\partial G_{L_i}^i(\mathbf{U}_i(L_i,T)),\beta_i}{\partial \mathbf{U}}^T m_{CL,i} + (\mathbf{F}_{\mathbf{U}}^T(\mathbf{U}_i;\beta_i)\mathbf{m}_i)(L,t) = J_{\mathbf{U}}^{rb}(\mathbf{U}_i) & t \in (0,T),\ i=2,3 \\
\dfrac{\partial Q_1(L_1,t)}{\partial \mathbf{U}} m_{CC,1} + \dfrac{\partial P_1(L_1,t)}{\partial U}(m_{CCL_1,2} + m_{CCL_1,3}) + \\
\qquad + (\mathbf{F}_{\mathbf{U}}^T(\mathbf{U}_1;\beta_1)\mathbf{m}_1)(L_1,t) = -J_{\mathbf{U}}^{rb}(\mathbf{U}_1) & t \in (0,T) \\
\dfrac{\partial Q_2(0,t)}{\partial \mathbf{U}} m_{CC,1} + \dfrac{\partial P_2(0,t)}{\partial \mathbf{U}} m_{CCL_1,2} + \\
\qquad + (\mathbf{F}_{\mathbf{U}}^T(\mathbf{U}_2;\beta_2)\mathbf{m}_2)(0,t) = J_{\mathbf{U}}^{lb}(\mathbf{U}_2) & t \in (0,T) \\
\dfrac{\partial Q_3(0,t)}{\partial \mathbf{U}} m_{CC,1} + \dfrac{\partial P_3(0,t)}{\partial \mathbf{U}} m_{CCL_1,3} + \\
\qquad + (\mathbf{F}_{\mathbf{U}}^T(\mathbf{U}_3;\beta_3)\mathbf{m}_3)(0,t) = J_{\mathbf{U}}^{lb}(\mathbf{U}_3) & t \in (0,T) \\
m_{0i} = m_i(x,0) & x \in (0,L_i),\ i=1,2,3 \\
m_i(x,T) = 0 & x \in (0,L_i),\ i=1,2,3
\end{cases}
\tag{3.24}
$$

where the

$$
\overline{\mathbf{m}} = (\mathbf{m}_1, \mathbf{m}_2, \mathbf{m}_3, m_{C0,1}, m_{CL,2}, m_{CL,3}, m_{CC,1}, m_{CCL_1,2}, m_{CCL_1,3}, m_{01}, m_{02}, m_{03})^T
$$

is the vector of Lagrange multipliers and we choose $\bar{i} = 1$;

The strategy that we use to solve this problem is described in subsection 3.2.2. Now we want to focus on the treatment of the coupling conditions as shown in subsection 3.2.3.

The matrices and vectors in the coupling conditions system (3.20) have the form

$$
A = \begin{pmatrix}
\dfrac{\partial Q_1}{\partial \mathbf{U}_1} & \dfrac{\partial P_1}{\partial \mathbf{U}_1} & \dfrac{\partial P_1}{\partial \mathbf{U}_1} \\
\dfrac{\partial Q_2}{\partial \mathbf{U}_2} & \dfrac{\partial P_2}{\partial \mathbf{U}_2} & \\
\dfrac{\partial Q_3}{\partial \mathbf{U}_2} & & \dfrac{\partial P_3}{\partial \mathbf{U}_3}
\end{pmatrix} \in \mathbb{R}^{6\times 3} \qquad \mathbf{m}_{CC}^j = \begin{pmatrix} m_{CC,1} \\ m_{CCL_1,2} \\ m_{CCL_1,3} \end{pmatrix} \in \mathbb{R}^3
$$

$$\mathcal{F}^1 = \begin{pmatrix} \dfrac{\partial F_1^T}{\partial \mathbf{U}_1} & & \\ & \dfrac{\partial F_2^T}{\partial \mathbf{U}_2} & \\ & & \dfrac{\partial F_3^T}{\partial \mathbf{U}_3} \end{pmatrix} \in \mathbb{R}^{6\times 6}. \qquad \mathbf{m}^j = \begin{pmatrix} \mathbf{m}_1 \\ \mathbf{m}_2 \\ \mathbf{m}_3 \end{pmatrix} \in \mathbb{R}^6$$

$$\mathcal{J}^1 = \begin{pmatrix} -J^{rb}_{\mathbf{U}_1}(\mathbf{U}_1) \\ J^{lb}_{\mathbf{U}_2}(\mathbf{U}_2) \\ J^{lb}_{\mathbf{U}_3}(\mathbf{U}_3) \end{pmatrix} \in \mathbb{R}^6$$

where $\dfrac{\partial F_i}{\partial \mathbf{U}_i} = \mathbf{F}^T_{\mathbf{U}_i}(\mathbf{U}_i;\beta_i), \quad i = 1,2,3,$

$$\frac{\partial Q_i(x,t)}{\partial \mathbf{U}_i} = \begin{pmatrix} 0 \\ 1 \end{pmatrix} \quad i = 1,2,3$$

and

$$\frac{\partial P_i(x,t)}{\partial \mathbf{U}_i} = \begin{pmatrix} -\rho\dfrac{Q_i^2(x,t)}{A_i^3(x,t)} + \dfrac{\beta}{2\sqrt{A_i(x,t)A_{i0}}} \\ \rho\dfrac{Q_i(x,t)}{A_i(x,t)} \end{pmatrix} \quad i = 1,2,3$$

Therefore the matrix B has the form

$$B = \begin{pmatrix} \dfrac{1}{(\partial P_1/\partial \mathbf{U}_1)_1} & 0 & -\dfrac{1}{(\partial P_2/\partial \mathbf{U}_2)_1} & 0 & -\dfrac{1}{(\partial P_3/\partial \mathbf{U}_3)_1} & 0 \\ -\dfrac{(\partial P_1/\partial \mathbf{U}_1)_2}{(\partial P_1/\partial \mathbf{U}_1)_1} & 1 & \dfrac{(\partial P_2/\partial \mathbf{U}_2)_2}{(\partial P_2/\partial \mathbf{U}_2)_1} & -1 & 0 & 0 \\ -\dfrac{(\partial P_1/\partial \mathbf{U}_1)_2}{(\partial P_1/\partial \mathbf{U}_1)_1} & 1 & 0 & 0 & \dfrac{(\partial P_3/\partial \mathbf{U}_3)_2}{(\partial P_3/\partial \mathbf{U}_3)_1} & -1 \end{pmatrix} \in \mathbb{R}^{3\times 6}$$

where $\left(\dfrac{\partial P_i}{\partial \mathbf{U}_i}\right)_j$ is the j-th component of $\left(\dfrac{\partial P_i}{\partial \mathbf{U}_i}\right)$. We note with some trivial computations that $BA = 0$ i.e. the rows of B and the columns of A are orthogonal. By multiplying the coupling conditions system by B, we obtain the reduced 3×3 system

$$B\mathcal{F}^1\mathbf{m}^1 = B\mathcal{J}^1.$$

In this way we obtained three scalar conditions on $\mathbf{m}_1$, $\mathbf{m}_2$ and $\mathbf{m}_3$ that together with suitable compatibility conditions obtained by extrapolation of the characteristics as described in Subsection 3.1.5 allow us to solve the adjoint problem for the bifurcation. Then, the vector $\mathbf{m}^1_{CC}$ is computed by applying the pseudo-inverse matrix of A to the original coupling condition system

$$\mathbf{m}^1_{CC} = A^\dagger \left(\mathcal{J}^1 - \mathcal{F}^1\mathbf{m}^1\right).$$

Finally, the optimality condition can be written as

$$
\begin{aligned}
\frac{\partial \mathcal{L}}{\partial \beta_{TOT}}(\mathbf{U}_{TOT}, \beta_{TOT}, \overline{\mathbf{m}}_{TOT}) &= \frac{\partial J}{\partial \beta_{TOT}}(\mathbf{U}_{TOT}, \beta_{TOT}) \\
&+ \sum_{i=1}^{3} \int_0^T \int_0^{L_i} \left(\left(\frac{\partial}{\partial \beta_i} \frac{\partial \mathbf{F}(\mathbf{U}_i; \beta_i)}{\partial x} + \frac{\partial \mathbf{S}}{\partial \beta_i}(\mathbf{U}_i; \beta_i) \right), \mathbf{m}_i \right) dxdt + \\
&+ \int_0^T \left(\frac{\partial G_0^1}{\partial \beta_1}(\mathbf{U}_1(0,t), \beta_1), m_{C0,1} \right) dt \\
&+ \sum_{k=2}^{3} \int_0^T \left(\frac{\partial G_L^k}{\partial \beta_k}(\mathbf{U}_k(L_k,t), \beta_k), m_{CL,k} \right) dt + \\
&+ \sum_{k=2}^{3} \int_0^T \left(\frac{\partial P_1}{\partial \beta_1}(L_1,t) - \frac{\partial P_k}{\partial \beta_k}(0,t), m_{CCL_1,k} \right)
\end{aligned}
\tag{3.25}
$$

3.3 Implementation aspects

The solvers for KKT conditions described in Chapter 2 and Chapter 3 and the optimization methods presented in Section 1.4 have been implemented in `LifeV`[2], a C++ finite element library. The solvers for the state and the adjoint problems are partially based and follow the strategy of the geometrical multiscale framework described in details in [Malossi, 2012]. This choice would permit further development in the direction of parameter estimation for other fluid structure interaction models, like 3D-FSI models.

We briefly describe the main classes that have set up to solve the problem.

`LineSearch` is the class that implements the finite dimension optimization techniques that are presented in Section 1.4 and updates the value of the parameter at each iteration of the optimization method. It also implements a scaling technique of the step length of parameter update in order to stay in the region of admissibility (for example, $\beta > 0$).

`OneDFSIKKTNetwork` is the class that sets up and solves the KKT conditions. It manages the time loop applied to a single model or to a network. It also handles the memorization of the state model solution and the measurements that are needed for the adjoint model.

`MultiscaleData` is a data container for the global parameters of the problem.

`MultiscaleModel` is a base abstract class from which all the specific model classes are derived. It provides a set of transparent interfaces to set up, update and solve the specific problems.

`MultiscaleCoupling` is a base abstract class from which all the specific coupling conditions are derived, both for state and adjoint problems.

`MultiscaleCommunicatorsManager` is a class designed to assign each specific model to a different subset of processors or cluster nodes.

[2] `http://lifev.org`

`OneDFSISolver` is the class that solves each single vessel model, both for state and adjoint problem. It implements the numerical discretizations that have been described in subsection 2.1.4 and subsection 3.1.3.

`OneDFSIBC` is the class that manages the imposition of boundary values for each single vessel model and passes it to the `OneDFSISolver` class.

We underline that all these classes except for `OneDFSISolver` and `OneDFSIBC` are managed through common abstract interfaces and make no assumptions regarding equations, geometries and numerical approximations.

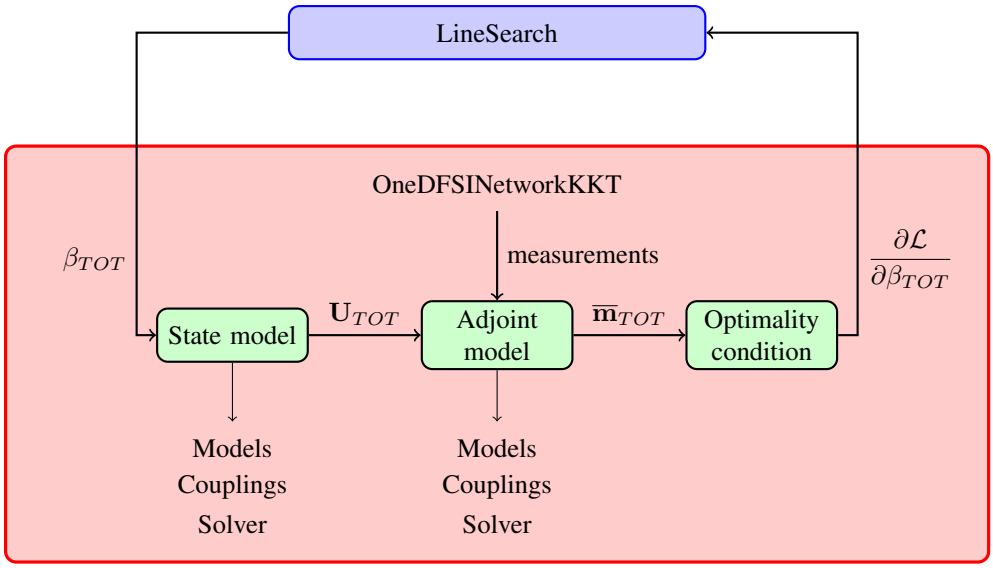

Figure 3.4: *Implementation of one iteration of optimal control for 1D-FSI network model.*

Figure 3.4 represents a schematic overview of the structure of one optimization framework iteration. Starting from `LineSearch` class, a set of parameters is passed to `OneDFSINetwork` class that first solves the state problem in the variable $\mathbf{U}_{TOT}$, then solves the adjoint problem in the variable $\overline{\mathbf{m}}_{TOT}$ using also the measurements stored in it. Finally `OneDFSINetwork` class computes the optimality condition that is passed to `LineSearch` class to check if a optimal control problem solution has been found or it is necessary to continue with the optimization process.

We now details the main features of our implementation.

Geometrical multiscale framework We adopt the geometrical multiscale strategy developed and described in details in [Malossi, 2012]. In our code, the `Linesearch` class creates one instance of a geometrical multiscale model for state equation and another for the adjoint equation. Each instance in turn makes use of a factory design pattern to create the instances of the given set of specific models, coupling conditions, as well as of the specific algorithm for the solution of the nonlinear interface problem for the state problem (for the adjoint problem we solve the linear system (3.21) with `LAPACK` routines). At the level of the geometrical multiscale model class, all these elements are seen as black boxes, managed through common abstract interfaces, without

any preliminary assumption regarding the equations, the geometries, and the numerical approximations behind each object. In other words, the geometrical multiscale model class acts as a global container of the elements in the network. The description of network geometry and topology, parameters of models and algorithms, the set of interface and measurement types and values are provided through a set of data files. We note that this choice permits future extensions to apply analogous parameter estimation techniques to other models for vascular vessels like, for instance, three dimensional fluid structure interactions.

Parallelization of model solutions The parallelism is handled by the multiscale communicators manager, which distributes the models across the available processors and cluster nodes. The 1D-FSI models are distributed one per each available processor. If the number of models exceeds the number of processors, the communicators manager assigns more models to each processor.

Parameters distribution We allow different distributions of parameters, that we estimate, in each vessels. In particular, we consider three possible distributions:

uniform We consider that the parameter is constant on the vessel and, therefore, we have to estimate one quantity per vessel.

linear We consider that the parameter is linearly distributed on the vessel or on part of it. In other words, when we consider the parameter linearly distributed on one vessel, we fix the values β_1 and β_2 of the parameter at each end of the vessel, while, inside of the vessel, the parameter is computed by the formula

$$\beta(x) = \beta_2 \frac{x}{L} + \beta_1 \frac{L - x}{L}.$$

Therefore, in our estimation process we have to compute two values of them parameter for each vessels or part of it.

pointwise We consider that the parameter possibly has a different value on each node of the discretization. We underline that, while this distribution may be a good approximation of the real properties of a vessel, especially in pathological conditions, we can not expect that this choice is proficiently usable in parameter estimation, particularly in real application, due to the large number of data necessary.

Optimization techniques In the `LineSearch` class, we implement the finite dimensional optimization techniques described in Subsection 1.4.1. We implement these techniques serially because, reasonably, the number of value of parameters that we compute is largely smaller than the number of degrees of freedom in the finite elements discretization of the vessels.

CHAPTER 4

Application of parameter estimation method: numerical tests and real data applications

In this chapter we apply the framework illustrated in the previous chapters. In particular, in the first section we test our method, in a full controlled environment, to validate the methodology and to assess the reliability and accuracy of the whole procedure and of the different optimization techniques that we employ. In the second section, we describe the application to the case of elastic parameter estimation in a carotid bifurcation exploiting real medical data.

4.1 Numerical tests

We first present some tests to validate the methodology described in Chapters 2 and 3. These tests are purely *in silico*, i.e. we use only synthetic data. In particular

(i) we set a goal (scalar or vectorial) parameter β^{**} within a physiological range;

(ii) we generate observations A_M by solving the state model with β^{**} as compliance parameter;

(iii) starting from an initial approximation β_0, we apply the parameter estimation method to retrieve β^{**} as solution of the procedure.

We choose as cost functional

$$J(\mathbf{U}, \beta) = \frac{1}{2} \sum_{k=0}^{N_t} \sum_{i=0}^{N_x} j(\mathbf{U}_i^k, \beta_i) = \frac{1}{2} \sum_{k=0}^{N_t} \sum_{i=0}^{N_x} \left(A(x_i, t_k) - A_M(x_i, t_k)\right)^2 . \tag{4.1}$$

where $\mathbf{U}_i^k = \mathbf{U}(x_i, t_k)$, $\beta_i = \beta(x_i)$, $A(x,t)$ is the first component of the state equation solution $\mathbf{U}(x,t)$, namely the section area of the vessel, $A_M(x,t)$ are the section area measurements and $\{x_i\}_{i=1}^{N_x}$ and $\{t_k\}_{k=0}^{N_t}$ the space and time nodes on which measurements are taken.

If not explicitly stated otherwise, we assume that the observations A_M are available at each grid point x_i and at each time t_k. In all the simulations of the present section we set in (2.20) $A^0 = 1$ cm^2, $\rho = 1$ g/cm^3, $K_R = 0$. The time and spatial discretization parameters are $\Delta t = 10^{-5}$ s and $h = 0.1$ cm, respectively. Then, unless explicitly stated otherwise, we impose at the inlet a condition on the flow rate

$$Q(0,t) = g_0(t) = \begin{cases} \sin^2\left(\dfrac{2\pi t}{0.005}\right) & t \leqslant 0.005, \\ 0 & t > 0.005. \end{cases} \tag{IC}$$

and at the outlet a condition on the section area

$$A(L,t) = A^0(t) = 1. \tag{OC}$$

We note that, with these choices of boundary conditions, the boundary terms vanish in the optimality conditions (3.15) and (3.22).

For what concerns the optimization methods, we choose as stopping criterion a control on the relative decrease of the norm of $\partial\mathcal{L}(\mathbf{U},\beta)/\partial\beta$, i.e. we stop the optimization process when

$$\left\| \frac{\partial \mathcal{L}^k}{\partial \beta} \right\|_2 \leqslant toll \left\| \frac{\partial \mathcal{L}^0}{\partial \beta} \right\|_2, \tag{4.2}$$

where $\dfrac{\partial \mathcal{L}^k}{\partial \beta}$ is the optimality condition at the k-th iteration of the optimization process.

In this section, we consider three optimization methods:

- standard Steepest Descent (SD), with Armijo rule step selection;
- Barzilai-Borwein (BB), with non monotone line search;
- BFGS, with Armijo rule step selection.

Finally, regarding the parameters of the optimization process, we set

- the maximum number of line search iteration $N_{max}^{LS} = 1000$,
- the maximum number of backtracking iteration in step length choice $N_{max}^{B} = 10$,
- the tolerance $toll = 10^{-10}$,
- the memory parameter in non monotone step selection (1.32) $M = 5$.

Thanks to the low computational effort that the 1D-FSI model requires, all tests presented in this chapter have been performed on a standard laptop provided with Intel Core i7 CPU and 4.0 GB RAM.

4.1.1 Parameter estimation on a single vessel

In this subsection we test our framework on a simple case, i.e. a network formed by a single vessel. We consider the state model (2.15), the adjoint model (3.3) and the optimality condition (3.15), where $L = 5.0$ cm and $T = 0.1$ s.

We test two cases:

(i) we consider a uniformly distributed parameter on the whole vessel (i.e. we have to estimate a scalar parameter β) as in Figure 4.1;

(ii) we consider a linearly distributed parameter on the vessel (i.e. we have to compute two parameters (β_1, β_2) as in Figure 4.2, since

$$\beta = \beta_2 \frac{x}{L} + \beta_1 \frac{L - x}{L}.$$

Uniformly distributed parameter case

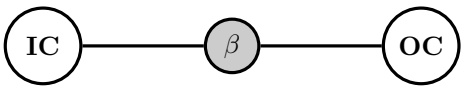

Figure 4.1: *Schematic representation of a single vessel with a single parameter.*

In this test, we suppose that the parameter is uniformly distributed over the vessel and, therefore, we have to compute only one parameter , as represented in Figure 4.1. We choose $\beta_0 = 10^6$ dyn/cm^2 and $\beta^{**} = 1.1 \cdot 10^6$ dyn/cm^2. In Table 4.1 we show the result of this test case.

	number of iterations	value of J	β	$\left\|\frac{\partial \mathcal{L}}{\partial \beta}\right\|$
Steepest Descent	1000	$7.6287 \cdot 10^9$	$1.083986 \cdot 10^6$	4.815336
Barzilai-Borwein	8	$1.3885 \cdot 10^{-15}$	$1.1 \cdot 10^6$	$1.4619 \cdot 10^{-13}$
BFGS	8	$1.3885 \cdot 10^{-15}$	$1.1 \cdot 10^6$	$1.4619 \cdot 10^{-13}$

Table 4.1: *Results of the test in the case of uniformly distributed parameter on the whole vessel.*

We note that by using steepest descent, the maximum number of line search iterations, that we have set to 1000, is reached without having reached convergence, while, by using the other methods, the goal parameter β^{**} is finally obtained. This is due to the well known slow convergence of the steepest descent method. We decided to stop using steepest descent method because of excessively slow convergence even for this very simple test. We also note that the Barzilai-Borwein method and the BFGS method have the same behaviour: this is due to the fact that in the case of the minimization of a scalar function, the two methods coincide.

Linearly distributed parameter

In this test, we assume that the parameter is linearly distributed over the vessel and, therefore, we have to identify two parameters (one for each end of the vessel), as repre-

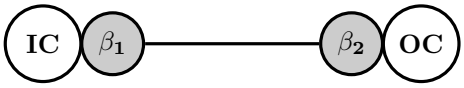

Figure 4.2: *Schematic representation of a single vessel with a couple of parameters.*

sented in Figure 4.2. We choose $\beta_0 = (10^6, 10^6)$ dyn/cm^2 and $\beta^{**} = (0.9 \cdot 10^6, 1.1 \cdot 10^6)$ dyn/cm^2. In Table 4.2, we show the result obtained in this test case. We note that BB and BFGS do not have any more identical behaviour. However they reach the goal parameter and they have still a similar performance.

	number of iterations	value of J	$\left\|\frac{\partial \mathcal{L}}{\partial \beta}\right\|$
Barzilai-Borwein	16	$5.3567 \cdot 10^{-13}$	$2.5387 \cdot 10^{-12}$
BFGS	18	$3.4210 \cdot 10^{-13}$	$1.8752 \cdot 10^{-12}$

Table 4.2: *Results for the test in the case of a linearly distributed parameter on the vessel.*

4.1.2 Parameter estimation on a bifurcation

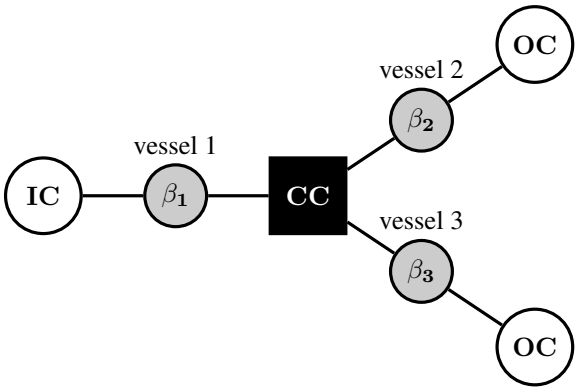

Figure 4.3: *Schematic representation of a bifurcation.*

In this subsection we test our method on a bifurcation network represented in Figure 4.3. We consider the state model (3.23), the adjoint model (3.24) and the optimality condition (3.25) and we set $L_i = 5.0$ cm, $i = 1, 2, 3$ and $T = 0.1$ s. We also assume that on each vessel only one compliance parameter value is defined. In particular, we set $\beta_0 = (10^6, 10^6, 10^6)$ and $\beta^{**} = (1.1 \cdot 10^6, 1.1 \cdot 10^6, 1.1 \cdot 10^6)$. In Table 4.3, we show the results for this test case.

We note that the number of iterations of the two methods (BB and BFGS) is similar and we can not state with certainty which of the two has better performance. However we recall that the BB method is simpler and it has computational advantages because it is natively matrix-free (we recall that also a matrix-free version of BFGS exists, but it is slightly more complex than the standard version that we have implemented). For this reason, in the following, we consider only the BB method in our tests.

	number of iterations	value of J	$\left\|\frac{\partial \mathcal{L}}{\partial \beta}\right\|$
Barzilai-Borwein	27	$2.4315 \cdot 10^{-10}$	$1.2135 \cdot 10^{-10}$
BFGS	26	$1.1523 \cdot 10^{-10}$	$8.9764 \cdot 10^{-10}$

Table 4.3: *Results of the test in the case of uniformly distributed parameters on each vessel of a bifurcation.*

Robustness of the method

We now study the robustness of our method when we change the initial approximation. We consider the same configuration that we presented for the previous test and we use only BB method. In Table 4.4, we show the number of iterations that are necessary to reach convergence with different values of the initial approximation β_0. We note that, in a reasonable range around β^{**}, the behaviour of the method substantially does not change and, therefore, we rely on the robustness of our method.

β_0 (dyn/cm^2)	number of iterations
0.5×10^6	36
0.75×10^6	31
1.0×10^6	27
1.25×10^6	25
1.5×10^6	30
2.0×10^6	45

Table 4.4: *Number of iterations necessary for the convergence of the bifurcation test for different values of initial approximations β_0.*

Simulations with noise

We are now interested to study the effect of the presence of noisy data, because real data are always affected by noise. In particular, at each time step and on each discretization node, we add a Gaussian white noise $\omega_{i,k}$ to the observations

$$\widetilde{A}_M(x_i, t_k) = A_M(x_i, t_k) + \omega_{i,k},$$

where A_M is the solution of state model with goal parameter β^{**} and we consequently consider the functional

$$J(\mathbf{U}) = \frac{1}{2} \sum_{k=0}^{N_t} \sum_{i=0}^{N_x} \left(A(x_i, t_k) - \widetilde{A}_M(x_i, t_k) \right)^2,$$

instead of (4.1)

More precisely, we take

$$\omega_{i,k} = P M_k G_{i,k},$$

where P is the percentage of error, M_k is the maximum in absolute value of $\{A_M(x_i, t_k),\ i = 0 \dots N_x\}$ and $G_{i,k}$ is a sample of a normal distribution with null mean and unit variance.

In Table 4.5 we report the mean error on the estimate over 5 simulations corresponding to 5 different realizations of noise for different values of the percentage of error P. We note that the computed solution is still in a neighbourhood of the exact solution and, even in presence of large noise, the mean error is below 6%.

	P		
	1%	5%	10%
$\frac{\|\beta^{**} - \beta_N^{**}\|}{\beta^{**}}$	1.21%	3.74%	5.89%

Table 4.5: *Mean percentage error of the five estimates for the different values of percentage of noise.*

Treatment of sparse data

In the previous tests, we assumed to be able to observe the solution at each point of the mesh and at each time step. This assumption in real application is unrealistic: typically the grid on which data are observed is considerably coarser than the grid on which the solution is computed. This latter must be refined enough to satisfy the CFL condition (2.29). Therefore, we need to be able to handle problems with a small number of observations. We recall that observations are needed only in the computation of the functional J.

We identify two possible approaches to treat this issue:

Linear interpolation in space (LI): we interpolate in space the observations to have measurements on each grid point.

Localised observations (LO): we exploit only the collected observations, i.e. we consider the functional composed by the sum of the terms

$$\widetilde{j}(\mathbf{U}_i^k, \beta_i) = \begin{cases} j(\mathbf{U}_i^k, \beta_i) & \text{if observation has been collected in the grid point } (x_i, t_k), \\ 0 & \text{otherwise,} \end{cases}$$

where (x_i, t_k) is a point in the space-time discretization grid, $\mathbf{U}_i^k = \mathbf{U}(x_i, t_k)$, $\beta_i = \beta(x_i)$ and $j(\mathbf{U}_i^k, \beta_i)$ is the term in the full functional depending on the point (x_i, t_k).

We analyze the behaviour of this two approaches in the first test case of this subsection, i.e. we consider a bifurcation where on each vessel a one parameter value is defined and we set $\beta_0 = (10^6, 10^6, 10^6)$ dyn/cm^2 and $\beta^{**} = (1.1 \cdot 10^6, 1.1 \cdot 10^6, 1.1 \cdot 10^6)$ dyn/cm^2. We have considered different combinations of time steps and space positions in which observations have been collected, but the results are analogous in all cases. In Table 4.6, we show the results in the case in which we use two points per vessel in space and ten instants in time as observations, while the computational grid is composed by fifty elements per vessel in space and 1000 instants in time. This test has been performed using the Barzilai Borwein method.

	Vessel 1	Vessel 2	Vessel 3	Number of iterations
β^{**}_{LO} (dyn/cm^2)	$1.1 \cdot 10^6$	$1.1 \cdot 10^6$	$1.1 \cdot 10^6$	26
β^{**}_{LI} (dyn/cm^2)	$1.0520 \cdot 10^6$	$1.1554 \cdot 10^6$	$1.1554 \cdot 10^6$	24

Table 4.6: *Comparison between the sparse data approach and linear interpolation approach, where β^{**}_{LO} is the parameter set that we obtain with LO approach and β^{**}_{LI} is the parameter set that we obtain with LI approach*

We note that with LO approach we are able to reach the goal parameters, while by using LI approach we end in another set of parameters. This different behaviour is due to the fact that LI approach reconstructs a set of observation that is not necessarily the same generated by the goal parameters and is not compatible with system dynamics, while in the LO approach observations are a subset of the ones generated by the goal parameters. The drawback of LO approach is that a slightly larger number of iterations is needed to converge, but this increase is not so substantial. Therefore, we conclude that LO approach is preferable. For sparsity in time, analogous considerations can be done and, so, we use LO approach both in time and in space.

4.1.3 Parameter estimation on more complex networks

We test our method also on more complex networks. We now present the application to the network in Figure 4.4 composed by seven vessels that we take of equal length $L_i = 5.0$ cm, $i = 1, \dots, 7$ and we take $T = 0.5$ s. We consider parameters uniformly distributed on each vessel: therefore, we have to estimate seven parameters. We assume that on each vessel the goal parameter is equal to $1.1 \cdot 10^6$ and the initial guess is equal to 10^6. Even in this test, our method is able to reach the goal parameters and in Table 4.7, we report the output regarding the convergence of this test case.

	number of iterations	value of J	$\left\| \frac{\partial \mathcal{L}}{\partial \beta} \right\|$
BB	33	$2.4512 \cdot 10^{-9}$	$1.5620 \cdot 10^{-10}$

Table 4.7: *Results for rhombus network*

4.2 Real data application: estimation of elastic parameters in carotid bifurcation

In this section we analyze the application of the methodology that we have described in Chapter 3 to the estimation of the compliance parameters in carotid bifurcations, employing real medical data.

The carotid artery are large arteries whose pulse can be felt on both sides of the neck under the jaw and whose function is to supply oxygenated blood to the brain and to the rest of the head. The anatomy of the carotid is shown in Figure 4.5. The two sides of

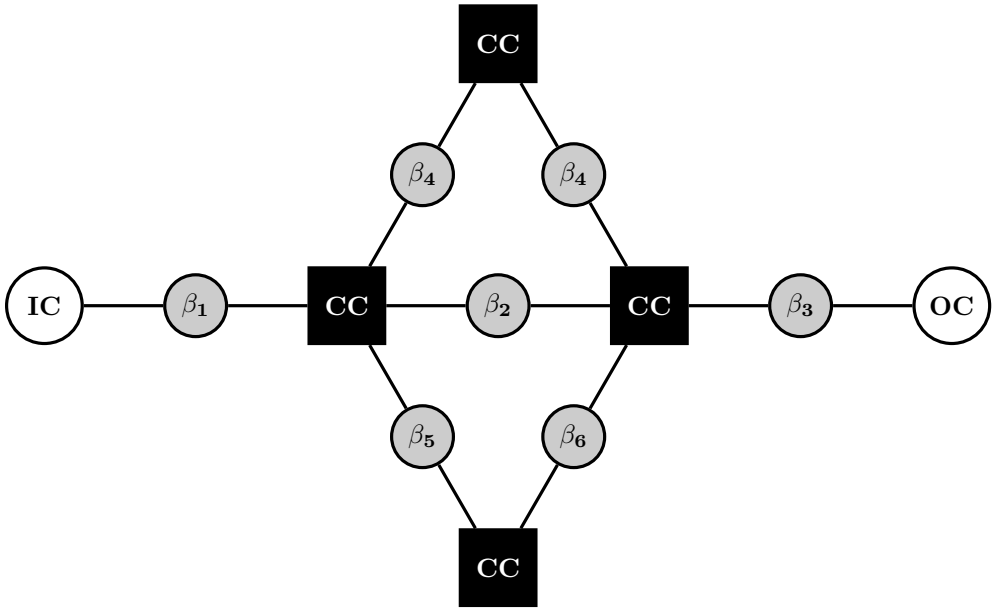

Figure 4.4: *Schematic representation of rhombus network.*

the carotid artery (that in the first part is called *common carotid artery*) have different origins; on the right side it starts from the brachiocephalic trunk (a branch of the aorta) while on the left side it comes directly off the aortic arch. At the throat it forks into the internal and external carotid arteries. The *internal carotid artery* supplies the brain, and the *external carotid artery* supplies the face.

This fork is a common site for atherosclerosis, an inflammatory buildup of atheromatous plaque that can narrow the lumen of carotid arteries (see Figure 4.5). When the stenosis due to the plaque is strong, intervention (carotid stenting or carotid thromboendarterectomy) is necessary. Carotid stenting consists in the insertion of a slender, metal-mesh tube, called a stent, which expands inside the carotid artery to increase blood flow in areas blocked by plaque. In carotid thromboendarterectomy (TEA), the surgeon opens the artery, removes the plaque and then repairs the artery with stitches or a patch made with a vein or artificial material (patch graft). The *Carotid Revascularization Endarterectomy versus Stenting Trial* (CREST) reported that the results of stents and thromboendarterectomy were comparable. However, the *European International Carotid Stenting Study* (ICSS) found that stents had almost double the rate of complications and recommended that carotid thromboendarterectomy should remain the treatment of choice for patients suitable for surgery [Ederle et al., 2010].

We expect that the presence of the plaque or the insertion of a patch modifies the elastic properties of the vessels and try to identify the effective compliance by applying the adjoint-based parameter estimation technique developed in this thesis. In particular, in this section we analyze the application of our technique to the parameter estimation in a carotid that had surgery and in which a patch has been placed.

We first describe the data that have been used in this study and how they are processed to be used in the parameter estimation method (subsection 4.2.1). Then we present the results of the application of our method to the specific patient under study.

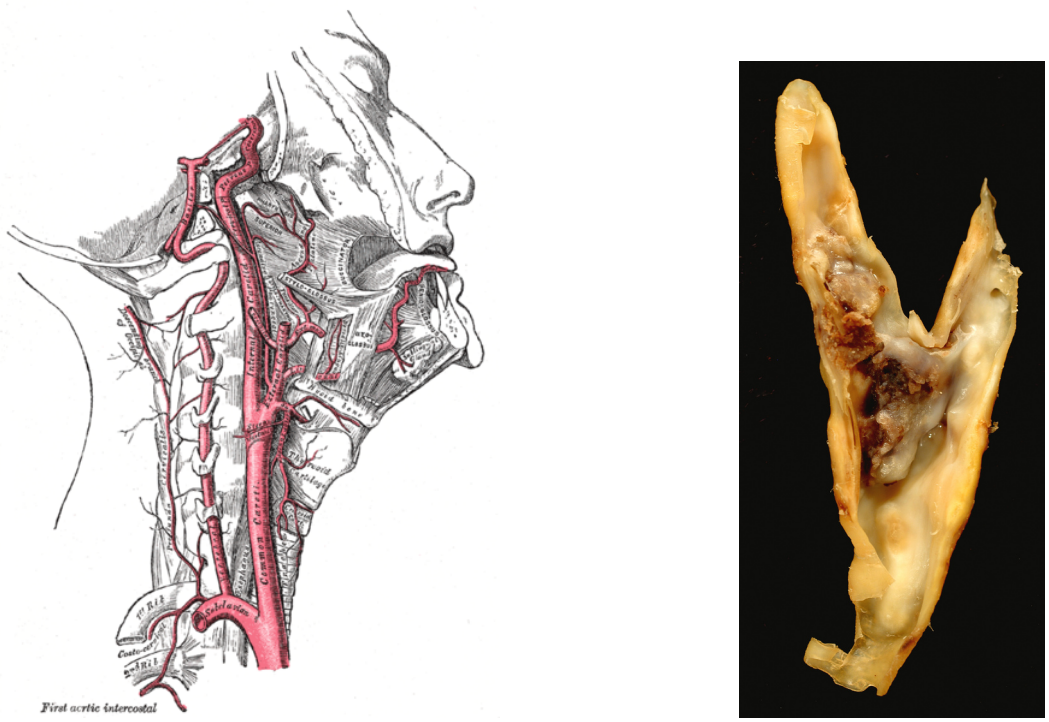

Figure 4.5: *Image on the left: anatomical table representing one carotid bifurcation. Source:*Henry Gray's Anatomy of the Human Body (1918).
Image on the right: Section of carotid artery with plaque. Source: wikipedia.org .

4.2.1 Real medical data

In this subsection we describe the data that have been collected and used in the application of adjoint-based parameter estimation framework to real carotid bifurcation. The data collected include *Echo-Color Doppler* (ECD) imaging to obtain the flow velocity inside the artery and *Magnetic Resonance Imaging* to compute the section area of the three vessels that form the carotid bifurcation. These data have been collected by Prof. Maurizio Domanin at the Unità Operativa di Chirurgia Vascolare Fondazione I.R.C.C.S. Cà Granda Ospedale Maggiore Policlinico di Milano within the project MACAREN@MOX, *MAthematichs for CARotid ENdarterectomy @ MOX*

Echo-Color Doppler Data

Carotid Echo-Color Doppler is a medical imaging procedure that uses reflected ultrasound waves to create images of an artery and to measure the velocity of blood cells in some locations within the artery. This technique does not require the use of contrast media or ionizing radiation and has a relative low cost. Thanks to this complete non-invasivity and also to the short acquisition time required, ECD scans are largely used in clinics, even though they provide a less rich and noisier information than other diagnostic devices. Figure 4.6 shows one ECD image. The ultrasounds image in the upper part of the figure represents the longitudinal section of the vessel. It also shows by a small gray box the position of the beam where blood particle velocities, in the longitudinal direction of the vessel, are measured; the dimension of the box relates to

the dimension of the beam. In the case considered in this picture, the acquisition beam is located at the center of the considered cross-section of the artery. The lower part of the ECD image is a graphical display of the acquired velocity signal during the time lapse of about three heart beats. This signal represents the histogram of the measured velocities, evolving in time. More precisely, the x-axis represents time and the y-axis represents velocity classes; for any fixed time, the gray-scaled intensity of pixels is proportional to the number of blood-cells in the beam moving at a certain velocity.

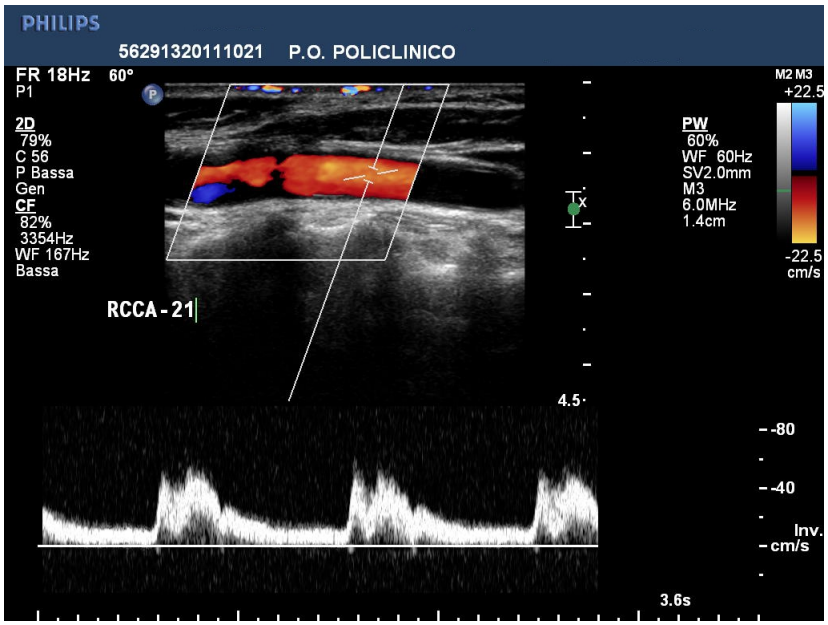

Figure 4.6: *Echo-color doppler image corresponding to the central point of the carotid section.*

Following [Buratti, 2011], the signal extracted from ECD image is obtained, after removing noise from the image with a threshold filter, computing the quantile of order 0.95 from all the histograms in time. This signal is then smoothed by projecting it on a Fourier basis with period estimated through Fourier transform (see the red line in the upper image in Figure 4.7). Finally, we obtain the time-dependent signal in the lower image in Figure 4.7, of period 0.924 s, that is used to prescribe the boundary condition at the inflow of the carotid bifurcation by imposing the following relation flow rate and cross section area,

$$Q(0,t) - v(t)A(0,t) = 0 \quad t \in [0, 0.924], \tag{4.3}$$

where $v(t)$ is the the time dependent signal obtained by ECD image.

Magnetic Resonance Imaging data

Magnetic resonance imaging (MRI) is a medical imaging technique used in radiology to visualize internal structures of the body in detail. MRI makes use of the property of proton nuclear magnetic resonance (NMR) that detects the presence of hydrogens (protons) by subjecting them to a large magnetic field to partially polarize the nuclear spins, then exciting the spins with properly tuned radio frequency radiation, and finally

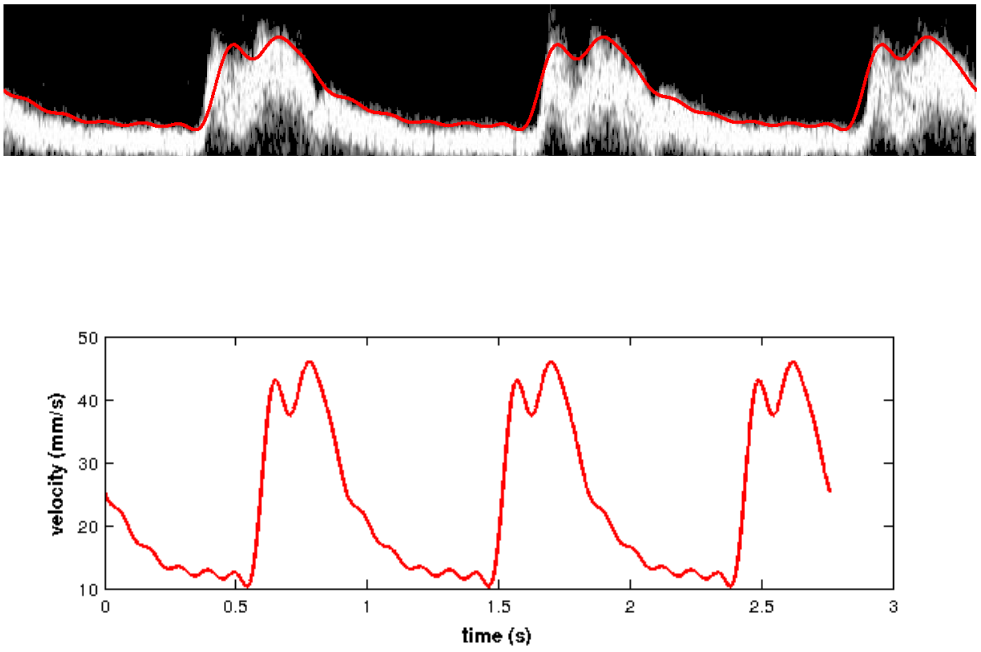

Figure 4.7: *Upper image: processed and denoised signal from ECG image in Figure 4.6. Lower image: velocity signal used to prescribe inflow boundary conditions.*

detecting weak radio frequency radiation from them as they relax from this magnetic interaction. Since the MRI uses proton NMR, it images the concentration of protons. Many of those protons are the protons in water, so MRI is particularly well suited for the imaging of soft tissue.

A large number of MRI sequences have been developed [Ridgway, 2010]. Here we used two dimensional *balanced steady state free precession* (bSSFP) technique, (also known with the commercial names of TrueFISP, FIESTA or bFFE) [Chavhan et al., 2008, Lee, 2010, Scheffler and Lehnhardt, 2003]. This technique is largely spread in medical applications thanks to the high signal-to noise ratio, the image contrast it offers and the possibility to observe time evolving phenomena.

In our specific application, through bSSFP we collected 17 slices of the carotid (as shown on the left of Figure 4.8) and its evolution in time in 25 instants during the heartbeat. On the right of Figure 4.8, the positions of the collected slices are shown on a three dimensional reconstruction of the carotid and in Figure 4.9 the positions of observations are indicated in a schematic plot. Each voxel in the image has dimension $1.103 \times 1.103 \times 1.103$ mm^3. We note that the dimension of the voxel is comparable to the variation of section area from one observation time step to another. Each slice of the three dimensional carotid is not exactly two dimensional, but has a thickness of 1.103 mm that we do not consider in our simulations. The minimum distance between consecutive slides is 6.0 mm. We point out that the MRI is performed on a sequence of heartbeats and then it is synchronized on a single heartbeat employing an electrocar-

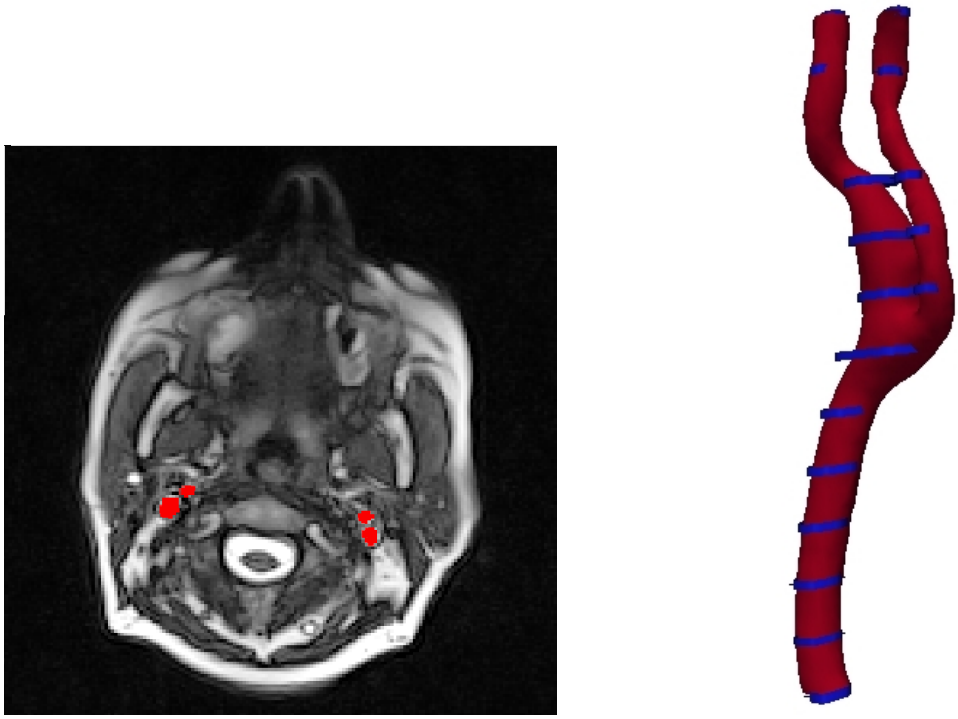

Figure 4.8: *Left image: one of the slices of the head collected through bSSFP. Carotid arteries are coloured in red.*
Right image: positions of the observed slices referred to a three dimensional reconstruction of the carotid.

diogram performed simultaneously to MRI acquisition and therefore these data are, in some sense, averaged over several heartbeats. From each slice we extract the contour of the carotids for each time instant that has been observed and we compute the area of the vessel. In Figure 4.10, we show one contour and its evolution in the subsequent observation. In Figure 4.11, we show the observations in three positions (positions 4, 10 and 15 in Figure 4.9).

We use these observations also to obtain the reference cross section area $A^0(x)$ of the patient. We compute it as the mean of the measured cross section area over an heartbeat. We report in Table 4.8 the computed mean cross section areas, compared values computed from literature values. We note that the values that we have are significantly different from that which are present in literature, for instance in [Reymond et al., 2011]. This gap is so pronounced that we point out the importance of using real data in parameter estimation.

4.2.2 Patient specific simulations

Here we describe how we have estimated the compliance parameter in the carotid artery, employing real medical data. Figure 4.12 depicts how the carotid bifurcation has been schematized. On the inflow we impose the velocity signal extracted from ECD imaging, shown in Figure 4.7. On the outflows we impose absorbing boundary conditions (2.32). We underline that absorbing boundary conditions do not represent the physiological be-

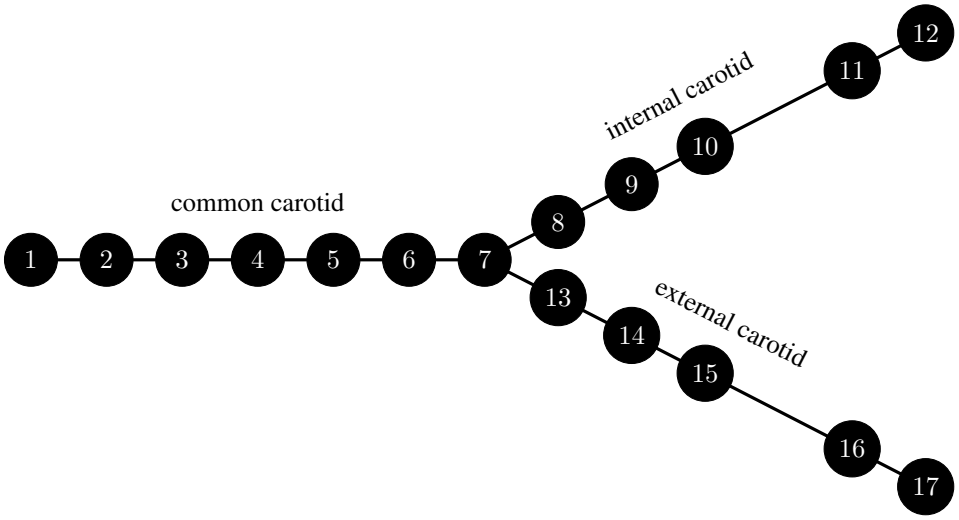

Figure 4.9: *Schematic representation of the position of MRI data on the bifurcation.*

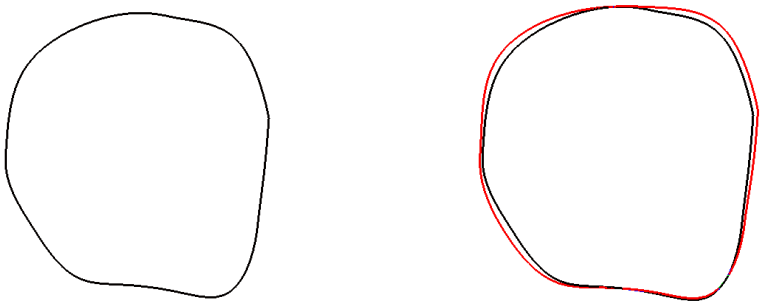

Figure 4.10: *Contour of the artery extracted from MRI (left) and comparison of contours of the same slice at different observation times (right).*

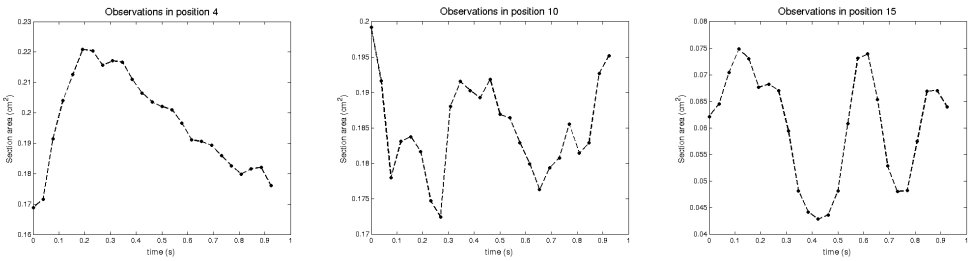

Figure 4.11: *Variation of the observations in time in position* 4*,* 10 *and* 15 *of Figure 4.9 in the carotid bifurcation.*

haviour of blood flow at the outflow of the carotid, but we choose this type of boundary conditions to avoid the formation of spurious modes that can deeply affect parameter estimation techniques in the case of hyperbolic systems. In further developments of this work, it may be interesting to study the impact of this choice and other possible choice of boundary conditions (e.g. *standard boundary conditions* [Vignon-Clementel

	Common Carotid		Internal Carotid		External Carotid	
	proximal	distal	proximal	distal	proximal	distal
Observed	0.1594	0.4730	0.3386	0.0526	0.0648	0.0657
Literature	3.1426	1.5394	1.0207	0.9318	0.7854	0.6544

Table 4.8: *Comparison of reference section areas computed starting from MRI observations versus the same quantities computed from literature values in [Reymond et al., 2011] (all values are in cm^2).*

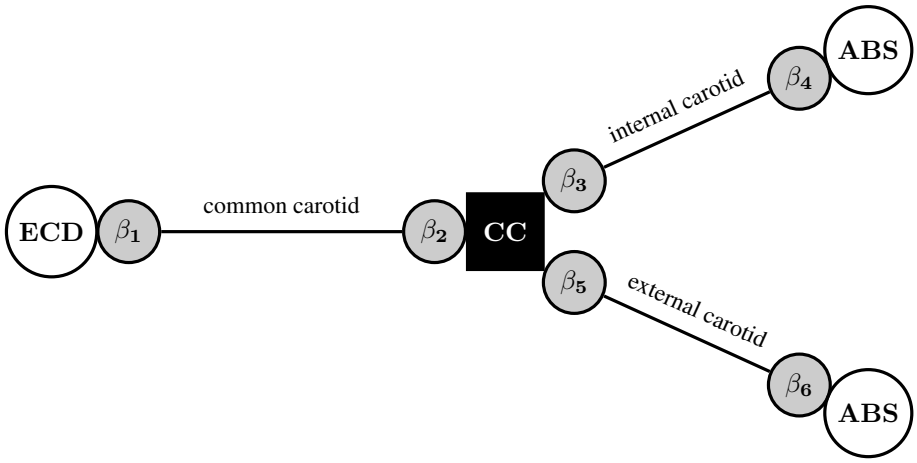

Figure 4.12: *Schematic representation of the simulation design for carotid bifurcation, employing real observations.*

et al., 2010]). We use the values of section areas extracted from MRI measurements to compute the cost functional (4.1) and we face the sparsity of these data adopting the LO approach described in subsection 4.1.2.

We point out that no physiological initial conditions are available and, obviously, we can not expect that the output of 1D-FSI model with zero initial conditions matches physiological observations. However, due to the hyperbolic nature of 1D-FSI model, we can assume that, after a suitable time, the solution of the 1D-FSI model does not depend on the initial conditions, if non reflective boundary conditions are imposed at the outflow. To prove that this assumption is true, we solve the 1D-FSI model on a bifurcation network with physiological inflow conditions, absorbing outflow conditions and zero initial conditions over three heartbeats. In Figure 4.13, we show the section area in the middle of one of the vessels after the bifurcation. We note that the influence of the initial conditions is lost after a time that is largely smaller that a single heartbeat and a periodic solution is reached. Therefore, in our parameter estimation process, we simulate two heartbeats of state model: after the first one, we are sure to have reached the periodic solution for the state solution and we make use of the second period to solve the adjoint problem and to compute the optimality condition.

In our simulation, we consider each vessel to be 3.6 cm long, i.e. $L_i = 3.6$ cm. We discretize each vessel in 12 elements and therefore $h = 0.3$ cm. We recall that the period of the inflow signal is 0.924 s and, therefore, we consider the duration of a single heartbeat equal to 0.924 s.

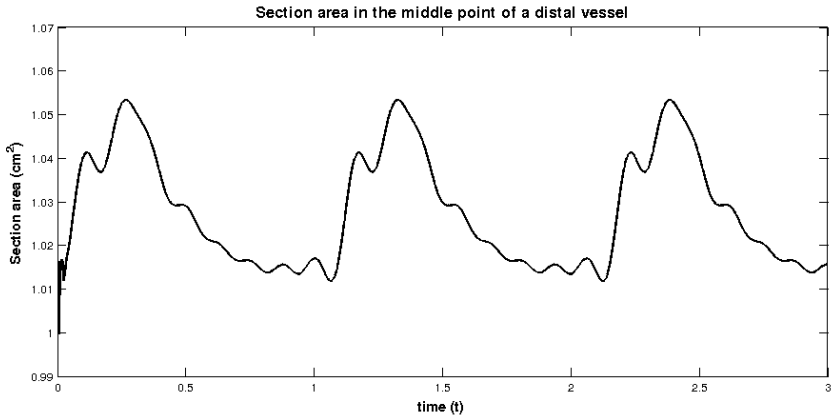

Figure 4.13: *Section area simulated by a 1D-FSI model with zero initial conditions*

We consider a linearly variable distribution of the parameter in each vessel. We consequently have to estimate two parameter values per vessel and six values in total (as shown in Figure 4.12). We set as initial approximation $\beta_0 = (10^6, 10^6, 10^6, 10^6, 10^6, 10^6)$ dyn/cm^2. We make use of Barzilai Borwein method as line search method.

In Table 4.9, we show the results of the simulation. We report the value of the compliance parameter β and the Young modulus E computed by inverting the relation (2.18), i.e by the formula

$$E(x) = \beta(x)\frac{1-\nu^2}{h_0(x)}\sqrt{\frac{A^0(x)}{\pi}}.$$

where we take the vessel thickness $h_0(x)$ equal to the 10% of the vessel diameter computer from vessel reference area $A^0(x)$. We recall that the Young modulus describes the elastic properties of the vessel walls.

	Common Carotid		Internal Carotid		External Carotid	
	β_1	β_2	β_3	β_4	β_5	β_6
Compliance Parameter	$1.022 \cdot 10^6$	$1.018 \cdot 10^6$	$1.074 \cdot 10^6$	$0.983 \cdot 10^6$	$0.974 \cdot 10^6$	$1.0236 \cdot 10^6$
Young modulus	$6.839 \cdot 10^6$	$6.808 \cdot 10^6$	$10.804 \cdot 10^6$	$9.882 \cdot 10^6$	$8.764 \cdot 10^6$	$9.214 \cdot 10^6$

Table 4.9: *Results for the real patient application.*

We note that there is clear difference between the Young modulus in the neighbourhood of the bifurcation. These results seems to be in accordance with effects due to the presence of a patch near the carotid bifurcation.

In Table 4.10, we report the quantities regarding the convergence of our method. We note that in this case the final value of J is not as close to zero as in *in silico* tests, as expected. This occurrence is due to the presence of noise in the measurements and to the model approximation.

number of iterations	value of J	$\left\|\frac{\partial \mathcal{L}}{\partial \beta}\right\|$
28	$7.537 \cdot 10^{-4}$	$1.4765 \cdot 10^{-11}$

Table 4.10: *Convergence quantities in the real patient application.*

Conclusions

In this thesis we have developed a parameter estimation technique to compute the elastic properties of networks of blood vessels by employing real observations. Elastic properties of vessels are can not to be measured directly in vivo in a non-invasive way. We modelled the networks with well known 1D-FSI models. These are reduced models (and consequently less computationally expensive than three dimensional models) but nevertheless they are able to capture the main characteristics of the physical phenomena, like the propagation of pressure waves. These models depend on the so called compliance parameter that takes into account the properties of the wall and in particular the elastic features. Our goal is precisely to estimate the compliance parameter.

The method that we developed can be placed in the wider class of data assimilation that consists in combining in an optimal way the mathematical information provided by the models and the physical information given by the observations, generally sparse and noisy. Data assimilation had a huge development in the last two decades in the field of cardiovascular simulations.

One of the major novelties of our methods stay in the fact that it is the first attempt to estimate a parameter in one dimensional network models by a variational data assimilation approach. Firstly, we define a cost functional that takes into account the difference between the observations and the output of the 1D-FSI model and consequently we introduced the Lagrangian functional that we minimized by solving the coupled system of first order conditions (the so-called KKT conditions), composed by the state equation, the adjoint equation and the optimality condition. Therefore we have built up an iterative optimization framework in which we first solve the state and adjoint equation and, then, we update the parameter by computing the optimality condition and applying finite dimensional optimization methods, until a certain tolerance is reached. In this process, a particular attention had been devoted to the treatment of adjoint boundary conditions and adjoint coupling conditions.

We implemented this framework in `LifeV`, a C++ finite elements library, partially following the geometrical multiscale strategy proposed in [Formaggia et al., 1999] and

developed in [Malossi, 2012]. In particular, we are able to manage and estimate different distributions of the parameter (constant, linear and pointwise) inside each vessel or part of vessel.

After having tested the method and our implementation, we applied it to a patient specific case employing real medical data, which is another of the main contributions of our work. In particular, we studied and preprocessed real observations and then we estimated the elastic properties of carotid that had undergone thromboendoarteroctomy with patch insertion. The results of the application of our method seems to be in agreement with medical hypothesis.

We can imagine some further developments of our work. First, it would be interesting to compare the numerical behaviour of our framework with previously published works, especially the ones in subsection 1.1.3. The most trivial development of the presented framework is the estimation of other parameters of the 1D-FSI model. Other possible more complex extensions include the estimation of physiological boundary and initial conditions or the application to different vascular models, by exploiting the geometrical multiscale implementation of differential problems.

Bibliography

[Agoshkov, 2003] Agoshkov, V. (2003). Optimal Control and Adjoint Equation Methods in Problems of Mathematical Physics. *Institute of Numerical Mathematics, Russian Academy of Sciences, Moscow (in Russian)*.

[Alastruey et al., 2007] Alastruey, J., Parker, K., and Peiró, J. (2007). Modelling the circle of Willis to assess the effects of anatomical variations and occlusions on cerebral flows. *Journal of biomechanics*, 40(8):1794–1805.

[Alekseev et al., 1987] Alekseev, V., Tikhomirov, V., and Fomin, S. (1987). *Optimal control*. Plenum Press.

[Ambadan and Tang, 2009] Ambadan, J. and Tang, Y. (2009). Sigma-Point Kalman Filter Data Assimilation Methods for Strongly Nonlinear Systems. *Journal of the Atmospheric Sciences*, 66(2):261–285.

[Avolio, 1980] Avolio, A. (1980). Multi-branched model of the human arterial system. *Medical & biological engineering & computing*, 18(6):709–18.

[Aziz, 1977] Aziz, A. (1977). *Control theory of systems governed by partial differential equations*. Academic Press.

[Balocco et al., 2010] Balocco, S., Basset, O., Courbebaisse, G., Boni, E., Frangi, A., Tortoli, P., and Cachard, C. (2010). Estimation of the viscoelastic properties of vessel walls using a computational model and Doppler ultrasound. *Physics in medicine and biology*, 55(12):3557–75.

[Banghert, 2008] Banghert, W. (2008). A framework for the adaptive finite element solution of large inverse problems. *SIAM Journal on Scientific Computing*.

[Barzilai and Borwein, 1988] Barzilai, J. and Borwein, J. (1988). Two-point step size gradient methods. *IMA Journal of Numerical Analysis*, 8(1):141–148.

[Bertoglio et al., 2012] Bertoglio, C., Moireau, P., and Gerbeau, J. (2012). Sequential parameter estimation for fluid–structure problems: Application to hemodynamics. *International Journal for Numerical Methods in Biomedical Engineering*, 28(4):434–455.

[Blanco et al., 2007] Blanco, P., Feijóo, R., and Urquiza, S. (2007). A unified variational approach for coupling 3D–1D models and its blood flow applications. *Computer Methods in Applied Mechanics and Engineering*, 196(41-44):4391–4410.

[Blanco et al., 2012] Blanco, P., Watanabe, S., and Feijóo, R. (2012). Identification of vascular territory resistances in one-dimensional hemodynamics simulations. *Journal of biomechanics*, 45(12):2066–73.

[Blum et al., 2008] Blum, J., Le Dimet, F., and Navon, I. (2008). Data assimilation for geophysical fluids. *Handbook of Numerical Analysis*, 14(Computational Methods for the Atmosphere and the Oceans):377–434.

[Bogaers et al., 2012] Bogaers, A., Kok, S., Reddy, B., and Fran, T. (2012). Inverse parameter identification for a branching 1D arterial network.

[Boron and Boulpaep, 2008] Boron, W. and Boulpaep, E. (2008). *Medical physiology*. Saunders.

[Bunks et al., 1995] Bunks, C., Saleck, F., Zaleski, S., and Chavent, G. (1995). Multiscale seismic waveform inversion. *Geophysics*, 60(5):1457–1473.

[Buratti, 2011] Buratti, P. (2011). Analysis of Doppler blood flow velocity in carotid arteries for the detection of atherosclerotic plaques.

[Canic et al., 2005] Canic, S., Ravi-Chandar, K., Krajcer, Z., Mirkovic, D., and Lapin, S. (2005). Mathematical model analysis of Wallstent and AneuRx: Dynamic responses of bare-metal endoprosthesis compared with those of stent-graft. *Texas Heart Institute Journal*, 32(4):502.

[Cannarsa and Coron, 2010] Cannarsa, P. and Coron, J. (2010). *Control of partial differential equations*. Springer.

[Cauchy, 1847] Cauchy, A. (1847). Méthode générale pour la résolution des systemes d'équations simultanées. *Comp. Rend. Sci. Paris*, 25(1847):536–538.

[Chandrasekar et al., 2008] Chandrasekar, J., Kim, I., Bernstein, D., and a.J. Ridley (2008). Reduced-rank unscented Kalman filtering using Cholesky-based decomposition. *International Journal of Control*, 81(11):1779–1792.

[Chavhan et al., 2008] Chavhan, G., Babyn, P., Jankaria, B., Cheng, H., and Shroff, M. (2008). Steady-State MR Imaging Sequences: Physics, Classification, and Clinical Applications1. *Radiographics*, 28(4):1147–1161.

[Courtier et al., 1993] Courtier, P., Derber, J., Errico, R., Louis, J., and Vukićević, T. (1993). Important literature on the use of adjoint, variational methods and the Kalman filter in meteorology. *Tellus A*, 45(15):342–357.

[Crosetto, 2011] Crosetto, P. (2011). *Fluid-Structure Interaction Problems in Hemodynamics: Parallel Solvers, Preconditioners, and Applications*. PhD thesis, École polytechnique fédérale de Lausanne, Switzerland.

[Dai and Fletcher, 2005] Dai, Y. and Fletcher, R. (2005). On the asymptotic behaviour of some new gradient methods. *Mathematical Programming*, 103(3):541–559.

[D'Elia, 2011] D'Elia, M. (2011). *Assimilation of velocity data into fluid dynamic simulations, an application to computational hemodynamics*. PhD thesis, Emory University.

[D'Elia et al., 2012] D'Elia, M., Mirabella, L., Passerini, T., Perego, M., Piccinelli, M., Vergara, C., and Veneziani, A. (2012). Applications of Variational Data Assimilation in Computational Hemodynamics. In *Modeling of Physiological Flows*, number 3, pages 363–394. Springer Milan.

[Dennis and Schnabel, 1987] Dennis, J. and Schnabel, R. (1987). *Numerical methods for unconstrained optimization and nonlinear equations*.

[Deparis et al., 2006] Deparis, S., Discacciati, M., Fourestey, G., and Quarteroni, A. (2006). Fluid–structure algorithms based on Steklov–Poincaré operators. *Computer Methods in Applied Mechanics and Engineering*, 195(41-43):5797–5812.

[Devault et al., 2008] Devault, K., Gremaud, P., Novak, V., Olufsen, M., Vernières, G., and Zhao, P. (2008). Blood Flow in the Circle of Willis: Modeling and Calibration. *Multiscale modeling & simulation : a SIAM interdisciplinary journal*, 7(2):888–909.

[du Plessis, 1967] du Plessis, R. (1967). Poor man's explanation of kalman filtering. *Autonectics Division of North American Rockwell Corporation*.

[Dumas, 2008] Dumas, L. (2008). Inverse problems for blood flow simulation. In *EngOpt 2008 - International Conference on Engineering Optimization*, number June.

[Dumas et al., 2012] Dumas, L., Boutouyrie, P., and Bozec, E. (2012). An optimal reconstruction of the human arterial tree from doppler echotracking measurements. *Proceedings of the fourteenth international conference on Genetic and evolutionary computation conference companion - GECCO Companion '12*, page 517.

[Ederle et al., 2010] Ederle, J., Dobson, J., Featherstone, R. L., Bonati, L. H., van der Worp, H. B., de Borst, G. J., Gaines, P., Dorman, P. J., MacDonald, S., Lyrer, P. A., and Others (2010). Carotid artery stenting compared with endarterectomy in patients with symptomatic carotid stenosis (International Carotid Stenting Study): an interim analysis of a randomised controlled trial. *Lancet*, 375(9719):985–997.

[Epanomeritakis et al., 2008] Epanomeritakis, I., Akçelik, V., Ghattas, O., and Bielak, J. (2008). A Newton-CG method for large-scale three-dimensional elastic full-waveform seismic inversion. *Inverse Problems*, 24(3):034015.

[Esmaily Moghadam et al., 2013] Esmaily Moghadam, M., Vignon-Clementel, I. E., Figliola, R., and Marsden, A. L. (2013). A modular numerical method for implicit 0D/3D coupling in cardiovascular finite element simulations. *Journal of Computational Physics*, 244:63–79.

[Euler, 1844] Euler, L. (1844). Principia pro motu sanguinis per arterias determinando. *Opera posthuma mathematica et physica anno*, pages 814–823.

[Evensen, 2003] Evensen, G. (2003). The Ensemble Kalman Filter: theoretical formulation and practical implementation. *Ocean Dynamics*, 53(4):343–367.

[Evensen, 2009] Evensen, G. (2009). *Data assimilation: the ensemble Kalman filter*. Springer.

[Faggiano et al., 2012] Faggiano, E., Bonnemain, J., Quarteroni, A., and Deparis, S. (2012). A patient-specific framework for the analysis of the haemodynamics in patients with ventricular assist device.

[Farrell and Ioannou, 2001] Farrell, B. and Ioannou, P. (2001). State Estimation Using a Reduced-Order Kalman Filter. *Journal of the Atmospheric Sciences*, 58(23):3666–3680.

[Fernández-Cara and Zuazua, 2003] Fernández-Cara, E. and Zuazua, E. (2003). Control Theory: History, mathematical achievements and perspectives. *Notes, Universidad de Sevilla and Universidad Autónoma Madrid, Spain*.

[Fletcher, 2005] Fletcher, R. (2005). On the Barzilai-Borwein method. In *Optimization and control with applications*, pages 235–256. Springer.

[Formaggia et al., 2003] Formaggia, L., Lamponi, D., and Quarteroni, A. (2003). One-dimensional models for blood flow in arteries. *Journal of Engineering Mathematics*, 47(3/4):251–276.

[Formaggia et al., 2006] Formaggia, L., Lamponi, D., Tuveri, M., and Veneziani, A. (2006). Numerical modeling of 1D arterial networks coupled with a lumped parameters description of the heart. *Computer methods in biomechanics and biomedical engineering*, 9(5):273–88.

[Formaggia et al., 1999] Formaggia, L., Nobile, F., Quarteroni, A., and Veneziani, A. (1999). Multiscale modelling of the circulatory system: a preliminary analysis. *Computing and visualization in science*, 2(2-3):75–83.

[Formaggia et al., 2009] Formaggia, L., Quarteroni, A., and Veneziani, A. (2009). *Cardiovascular Mathematics: Modeling and simulation of the circulatory system*.

[Gerbeau et al., 2005] Gerbeau, J., Vidrascu, M., and Frey, P. (2005). Fluid–structure interaction in blood flows on geometries based on medical imaging. *Computers & Structures*, 83(2-3):155–165.

[Gillijns et al., 2006] Gillijns, S., Mendoza, O., Chandrasekar, J., De Moor, B., Bernstein, D., and Ridley, A. (2006). What is the ensemble Kalman filter and how well does it work? In *American Control Conference, 2006*, page 6 pp. IEEE.

[Glowinski, 1992] Glowinski, R. (1992). Ensuring well-posedness by analogy: Stokes problem and boundary control for the wave equation. *Journal of Computational Physics*, 103(2):189–221.

[Glowinski and Li, 1990] Glowinski, R. and Li, C. (1990). On the numerical implementation of the Hilbert uniqueness method for the exact boundary controllability of the wave equation. *C. R. Acad. Sci. Paris Sér. I Math*, 311(2):135–142.

[Glowinski et al., 1990] Glowinski, R., Li, C., and Lions, J. (1990). A numerical approach to the exact boundary controllability of the wave equation. I. Dirichlet controls: description of the numerical methods. *Japan Journal of Applied Mathematics*, 7:1–76.

[Grinberg and Karniadakis, 2008] Grinberg, L. and Karniadakis, G. (2008). Outflow boundary conditions for arterial networks with multiple outlets. *Annals of biomedical engineering*, 36(9):1496–514.

[Grippo et al., 1989] Grippo, L., Lampariello, F., and Lucidi, S. (1989). A truncated Newton method with nonmonotone line search for unconstrained optimization. *Journal of Optimization Theory and Applications*, 60(3):401–419.

[Grippo and Sciandrone, 2002] Grippo, L. and Sciandrone, M. (2002). Nonmonotone Globalization Techniques for the Barzilai-Borwein Gradient Method. *Computational Optimization and Applications*, 23:143–169.

[Gronskis et al., 2013] Gronskis, A., Heitz, D., and Mémin, E. (2013). Inflow and initial conditions for direct numerical simulation based on adjoint data assimilation. *Journal of Computational Physics*, 242:480–497.

[Gunzburger, 1987] Gunzburger, M. (1987). *Perspectives in flow control and optimization*, volume 5. SIAM.

[Gunzburger, 2000] Gunzburger, M. (2000). Adjoint equation-based methods for control problems in incompressible, viscous flows. *Flow, Turbulence and Combustion*, 65:249–272.

[Guyton and Hall, 2010] Guyton, A. and Hall, J. (2010). *Guyton and Hall Textbook of Medical Physiology*. Saunders.

[Harb et al., 2011] Harb, N., Labed, N., Domaszewski, M., and Peyraut, F. (2011). A new parameter identification method of soft biological tissue combining genetic algorithm with analytical optimization. *Computer Methods in Applied Mechanics and Engineering*, 200(1-4):208–215.

[Hedstrom, 1979] Hedstrom, G. W. (1979). Nonreflecting boundary conditions for nonlinear hyperbolic systems. *Journal of Computational Physics*, 30(2):222–237.

[Hinze et al., 2009] Hinze, M., Pinnau, R., Ulbrich, M., and Ulbrich, S. (2009). *Optimization with PDE Constraints. Mathematical Modelling: Theory and Applications, vol. 23*. Springer.

[Humpherys et al., 2012] Humpherys, J., Redd, P., and West, J. (2012). A Fresh Look at the Kalman Filter. *SIAM Review*, 54(4):801–823.

[Huo and Kassab, 2007] Huo, Y. and Kassab, G. (2007). A hybrid one-dimensional/Womersley model of pulsatile blood flow in the entire coronary arterial tree. *American journal of physiology. Heart and circulatory physiology*, 292(6):H2623–33.

[Ismail et al., 2013a] Ismail, M., Gee, M., and Wall, W. (2013a). CFD Challenge: Hemodynamic Simulation of a Patient-Specific Aortic Coarctation Model with Adjoint-Based Calibrated Windkessel Elements. In *Statistical Atlases and Computational Models of the Heart. Imaging and Modelling Challenges*, pages 44–52.

[Ismail et al., 2013b] Ismail, M., Wall, W., and Gee, M. (2013b). Adjoint-based inverse analysis of windkessel parameters for patient-specific vascular models. *Journal of Computational Physics*, 244:113–130.

[Jameson, 2003] Jameson, A. (2003). CFD for aerodynamic design and optimization: Its evolution over the last three decades. *AIAA Paper*, 3438.

[Julier and Uhlmann, 2004] Julier, S. and Uhlmann, J. (2004). Unscented Filtering and Nonlinear Estimation. *Proceedings of the IEEE*, 92(3):401–422.

[Julier et al., 2000] Julier, S., Uhlmann, J., and Durrant-Whyte, H. (2000). A New Method for the Nonlinear Transformation of Means and Covariances in Filters and Estimators. *IEEE transactions on Automatic Control*, 45(3):477–482.

[Kalman, 1960] Kalman, R. (1960). A new approach to linear filtering and prediction problems. *Journal of basic Engineering*, 82(1):35–45.

[Kalman and Bucy, 1961] Kalman, R. and Bucy, R. (1961). New results in linear filtering and prediction theory. *Journal of basic Engineering*, 83(3):95–108.

[Karamanoglu et al., 1994] Karamanoglu, M., Gallagher, D., Avolio, A., and O'Rourke, M. (1994). Functional origin of reflected pressure waves in a multibranched model of the human arterial system. *American Journal of Physiology-Heart and Circulatory Physiology*, 267(5):H1681—-H1688.

[Kelley, 1995] Kelley, C. (1995). Iterative Methods for Linear and Nonlinear Equations.

[Kim et al., 2009] Kim, H.-J., Vignon-Clementel, I., Figueroa, C., LaDisa, J., Jansen, K., Feinstein, J., and Taylor, C. (2009). On coupling a lumped parameter heart model and a three-dimensional finite element aorta model. *Annals of biomedical engineering*, 37(11):2153–69.

[Kolmogorov and Fomin, 1999] Kolmogorov, A. N. and Fomin, S. V. (1999). *Elements of the theory of functions and functional analysis*, volume 1. Courier Dover Publications.

[Küttler and Gee, 2010] Küttler, U. and Gee, M. (2010). Coupling strategies for biomedical fluid–structure interaction problems. *International Journal for Numerical Methods in Biomedical Engineering*, 26(3-4):305–321.

[Lagrée, 2000] Lagrée, P.-Y. (2000). An inverse technique to deduce the elasticity of a large artery. *The European Physical Journal Applied Physics*, 9(2):153–163.

[Lanzarone et al., 2007] Lanzarone, E., Liani, P., Baselli, G., and Costantino, M. (2007). Model of arterial tree and peripheral control for the study of physiological and assisted circulation. *Medical engineering & physics*, 29(5):542–55.

[Lee, 2010] Lee, J. (2010). Balanced steady state free precession fMRI. *International Journal of Imaging Systems and Technology*, 20(1):23–30.

[LeVeque, 2002] LeVeque, R. (2002). *Finite volume methods for hyperbolic problems*.

[Liang and Liu, 2005] Liang, F. and Liu, H. (2005). A closed-loop lumped parameter computational model for human cardiovascular system. *JSME International Journal Series C*, 48(4):484–493.

[Lions, 1972] Lions, J. (1972). *Optimal control of systems described by partial differential equations*. Mir, Moscow.

[Lions, 1987] Lions, J. (1987). *Some aspects of the optimal control of distributed parameter systems*, volume 6. Society for Industrial and Applied Mathematics.

[Lombardi, 2013] Lombardi, D. (2013). Inverse problems in 1D hemodynamics on systemic networks: A sequential approach. *International Journal for Numerical Methods in Biomedical Engineering*.

[Luenberger, 2003] Luenberger, D. (2003). *Linear and nonlinear programming*. Springer.

[Malossi, 2012] Malossi, A. (2012). *Partitioned Solution of Geometrical Multiscale Problems for the Cardiovascular System: Models, Algorithms, and Applications*. Phd thesis, École polytechnique fédérale de Lausanne, Switzerland.

[Malossi et al., 2012] Malossi, A., Blanco, P., and Deparis, S. (2012). A two-level time time step technique for the partitioned of one-dimensional arterial networks. *Comput. Methods Appl. Mech. Engrg.*, 237-240:212–226.

[Manzoni et al., 2012] Manzoni, A., Quarteroni, A., and Rozza, G. (2012). Model reduction techniques for fast blood flow simulation in parametrized geometries. *International Journal for Numerical Methods in Biomedical Engineering*, 28(6-7):604–625.

[Marchesseau et al., 2013] Marchesseau, S., Delingette, H., Sermesant, M., Cabrera-Lozoya, R., Tobon-Gomez, C., Moireau, P., Figueras i Ventura, R., Lekadir, K., Hernandez, A., Garreau, M., Donal, E., Leclercq, C., Duckett, S., Rhode, K., Rinaldi, C., Frangi, A., Razavi, R., Chapelle, D., and Ayache, N. (2013). Personalization of a cardiac electromechanical model using reduced order unscented Kalman filtering from regional volumes. *Medical image analysis*, 17(7):816–829.

[Martin et al., 2005] Martin, V., Clément, F., Decoene, A., and Gerbeau, J. (2005). Parameter identification for a one-dimensional blood flow model. *ESAIM: Proceedings*, 14:174–200.

[Maurer, 1981] Maurer, H. (1981). First and second order sufficient optimality conditions in mathematical programming and optimal control. In *Mathematical Programming at Oberwolfach*, pages 163–177. Springer.

[Maurer and Zowe, 1979] Maurer, H. and Zowe, J. (1979). First and second-order necessary and sufficient optimality conditions for infinite-dimensional programming problems. *Mathematical Programming*, 16(1):98–110.

[Micu, 2002] Micu, S. (2002). Uniform boundary controllability of a semi-discrete 1-D wave equation. *Numerical Mathematics*, 91:723–768.

[Migliavacca et al., 2006] Migliavacca, F., Balossino, R., Pennati, G., Dubini, G., Hsia, T., de Leval, M., and Bove, E. (2006). Multiscale modelling in biofluidynamics: application to reconstructive paediatric cardiac surgery. *Journal of biomechanics*, 39(6):1010–20.

[Milišić and Quarteroni, 2004] Milišić, V. and Quarteroni, A. (2004). Analysis of lumped parameter models for blood flow simulations and their relation with 1D models. *ESAIM; Modelling and Numerical Analysis*, 38:613–632.

[Mohammadi and Pironneau, 2001] Mohammadi, B. and Pironneau, O. (2001). *Applied shape optimization for fluids*, volume 28. Oxford University Press Oxford.

[Moireau and Chapelle, 2010] Moireau, P. and Chapelle, D. (2010). Reduced-order Unscented Kalman Filtering with application to parameter identification in large-dimensional systems. *ESAIM: Control, Optimisation and Calculus of Variations*, 17(2):380–405.

[Moireau et al., 2008] Moireau, P., Chapelle, D., and Le Tallec, P. (2008). Joint state and parameter estimation for distributed mechanical systems. *Computer Methods in Applied Mechanics and Engineering*, 197(6-8):659–677.

[Moireau et al., 2009] Moireau, P., Chapelle, D., and Le Tallec, P. (2009). Filtering for distributed mechanical systems using position measurements: perspectives in medical imaging. *Inverse Problems*, 25(3):035010.

[Moireau et al., 2012] Moireau, P., Xiao, N., Astorino, M., Figueroa, C. a., Chapelle, D., Taylor, C. a., and Gerbeau, J.-F. (2012). External tissue support and fluid-structure simulation in blood flows. *Biomechanics and modeling in mechanobiology*, 11(1-2):1–18.

[Mynard and Nithiarasu, 2008] Mynard, J. and Nithiarasu, P. (2008). A 1D arterial blood flow model incorporating ventricular pressure, aortic valve and regional coronary flow using the locally conservative Galerkin (LCG) method. (March):367–417.

[Navon, 2009] Navon, I. (2009). Data assimilation for numerical weather prediction: a review. In *Data Assimilation for Atmospheric, Oceanic and Hydrologic Applications.*, pages 21–65.

[Netter and Colacino, 1989] Netter, F. and Colacino, S. (1989). *Atlas of human anatomy*. Ciba-Geigy Corporation.

[Nichols et al., 2011] Nichols, W., O'Rourke, M., and Vlachopoulos, C. (2011). *McDonald's blood flow in arteries: theoretical, experimental and clinical principles*. CRC Press.

[Nobile, 2001] Nobile, F. (2001). Numerical approximation of fluid-structure interaction problems with application to haemodynamics. *PhD, Ecole Polytechnique F{é}derale de Lausanne, Switzerland*.

[Nocedal, 1992] Nocedal, J. (1992). Theory of algorithms for unconstrained optimization. *Acta numerica*.

[Nocedal and Wright, 1999] Nocedal, J. and Wright, S. (1999). *Numerical Optimization*. Springer Series in Operations Research and Financial Engineering. Springer-Verlag, New York.

[Olufsen et al., 2000] Olufsen, M., Peskin, C., Kim, W., Pedersen, E.M, Nadim, A., and Larsen, J. (2000). Numerical simulation and experimental validation of blood flow in arteries with structured-tree outflow conditions. *Annals of biomedical engineering*, 28(11):1281–99.

[Ottesen et al., 2004] Ottesen, J., Olufsen, M., and Larsen, J. (2004). *Applied mathematical models in human physiology*, volume 9. SIAM.

[Penenko, 2009] Penenko, V. V. (2009). Variational methods of data assimilation and inverse problems for studying the atmosphere, ocean, and environment. *Numerical Analysis and Applications*, 2(4):341–351.

[Perego et al., 2011] Perego, M., Veneziani, A., and Vergara, C. (2011). A Variational Approach for Estimating the Compliance of the Cardiovascular Tissue: An Inverse Fluid-Structure Interaction Problem. *SIAM Journal on Scientific Computing*, 33(3):1181–1211.

[Pope et al., 2008] Pope, S., Ellwein, L., Zapata, C., Novak, V., Kelley, C., and Olufsen, M. (2008). Estimation and identification of parameters in a lumped cerebrovascular model. *Mathematical Biosciences and Engineering*, 6(1):93–115.

[Pozzoli, 2012] Pozzoli, M. (2012). *Efficient partitioned algorithms for the solutions of fluid-structure interaction problems in haemodynamics*. PhD thesis, Politecnico di Milano, Italy.

[Quartapelle, 1993] Quartapelle, L. (1993). *Numerical Solution of the Incompressible Navier–Stokes Equations*. Springer-Verlag.

[Quarteroni and Formaggia, 2004] Quarteroni, A. and Formaggia, L. (2004). Mathematical modelling and numerical simulation of the cardiovascular system. *Handbook of numerical analysis*, 12:3–127.

[Quarteroni et al., 2000] Quarteroni, A., Tuveri, M., and Veneziani, A. (2000). Computational vascular fluid dynamics: problems, models and methods. *Computing and Visualization in Science*, 2(4):163–197.

[Raydan, 1993] Raydan, M. (1993). On the Barzilai and Borwein choice of steplength for the gradient method. *IMA Journal of Numerical Analysis*, 13(3):321–326.

[Raydan, 1997] Raydan, M. (1997). The Barzilai and Borwein gradient method for the large scale unconstrained minimization problem. *SIAM Journal on Optimization*, 7(1):26–33.

[Raydan and Svaiter, 2002] Raydan, M. and Svaiter, B. (2002). Relaxed Steepest Descent and Cauchy-Barzilai-Borwein Method. *Computational Optimization and Applications*, 21:155–167.

[Reichle et al., 2002] Reichle, R., Walker, J., Koster, R., and Houser, P. (2002). Extended versus ensemble Kalman filtering for land data assimilation. *Journal of Hydrometeorology*, 3:728–740.

[Reichold et al., 2009] Reichold, J., Stampanoni, M., Keller, L., Buck, A., Jenny, P., and Weber, B. (2009). Vascular graph model to simulate the cerebral blood flow in realistic vascular networks. *Journal of cerebral blood flow and metabolism : official journal of the International Society of Cerebral Blood Flow and Metabolism*, 29(8):1429–43.

[Reymond et al., 2011] Reymond, P., Bohraus, Y., Perren, F., Lazeyras, F., and Stergiopulos, N. (2011). Validation of a patient-specific one-dimensional model of the systemic arterial tree. *American journal of physiology. Heart and circulatory physiology*, 301(3):H1173–82.

[Reymond et al., 2009] Reymond, P., Merenda, F., Perren, F., Rüfenacht, D., and Stergiopulos, N. (2009). Validation of a one-dimensional model of the systemic arterial tree. *American journal of physiology. Heart and circulatory physiology*, 297(1):H208–22.

[Ridgway, 2010] Ridgway, J. (2010). Cardiovascular magnetic resonance physics for clinicians: part I. *Journal of cardiovascular magnetic resonance : official journal of the Society for Cardiovascular Magnetic Resonance*, 12(1):71.

[Robinson and Lermusiaux, 2000] Robinson, A. and Lermusiaux, P. (2000). Overview of data assimilation. *Harvard reports in physical/interdisciplinary ocean science*, (62).

[Scheffler and Lehnhardt, 2003] Scheffler, K. and Lehnhardt, S. (2003). Principles and applications of balanced SSFP techniques. *European radiology*, 13(11):2409–18.

[Segers et al., 2003] Segers, P., Stergiopulos, N., Westerhof, N., Wouters, P., Kolh, P., and Verdonck, P. (2003). Systemic and pulmonary hemodynamics assessed with a lumped-parameter heart-arterial interaction model. *Journal of Engineering Mathematics*, 47(3/4):185–199.

[Sermesant et al., 2006] Sermesant, M., Moireau, P., Camara, O., Sainte-Marie, J., Andriantsimiavona, R., Cimrman, R., Hill, D., Chapelle, D., and Razavi, R. (2006). Cardiac function estimation from MRI using a heart model and data assimilation: advances and difficulties. *Medical image analysis*, 10(4):642–56.

[Sherwin et al., 2003] Sherwin, S., Franke, V., Peiró, J., and Parker, K. (2003). One-dimensional modelling of a vascular network in space-time variables. *Journal of Engineering Mathematics*, 47(3/4):217–250.

[Shi et al., 2011] Shi, Y., Lawford, P., and Hose, R. (2011). Review of zero-D and 1-D models of blood flow in the cardiovascular system. *Biomedical engineering online*, 10(1):33.

[Simon, 2006] Simon, D. (2006). *Optimal state estimation: Kalman, H infinity, and nonlinear approaches*. Wiley. com.

[Sokolowski and Zolesio, 1992] Sokolowski, J. and Zolesio, J. (1992). *Introduction to shape optimization*. Springer.

[Spilker and Taylor, 2010] Spilker, R. and Taylor, C. (2010). Tuning multidomain hemodynamic simulations to match physiological measurements. *Annals of biomedical engineering*, 38(8):2635–48.

[Stå lhand, 2009] Stå lhand, J. (2009). Determination of human arterial wall parameters from clinical data. *Biomechanics and modeling in mechanobiology*, 8(2):141–8.

[Stå lhand and Klarbring, 2005] Stå lhand, J. and Klarbring, A. (2005). Aorta in vivo parameter identification using an axial force constraint. *Biomechanics and modeling in mechanobiology*, 3(4):191–9.

[Stergiopulos et al., 1999] Stergiopulos, N., Westerhof, B. E., and Westerhof, N. (1999). Total arterial inertance as the fourth element of the windkessel model. *The American journal of physiology*, 276(1 Pt 2):H81–8.

[Stergiopulos et al., 1992] Stergiopulos, N., Young, D., and Rogge, T. (1992). Computer simulation of arterial flow with applications to arterial and aortic stenoses. *Journal of biomechanics*, 25(12):1477–1488.

[Sun and Yuan, 2006] Sun, W. and Yuan, Y. (2006). *Optimization theory and methods: nonlinear programming*. Springer.

[Taylor and Figueroa, 2009] Taylor, C. and Figueroa, C. (2009). Patient-specific modeling of cardiovascular mechanics. *Annual review of biomedical engineering*, 11:109–134.

[Tezduyar and Sathe, 2007] Tezduyar, T. and Sathe, S. (2007). Modelling of fluid–structure interactions with the space–time finite elements: solution techniques. *International Journal for Numerical ...*, (January):855–900.

[Tezduyar et al., 2006] Tezduyar, T., Sathe, S., and Stein, K. (2006). Solution techniques for the fully discretized equations in computation of fluid–structure interactions with the space–time formulations. *Computer Methods in Applied Mechanics and Engineering*, 195(41-43):5743–5753.

[Thompson, 1987] Thompson, K. W. (1987). Time dependent boundary conditions for hyperbolic systems. *Journal of Computational Physics*, 68(1):1–24.

[Torii et al., 2008] Torii, R., Oshima, M., Kobayashi, T., Takagi, K., and Tezduyar, T. (2008). Fluid–structure interaction modeling of a patient-specific cerebral aneurysm: influence of structural modeling. *Computational Mechanics*, 43(1):151–159.

[Troianowski et al., 2011] Troianowski, G., Taylor, C. A., Feinstein, J. A., and Vignon-Clementel, I. E. (2011). Three-dimensional simulations in Glenn patients: clinically based boundary conditions, hemodynamic results and sensitivity to input data. *Journal of Biomechanical Engineering*, 133:111006.

[Tröltzsch, 2010] Tröltzsch, F. (2010). *Optimal control of partial differential equations: theory, methods, and applications*, volume 112. American Mathematical Soc.

[Tuan Pham et al., 1998] Tuan Pham, D., Verron, J., and Roubaud, M. (1998). A singular evolutive extended Kalman filter for data assimilation in oceanography. *Journal of Marine Systems*, 16(3-4):323–340.

[Ulbrich, 2001] Ulbrich, S. (2001). Optimal control of nonlinear hyperbolic conservation laws with source terms. *Technische Universitaet Muenchen*.

[Ursino, 1998] Ursino, M. (1998). Interaction between carotid baroregulation and the pulsating heart: a mathematical model. *The American journal of physiology*, 275(5 Pt 2):H1733–47.

[van den Doel and Ascher, 2012] van den Doel, K. and Ascher, U. (2012). The chaotic nature of faster gradient descent methods. *Journal of Scientific Computing*, 51(3):560–581.

[van der Merwe, 2004] van der Merwe, R. (2004). *Sigma-point Kalman filters for probabilistic inference in dynamic state-space models*. PhD thesis.

[van der Merwe and Wan, 2001] van der Merwe, R. and Wan, E. (2001). The square-root unscented Kalman filter for state and parameter-estimation. *Acoustics, Speech, and Signal Processing, 2001. Proceedings.(ICASSP'01). 2001 IEEE International Conference on.*, 6:3461–3464.

[Vignon and Taylor, 2004] Vignon, I. E. and Taylor, C. a. (2004). Outflow boundary conditions for one-dimensional finite element modeling of blood flow and pressure waves in arteries. *Wave Motion*, 39(4):361–374.

[Vignon-Clementel et al., 2006] Vignon-Clementel, I., Figueroa, A., Jansen, K., and Taylor, C. (2006). Outflow boundary conditions for three-dimensional finite element modeling of blood flow and pressure in arteries. *Computer Methods in Applied Mechanics and Engineering*, 195(29-32):3776–3796.

[Vignon-Clementel et al., 2010] Vignon-Clementel, I. E., Figueroa, C. a., Jansen, K. E., and Taylor, C. a. (2010). Outflow boundary conditions for 3D simulations of non-periodic blood flow and pressure fields in deformable arteries. *Computer methods in biomechanics and biomedical engineering*, 13(5):625–40.

[Wang et al., 2000] Wang, B., Zou, X., and Zhu, J. (2000). Data assimilation and its applications. *Proceedings of the National Academy of Sciences of the United States of America*, 97(21):11143–4.

[Wang and Parker, 2004] Wang, J. and Parker, K. (2004). Wave propagation in a model of the arterial circulation. *Journal of biomechanics*, 37(4):457–70.

[Wemple and Mockros, 1972] Wemple, R. and Mockros, L. (1972). Pressure and flow in the systemic arterial system. *Journal of biomechanics*, 5(6):629–641.

[Xi et al., 2011] Xi, J., Lamata, P., Lee, J., Moireau, P., Chapelle, D., and Smith, N. (2011). Myocardial transversely isotropic material parameter estimation from in-silico measurements based on a reduced-order unscented Kalman filter. *Journal of the mechanical behavior of biomedical materials*, 4(7):1090–102.

[Yang and Veneziani, 2013] Yang, H. and Veneziani, A. (2013). Variational estimation of cardiac conductivities by a data assimilation procedure. Technical report, Department of Mathematics and Computer Science, Emory University.

[Zuazua, 2005] Zuazua, E. (2005). Propagation, Observation, and Control of Waves Approximated by Finite Difference Methods. *SIAM Review*, 47(2):197–243.

[Zuazua, 2007] Zuazua, E. (2007). Controllability and observability of partial differential equations: some results and open problems. *Handbook of differential equations: evolutionary equations*, 3:527–621.